ABSTRACT

SHARMA, RACHITA. Principles and Engineering of Self-Propelling Particles. (Under the direction of Dr. Orlin D. Velev).

We report here the development and characterization of novel techniques for powering and actuating the self-propulsion of small particles, and potentially future microdevices, in liquids. This is a challenging research area because the interplay of forces acting on a small particle swimming in a liquid is very different from that acting on a macroscopic swimmer. The inertial forces, dominant at the macroscale, are overpowered by other effects such as Brownian collisions and viscous drag at microscales. Over the last decade, several techniques have been explored to propel different kinds of objects (a few millimeters or smaller in size) in liquids and to control or tune their motion. Self-propelling particles could find applications in performing a broad range of functions such as drug/vaccine delivery and medical diagnostics in the biomedical field, shuttling cargo and pumping/mixing fluid in lab-on-chip devices, and others. Recently, proof-of concept of their ability to perform some of these practical tasks has been demonstrated by various groups. We developed two new categories of self-propelling particles driven by a periodic cycle of Marangoni effect flows and catalytic activity of live cells, and proposed a novel technique based on AC field modulation for remotely controlling the direction of motion of the diode-based self-propelling particles. We also demonstrated a novel simple application of such autonomously propelling particles floating on water surface for rapid oil spill cleanup.

Our Marangoni effect driven self-propelling particles, comprising of an ethanol infused hydrogel, exhibit a unique pulsating motion in water over long duration. Their pulsation results from the emergence of a self-sustained periodic cycle of surface tension gradient driven flows. We developed scaling relations for the pulse interval and the distance propelled by these particles. On the basis of the quantification of this mass-transfer driven motion, we constructed floaters of different designs programmed to move in complex trajectories over the water surface. Such programmable “dancing” swimmers serve as early prototypes of functional autonomously propelling devices capable of performing practical tasks, as demonstrated by us in a follow-up project where we use them for efficient oil collection.

To achieve functionality, we incorporated an oil absorbent "payload" into the Marangoni effect driven particles, which already contain an "engine" component for self-propulsion. Such "engine-payload" particles self-propel over the oil-covered water surface while simultaneously collecting and dispersing the oil film. Oil gets collected into the absorbent end and the release of the surface active material from the hydrogel end causes oil film dispersion. We found that such mobile absorbents are more efficient (due to convective transport of oil) compared to immobile absorbents that depend on diffusion or natural drifting for gathering oil, which makes the former a viable alternative for tackling oil spills. The overall approach of enhancing the rate of mass-transfer by self-propelling an otherwise stationary particle may be also used to dramatically increase the efficiency of other processes such as catalysis.

A drawback prevalent with chemical Marangoni effect driven self-propulsion is that the motion is limited by the amount of "fuel" on-board the particle. With the objective of overcoming this drawback, we developed biocatalytic self-propelling particles that use yeast cells as catalyst to power their propulsion by fermenting glucose or decomposing hydrogen peroxide (H_2O_2) present in the surrounding solution. Catalytically driven propulsion in H_2O_2 has already been accomplished using synthetic catalysts or isolated enzymes. Our work is the first demonstration of employing live cells directly as catalysts for this process, and will stimulate further exploration of novel catalyst-fuel combinations.

Finally, we devised a novel technique for controlling the direction of motion of diode-based self-propelling prototypes of electronic microdevices on water. The diodes are remotely powered by an external uniform AC electric field, a technique reported earlier by Velev group. We found that by modifying the wave symmetry of the AC signal, the self-propelling diodes could be rotated due to their orientation-dependent polarizability and made to shuttle back and forth on water. Analogous to the dipole-dipole interactions, diodes prefer to orient such that the DC field across them is anti-parallel with respect to the external field. We believe that this new principle of AC field modulation driven control of the direction of motion of the self-propelling microcircuit elements is a first step towards the development of "intelligent" particles that can perform complex functions in the fields of MEMs and micro-robotics.

Principles and Engineering of Self-Propelling Particles

by
Rachita Sharma

A dissertation submitted to the Graduate Faculty of
North Carolina State University
in partial fulfillment of the
requirements for the degree of
Doctor of Philosophy

Chemical Engineering

Raleigh, North Carolina

2013

APPROVED BY:

_____	_____
Michael Flickinger	Jan Genzer
_____	_____
Michael Dickey	Orlin D. Velev Committee Chair

DEDICATION

This dissertation is dedicated to
my parents,
Renu Sharma and Rajendra K. Sharma,
and my brother,
Rajat Sharma,
who make everything possible for me
by their love, support and sacrifices.

BIOGRAPHY

Rachita Sharma was born on 5th November1986 in Rajhara, a small town in Chhattisgarh state of India. She grew up in Bhilai, another town in Chhattisgarh state, famous for its steel plant which is the largest in India and known for being the only manufacturer of rails in the country. Rachita did her entire schooling in Bhilai at Delhi Public School. After graduating from high school in 2004, she earned an admission into the Bachelor of Technology (B. Tech.) program for Chemical Engineering at the prestigious Indian Institute of Technology - Bombay (IIT Bombay), by clearing the extremely competitive Joint Entrance Exam (JEE) in 2004. Rachita finished her undergraduate education at IIT Bombay in May, 2008. She joined the PhD program at the Chemical & Biomolecular Engineering Department of North Carolina State University in Fall 2008, and since then she has been pursuing her graduate research under the guidance of Prof. Orlin D. Velev.

ACKNOWLEDGMENTS

I would like to acknowledge the help and support of several individuals without whom this work would not have been possible. Firstly, I would like to thank my advisor, Dr. Orlin D. Velev, for his excellent guidance and mentorship throughout the last ~ 5 years of my graduate research. He has been a constant source of motivation and encouragement for all of us, and most importantly he always has time for discussing our research progress in spite of his very busy schedule. I am grateful to Dr. Velev for all the fruitful discussions I had with him, which always gave me a sense of direction in my research. Thanks for everything, Dr. Velev!

I am thankful to all the members of my thesis committee, Dr. Jan Genzer, Dr. Michael Dickey and Dr. Michael Flickinger, for agreeing to serve on my thesis committee and for their time and constructive feedbacks. I must also thank Dr. Saad Khan for agreeing to be a substitute committee member during my Prelim. I would like to acknowledge all the CBE faculty members and staff members for their help and favors. I am lucky that I got a chance to work with such a dynamic research group. All my colleagues from Velev research group have been very nice and helpful to me. Thank you – Elena, Stephanie, Stoyan, Sejong, Burak, Jess, Hyung Jun, Alex, Jairus, Tian, Shan, Daniel, Bhuvnesh, Etienne, Yan, Naren, Selver, Anne-Laure!

I cannot thank enough my parents and my brother for being a driving force in my life. I give all the credit for my achievements to their endless love, support and sacrifices!

TABLE OF CONTENTS

LIST OF TABLES

LIST OF FIGURES

CHAPTER 1

General Introduction to Self-Propelling Particles

1.1 Definition

There is no universal definition of which particles should be called self-propelling (as compared to simply moving by external force), so we begin by building our own strict definition. A uniformly polarizable particle present in a uniform field (such as chemical, electrical, thermal, etc.) does not necessarily experience a net force (Figure 1.1a). When this field is non-uniform, it exerts a net force acting on the particle that may cause it to move (Figure 1.1b). However, we do not refer to such a particle as self-propelling. A self-propelling particle is one that can generate local field asymmetry around itself while the external field is uniform. This local asymmetry, coupled with a fluid flux, causes the particle to propel (Figure 1.1c). Self-propelling particles are dissipative systems as they are open to their environment and operate out of thermodynamic equilibrium. Momentum flux acting on these particles is coupled to the mass/thermal/electric flux generated by them due to their asymmetric design. Restoring the symmetry in their material or shape eliminates the generated coupled fluxes and brings the system to equilibrium (no propulsion).

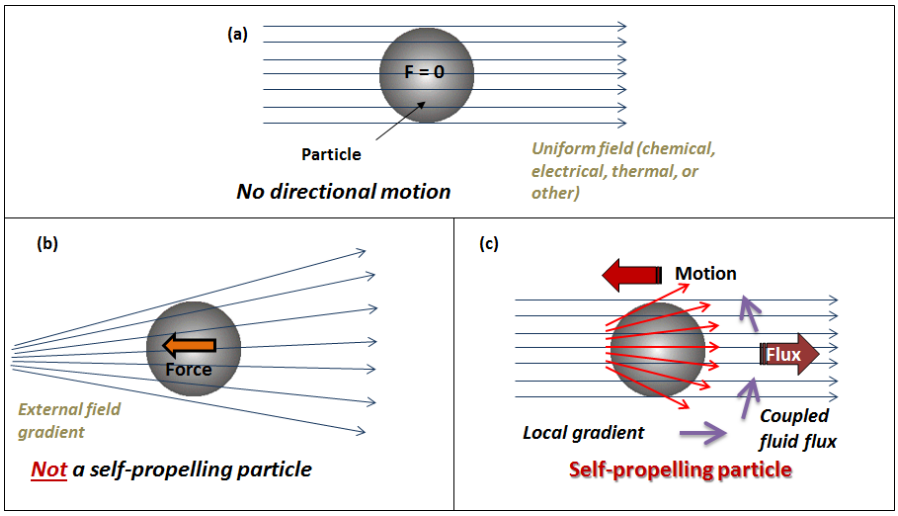

Figure 1.1 Definition of a self-propelling particle in terms of the source of the driving force. A particle under uniform field (a) does not exhibit directional motion. A particle whose motion originates from external field asymmetry (b) is not self-propelling, unlike a particle whose motion originates from local field asymmetry leading to a local flux (c).

1.2 Physical Challenges in Propelling Small Particles

As with several other research areas, the major inspiration behind self-propelling particles comes from the nature itself. Some common examples are the swimming of an *Escherichia coli* bacterium due to 'cork-screw' motion of its flagella driven by motor proteins,[1-3] and propulsion of a *Listeria* bacterium by the polymerization and cross-linking of actin protein into a comet-like tail behind the bacterium.[4,5] Biological motors, such as kinesin and myosin motor proteins, exhibit remarkable motion capabilities and are excellent examples of conversion of chemical energy, stored as adenosine triphosphate (ATP), into mechanical energy for propulsion (Fig. 1.2).[6,7] However, competing with nature is challenging as evolution has perfected the workings of these self-propelling "machines".

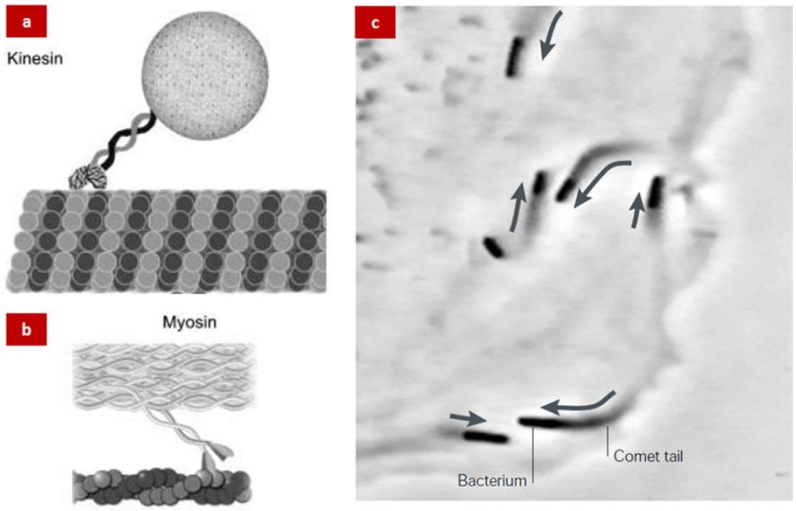

Figure 1.2 Schematic showing (a) a kinesin motor protein moving along a microtubule while carrying an intracellular cargo, and (b) a myosin motor protein moving along an actin filament.[6] (c) A micrograph illustrating movement of *Listeria monocytogenes* in an infected host cell. The comet tail behind the bacteria is clearly visible.[5]

As the dimension of a particle decreases by a factor of x, its volume shrinks by a factor of x^3 and the decrease in its surface area scales as x^2. Therefore, the surface area to volume ratio increases with decrease in size. This has several interesting consequences on the

interplay of forces acting on the particle.[8] (a) Surface forces, such as diffusiophoresis, electrophoresis, thermophoresis, etc., dominate over the inertial forces as they scale with the surface area and volume of the particle, respectively. (b) Drag forces become important compared to inertial forces since drag forces scale with the factor *x*, making swimming in water seem like swimming in molasses. In other words, ratio of inertial to viscous forces, defined as Reynolds number, *Re*, is small:

$$\mathrm{Re} = \frac{\rho v l}{\mu} \tag{1.1}$$

where ρ is the fluid density, μ is the fluid viscosity, v is the mean particle velocity and l is the characteristic linear dimension. Moreover, the fluid flows at low Reynolds number are microscopically reversible. This implies that under laminar regime reciprocating motion, for example, the opening-closing of a scallop shell, would not result in a net fluid flow or animal motion. Also, what a particle does at any moment is determined by the forces acting on it at that moment, and not by the forces acting on it in the past. (c) Brownian collisions become significant relative to inertial forces, as the frequency of collisions scales with the surface area. In short, Brownian collisions, viscous drag and surface phenomena become dominant over inertial forces as the particle size decreases. This renders the task of designing a self-propelling particle, a few millimeters or smaller in size, challenging. Scaling down macroscale motors and propellers to the microscale is complicated and they may not be as efficient as their correspondingly larger analogues because of the limitations of the above mentioned viscous, thermal, and interfacial microscale effects. Propulsion at macroscale is predominantly driven by the inertial forces, unlike propulsion at microscale that falls under the low Reynolds number regime. Therefore, novel techniques are required to supply power (or fuel) to propel small objects in liquids, which in itself is not straightforward due to their constrained dimensions and limited volumes.[9-15]

1.3 Brief Review of Self-Propelling Particles

A brief review of previously reported self-propelling particles that “swim” on liquid surfaces or within the bulk liquid, grouped on the basis on their propulsion mechanism, has been

made in this section. The major advantages and limitations of each propulsion mechanism are discussed and the means to overcome them are evaluated.

1.3.1 Marangoni Effect Driven Propulsion

One of the earliest known techniques of propelling objects in liquids is based on Marangoni effect or surface tension gradient driven flows.[16-17] The most commonly known Marangoni effect driven phenomena, such as the propulsion of certain insects on water surface, originate from chemical concentration gradients.[18] Camphor and soap "boats" are well known simple devices that self-propel on water.[19-29] The adsorption and spreading of the camphor and soap (surfactant) molecules decreases the surface tension of water. Therefore, chemical concentration gradient resulting from asymmetric release of camphor or soap molecules leads to surface tension asymmetry across the boat, causing it to propel due to force imbalance. The propulsion force, F, on a particle due to surface tension asymmetry scales as

$$F \propto \Delta\gamma \propto \frac{\Delta\gamma}{\Delta C}\Delta C \tag{1.2}$$

where $\Delta\gamma$ is the difference in surface tension and ΔC is the difference in the concentration of the surface-active material across the particle. Assuming that the surface tension of the liquid-liquid mixture can be approximated as the sum of the surface tensions of all the components weighted according to their mole fractions in the mixture,[30] we obtain

$$\frac{\Delta\gamma}{\Delta C} = \text{constant} \tag{1.3}$$

which further simplifies eqn (1.2), as discussed in Chapter 2. Based on this same source of motion, gels infused with organic solvents (such as ethanol, tetrahydrofuran, etc.), have been propelled on water by Marangoni effect arising from the release and spreading of the solvent near one end of the gels.[31-35] Similarly, SU-8 microboats have been propelled by releasing isopropanol.[36] Recently, Xiao *et al.* have combined Marangoni effect with pH-responsive transition of superhydrophobicity-superhydrophilicity to mimic the movement of beetles on water.[37] However, a limitation in the design of particles that carry their "fuel" on-board is that their motion is limited, in terms of duration, by the amount of fuel contained by the

particle. A solution to this drawback is the alternative approach of generating Marangoni effect - by inducing temperature gradients, as surface tension of a fluid decreases with increase in temperature. An excellent example of transduction of light into mechanical energy is based on thermally induced Marangoni effect, where a composite of PDMS and vertically aligned carbon nanotubes (VANT) has been propelled on water by optical heating.[38] VANTs are localized on only one edge of the object and they act as light-activated thermal switches, which heat up the surrounding fluid locally leading to a temperature gradient across the object. These PDMS-VANT composite particles have also been shown to be effective in harnessing sunlight for thermal Marangoni effect driven propulsion. Such a particle can, in theory, keep propelling as long as it is exposed to the light source.

One common aspect in the motion of the floaters listed here is that the motion occurs at the air-liquid interface, as Marangoni effect is an interfacial phenomenon. Recently, Marangoni effect driven propulsion of a capsule motor at the liquid-liquid interface was reported.[39] Examples of various Marangoni effect driven self-propelling particles are shown in Fig. 1.3.

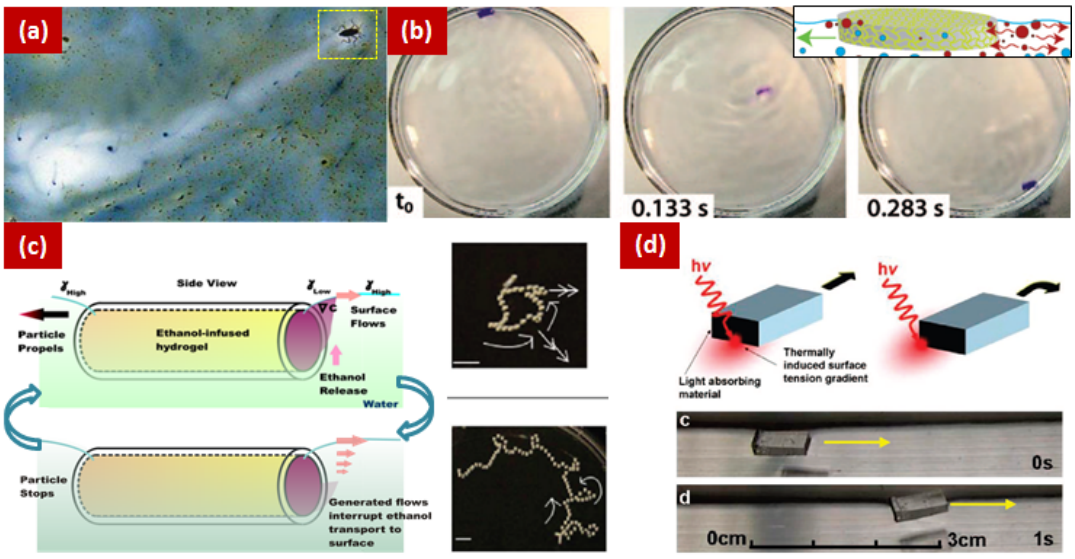

Figure 1.3 Examples of autonomously propelling particles based on Marangoni effect. (a) *Microvelia*, a semi-aquatic insect, moving by releasing surfactant (surfactant spreading visible by clearing of dye from water surface).[18] (b) Time-lapse snapshots of photopatterned poly-*N*-isopropylacrylamide gel, rectangular shaped, translating on water surface by releasing ethanol.[33] (c) Ethanol-infused hydrogel based particles pulsating in complex trajectories on water.[35] (d) Schematic illustrating the light-based activation of PDMS-VANT composite objects, along with snapshots showing its linear propulsion.[38]

1.3.2 Bubble Propulsion

The earliest self-propelling particles driven by catalytic reactions, reported by Ismagilov *et al.*, were based on propulsion originating from the ejection of gas bubbles.[40] These millimeter sized polydimethylsiloxane (PDMS) plates have been propelling on the surface of hydrogen peroxide (H_2O_2) solution due to the catalytic decomposition of H_2O_2 by platinum into water and oxygen (Fig. 1.4a). In addition to propulsion, these autonomously propelling plates have been shown to self-assemble into aggregates due to capillary interactions. Other examples of particles propelled by impulse of bubbles generated by catalytic reactions in H_2O_2 solution are silica microbeads propelled by synthetic catalase,[41] silica-platinum Janus microspheres (Fig. 1.4c)[42] and palladium doped cobalt ferrite microparticles.[43] In all these cases, asymmetric bubble release has been achieved by asymmetric placement of the catalyst on the particle. Using a slightly different approach, rolled-up microtubes as well as microtubes

prepared by templated-electrochemical deposition method have been propelled in H_2O_2 due to the catalytic activity of the platinum or catalase enzyme present in the interior of the microjets (Fig. 1.4b).[44-48] Although the catalyst has been symmetrically incorporated in the microtubes, bubble release from only one end of the microtubes was achieved by pressure differential across it owing to its conical shape.

Recently polymer stomatocytes, with entrapped Pt nanoparticles, have been propelled in H_2O_2 by releasing oxygen bubbles during controlled opening of the stomatocyte cavity.[49] Efforts have also been made towards exploring benign fuels, in place of H_2O_2, for powering these systems to broaden the scope of their practical applicability. For example, a biohybrid system comprising of carbon nanotubes functionalized with glucose oxidase and catalase enzymes has been shown to propel in a natural medium, glucose, by bubble recoil mechanism due to the concerted action of the two enzymes.[50] In all these examples of particles driven by bubble release, the source of bubble production is a catalytic reaction. The catalyst is incorporated into the particle design and the "fuel" that is decomposed by the catalyst is present in the external environment. This allows continuous particle propulsion, in principle, as long as the very big external pool of fuel is exhausted. The motion is well-defined at the air-liquid interface, however, when motion takes place in bulk liquid buoyancy effects arising from bubble generation impart additional complexity.[40] It has been observed in one of the previous studies that the motion driven by bubble recoil mechanism is not significantly affected by the ionic strength of the medium, making propulsion possible even in salt-rich environments. Velocity of Au-Pt microtubes was found to decrease by only 1-3% in the presence of 1M NaCl in H_2O_2 media relative to salt-free media.[45]

Contrasting results have been reported in another study where the motion of Pt catalytic bubble-propelled microjets has been found to be significantly inhibited in the presence of inorganic ions found in real world environments such as tap water, sea water or rain water.[51] Similarly, motion of such bubble-propelled microengines has been tested in other complex but practical media environments such as artificial blood samples (with added fuel H_2O_2).[52] It has been found that the two main components of animal blood, red blood cells and serum, individually suppress bubble ejection and particle motion even at high

dilutions. Also, typical organic and/or biological molecules (such as dimethyl sulfoxide, extracellular thiols, etc.) have been shown to negatively impact the propulsion of microjets comprising of Pt catalyst.[53] Such findings shed light on some of the challenges/limitations facing propulsion of catalytically driven particles in real-world environments and point out the directions for future work needed to improve the design of these particles, as further discussed in Section 1.4.

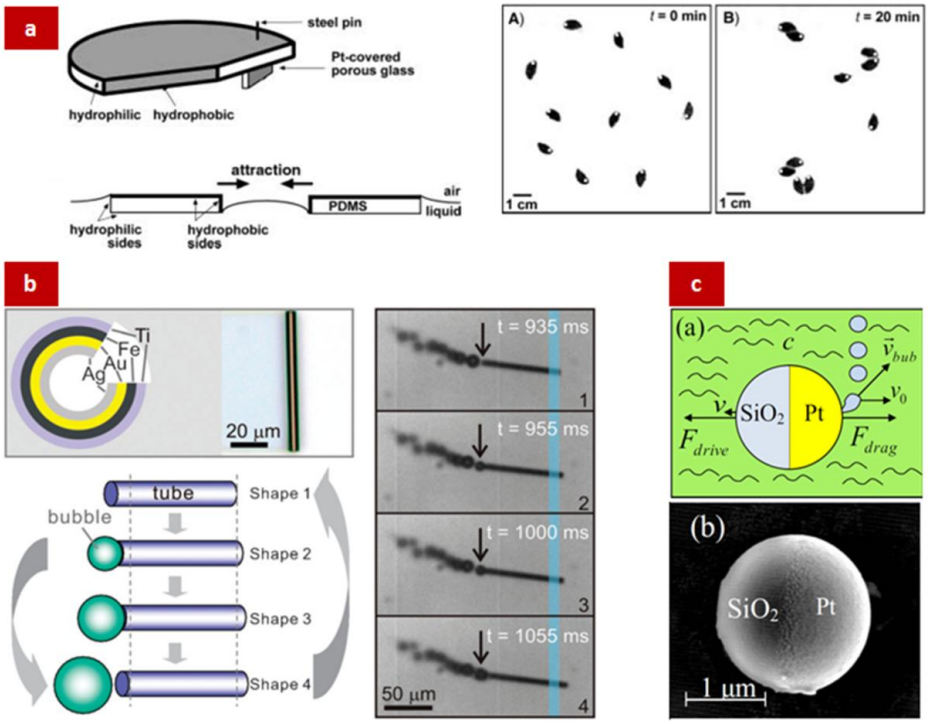

Figure 1.4 Examples of autonomously propelling particles based on bubble propulsion. (a) Schematic of millimeter sized hemicylindrical PDMS plates, with a small Pt catalyst-coated surface, that propel on the surface of H_2O_2 solution. The edges of the plates are patterned to create hydrophilic and hydrophobic regions, which induces capillary attraction between the plates causing them to self-assemble into dimers (as seen in the photograph after 20 min of floatation on the surface of H_2O_2).[40] (b) Schematic showing the composition of multilayered rolled-up microtubes, comprising of Ag catalyst in their interior. These "microrockets" propel in H_2O_2 solution due to generation, growth and release of oxygen bubbles, as illustrated by the time-lapse video frames and schematic.[44,46] (c) Pt-coated Janus silica microbead self-propels in H_2O_2 solution due to catalytic decomposition of H_2O_2 into water and oxygen bubbles.[42]

1.3.3 Self-Electrophoresis

The propulsion mechanism of self-electrophoresis was proposed by the team led by Mallouk and Sen, to explain the motion of bimetallic nanorods in H_2O_2 solution. Tethered Au-Ni nanorods have been shown to rotate in H_2O_2 solution,[54,55] and Au-Pt nanorods have been observed to propel in the direction opposite to that expected from the bubble recoil mechanism.[56] Due to the small size of the nanorods, the recoil generated from bubble release was insufficient to induce motion unlike that observed at macroscales, and other surface forces were dominant in comparison. The most significant force acting on the nanorods comes from the redox reactions at the Au and Pt ends, leading to an electron flux from Au towards Pt through the nanorods and a simultaneous proton flux in the same direction through the electrical double layer near the surface of the nanorods (Fig. 1.5a).[57] This (in effect electrophoretic) proton flux near the nanorod surface drags water molecules along, causing nanorods to propel reactively in the opposite direction. The velocity of the self-electrophoretically driven particles, u_{se}, can be estimated using the Helmholtz-Smoluchowski equation as

$$u_{se} = \mu_e E = \frac{\mu_e J}{k} \tag{1.4}$$

where E and J are the electric field and current density, respectively, due to the electrochemical reaction, μ_e is the electrophoretic mobility of the particle and k is the conductivity of the bulk solution.[58] The drastic difference between the propulsion mechanism in H_2O_2 solution of millimeter-sized catalytic particles reported by Ismagilov *et al.*[40] and that of the bimetallic nanorods highlights the unique physics governing motion at small scales.[10] The mechanism of hydronium flux driven propulsion of nanorods also has broad similarities to the proton gradient driven transport processes in cells.[14,59] Based on the same principle, carbon fibers with bioelectrocatalyst-coated end segments were autonomously propelled on the surface of glucose solution due to proton flux (accompanying current flow across the fiber) originating from the simultaneous redox reactions at its two ends (Fig. 1.5b).[60]

As can be deduced from eqn (1.4), the major drawback associated with this propulsion mechanism is that the particle velocity scales inversely with the conductivity of

the medium, which poses limitations to the propulsion of such particles in higher ionic strength real-world media such as biological samples. In spite of these challenges, over the past few years self-electrophoretically driven catalytic nanorods have garnered attention from various research groups and extensive work has been done to further improve their design with the aim of applying them to perform complex practical functions,[14,61,62] as discussed in Section 1.4.

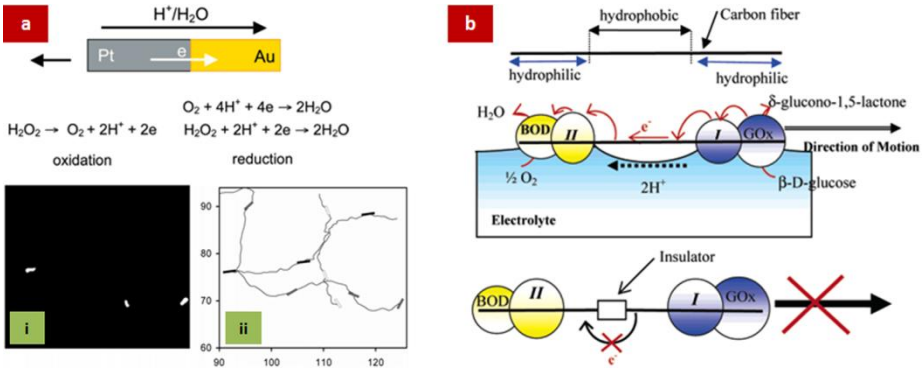

Figure 1.5 Examples of autonomously propelling particles based on self-electrophoresis principle. (a) Au-Pt nanorods[57] and (b) carbon fiber functionalized with bioelectrocatalysts at its ends[60] propel in H_2O_2 solution, driven by the flux of hydronium ions near its surface, due to redox reactions at its ends. Trajectories of three 2 µm long nanorods,[56] identified in panel (i) of (a), have been illustrated in panel (ii) of (a) during 5 min of their propulsion in H_2O_2 solution.

1.3.4 Other Propulsion Mechanisms

The asymmetric catalytic particles described in Sections 1.3.2 & 1.3.3 propel predominantly due to recoil from bubble release and self-electrophoresis, respectively. Other mechanisms by which such catalytic particles can be self-propelled include osmophoresis or diffusiophoresis resulting from the generation of a concentration gradient of soluble or nongaseous reaction products around them.[14,63] The speed and direction of motion depend on

nature of particle-solute interaction. Theoretical[64-67] and experimental[68,69] investigation of this phenomenon has been done by several groups in recent years.

External electric field driven effects have been extensively utilized to develop self-propelling particles. Velev group has reported that uniform external AC electric fields can be applied to selectively propel metallodielectric Janus particles due to induced-charge electrophoresis (Fig. 1.6a).[70] The origin of motion in this case exists in the asymmetry in the particle design. The electric double layer on the metallic side is more strongly polarized relative to the dielectric side. Consequently, the induced-charge electroosmotic flows near the metallic surface are stronger compared to the dielectric surface, resulting in propulsion of the metallodielectric Janus particticles due to induced-charge electrophoresis in the direction perpendicular to the applied electric field. An alternate method of propelling particles using uniform external AC electric fields is by breaking the symmetry of the medium rather than the particle, as demonstrated by Lavrentovich *et al*., based on the asymmetric distortions of liquid-crystal orientation around the particle.[71] Unlike electrophoresis in an isotropic medium, where the particle needs to be charged or asymmetric, liquid-crystal based electrophoresis can be applied to symmetric and uncharged particles. Lavrentovich et al. showed that particle motion along curvilinear tracks could be attained, in addition to motion parallel, anti-parallel and perpendicular to the electric field.

Velev group also came up with a novel technique to self-propel microcircuit elements such as semiconductor diodes, due to localized electroosmosis resulting from the rectification of the uniform external AC field by the diode,[72] without inducing bulk fluid flows generally prevalent during DC field application (Fig. 1.6b). Similar to eqn 1.4, diode propulsion velocity, u_d, can be estimated using Helmholtz-Smoluchowski equation as

$$u_d = \beta \frac{\varepsilon \varepsilon_0 \zeta}{2\mu} \left(E_{ext} - E_{d0} \right) \tag{1.5}$$

where ε and ε_0 are the dielectric permittivity of the media and vacuum, respectively, ζ is the potential in the plane of hydrodynamic shear, μ is the medium viscosity, β is the coefficient of hydrodynamic resistance, E_{ext} is the applied external field (based on peak-to-peak voltage) and E_{d0} is the intrinsic field across the diode. Based on the principle reported by Velev group

using millimeter-sized diodes, Calvo-Marzal *et al.* have propelled semiconductor diode nanowires synthesized by membrane template growth route,[73] which demonstrates that this technique is effective even at miniaturized scales. Similar to the self-electrophoretically driven motors, electroosmotically driven diodes need low ionic strength media for propulsion. Loget and Kuhn have recently reported electric field driven "propulsion" of conducting objects based on the principle of bipolar self-regeneration, where metal deposition takes place on one end of the particle and dissolution at the other, causing apparent motion of the object.[74] The same team has also applied the principle of bipolar electrochemistry to induce site-selective bubble generation due to water-splitting on metallic particles, leading to their self-propulsion.[75] Interestingly, the principle of bipolar electrochemistry driven water-splitting has also been used by Gao *et al.* to propel Al-Ga/Ti micromotors, without applying electric fields.[76] Other external fields used for powering the self-propulsion of particles in liquids include magnetic fields[77-81] (Fig. 1.6c & d) and ultrasound[82,83] (or acoustic waves), both of which are believed to be promising candidates for biomedical related applications as discussed in Section 1.4.

Significant efforts have also been directed towards interfacing biological motor proteins and intact cells with synthetic components to create a hybrid self-propelling system.[6,7,84-87] One of the main concerns associated with such systems is the differing compatibilities of the biological and synthetic components with the propulsion media, which makes finding/creating a mutually compatible media very difficult. Biological motors have evolved to function under physiological conditions, which demands high ionic strength media. Such media are unfavorable for the overall operation of the hybrid devices as decrease in the electrical double layer thickness at high ionic strength leads to aggregation of the devices.[14]

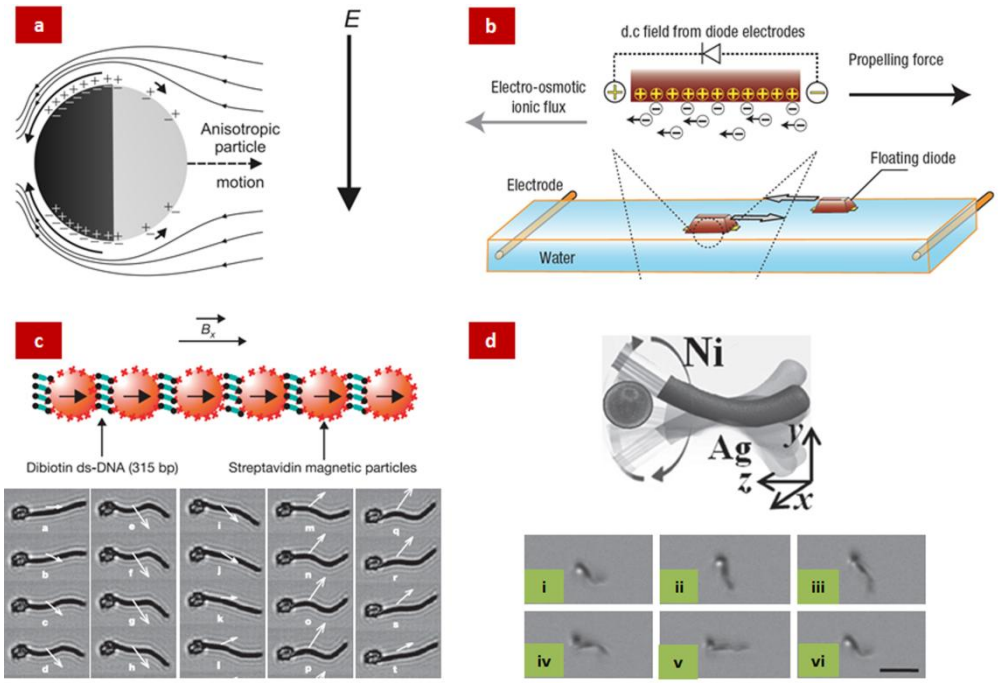

Figure 1.6 Examples of autonomously propelling particles powered by external electric or magnetic fields. (a) Schematic illustrating the principle of induced charge electrophoresis driven propulsion of metallodielectric Janus particles on application of uniform AC fields.[70] (b) Diodes, floating over the water surface due to capillarity, propel due to electroosmotic ionic flux near their surface, driven by the external uniform AC field rectified across the diode.[72] (c) Streptavidin-coated magnetic particles are bound into flexible filaments under external magnetic fields by biotinylated double-stranded DNA due to streptavidin-biotin interactions.[78] The beating pattern of motion of such a filament (24 μm long), attached to a red blood cell, driven by magnetic fields has been illustrated in the time-lapse images taken at 5 ms intervals.[78] (d) Time-lapse images (taken at 20 ms intervals) showing transportation of a 1 μm drug-loaded magnetic pol(d,l-lactic-*co*–glycolic acid) (PLGA) particle using a flexible Ni-Ag magnetic nanowire motor.[81]

1.4 Potential Applications of Self-Propelling Particles

Possible applications envisioned for self-propelling particles are as interdisciplinary as the techniques employed to design and develop such particles.[88] Emergent or collective behavior and self-assembly of autonomously moving particles is a cutting edge and rapidly growing research area, as understanding the interactions among self-propelling particles as well as their interactions with external stimuli may provide some insight into the dynamics of similar

phenomena observed in nature (such as swarming of bacteria, schooling of fish) and in turn may lead to the development of "intelligent" functional systems.[40] To this end, the team from Penn State has studied schooling behavior of light-driven AgCl motors due to diffusiophoresis,[89] and biomimetic response of synthetic motors to external stimuli such as chemotaxis and phototaxis has been analyzed by them as well as other groups[90-94] (Fig. 1.7a & b).

Self-assembly of catalytic self-propelling particles into dimers and the resulting complex coordinated movement of the aggregates has been studied by multiple groups[40,95-97] (Fig. 1.7c). Recently, Reinmüller *et al.* demonstrated cooperative self-propulsion, at low Reynolds number, of an emergent self-assembly of individually inactive particles.[98] Also, Palacci *et al.* recently reported "living crystals", comprising of self-propelling colloidal particles, that can constantly form, disassemble and re-form elsewhere.[99] As dynamic models for the origin of life, self-propelled oil droplets have also garnered much attention recently and research efforts are directed towards propulsion of oil droplets on water surface by Marangoni effect.[100-104]

Practical applications, such as efficient cargo transportation, using self-propelling particles demand high propulsion speed and control over the direction of motion.[105-108] A review article, by Wang and Manesh,[109] nicely summarizes the techniques that are based on external stimuli (such as magnetic,[44,110-113] thermal, [114,115] chemical,[93] electrochemical,[116] light[117,118]) developed to tune and control the direction and speed of nano/micromotors (catalytically driven in most of the cases). Another review article, from the same team,[105] discusses the various efforts that have been directed towards enhancement of the speed/power of the catalytic nanomotors by rational engineering of the design[45,47,57,112,119-123] of the nanomotors and careful selection of the fuel[44,58,112,122,124-126] for propulsion. Proof-of-concept of pick-up, transportation and delivery of cargo using self-electrophoresis driven nanorods and bubble propulsion driven microtubes has already been demonstrated.[113,126-128] As a next step towards advanced cargo delivery for biomedical applications, Kagan *et al.* reported directed delivery of polymeric and liposomal drug carriers using the self-electrophoretic nanomotors.[129] With continuing efforts from Wang's team and other groups,

selective capture (and subsequent transportation) of a range of cells and biomolecules (such as circulating tumor cells, bacteria, nucleic acids, proteins) from unprocessed complex media has been realized using biologically functionalized catalytic nanomotors (Fig. 1.8).[130-137]

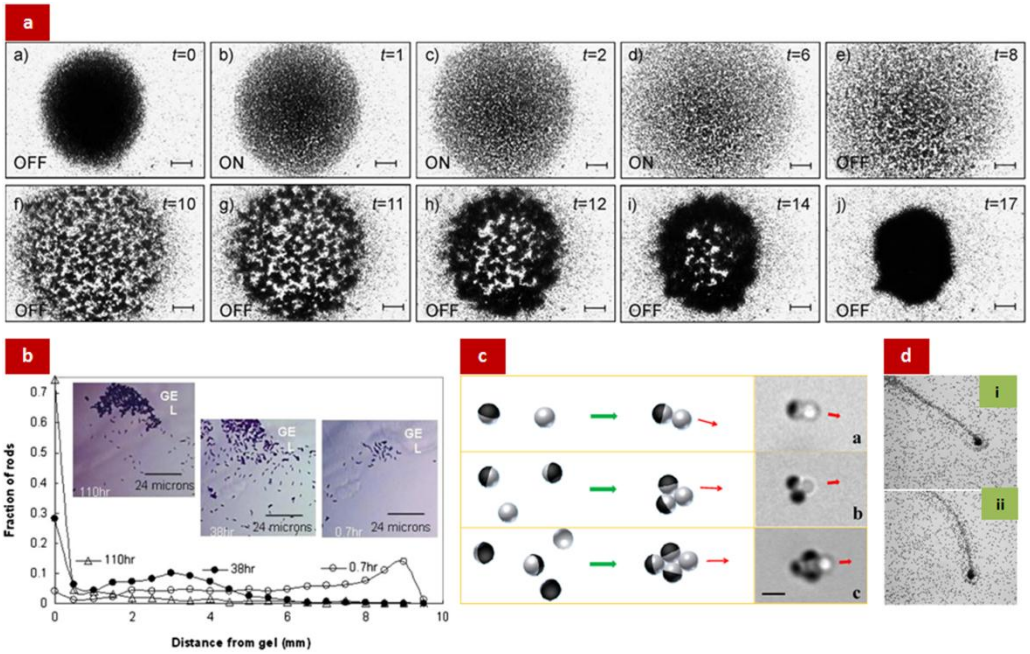

Figure 1.7 Examples of collective behavior exhibited by autonomously propelling particles. (a) Time-lapse images showing the effect of UV illumination on the schooling behavior of micron-sized AgCl particles. Interparticle spacing between AgCl particles, initially exposed to UV light, increases when UV source is turned off. Re-illuminating the particles with UV light causes them to school again. Each AgCl particle secretes ions as it moves under UV illumination, which triggers schooling of other AgCl particles into regions with higher particle concentration.[89] (b) Plot and time-lapse snapshots illustrating the chemotaxis of 2 μm long Pt-Au nanomotors towards a gel soaked in 30% H_2O_2, due to "active diffusion" caused by a combination of self-electrophoretic translation and Brownian rotation.[93] (c) Schematics and microscopic images showing assemblies of Janus motor and nonmotor particles into doublet, triplet and quadruplet assemblies, induced by hydrophobic surface interactions.[97] (d) A self-propelling complex of colloidal particles accumulated at a HCl-releasing cation-exchange raisin particle at two different times represented by micrographs (i) and (ii), where both the raisin and colloidal particles are phoretically inactive.[98] The diffusioosmotic solvent flows induced by the raisin particle confine the colloidal particles into the convection cells, resulting in propulsion of the self-assembled complex.

Proof-of-principle studies of applying self-propelling particles for biosensing have been reported as well.[136,138] These impressive results, attained over a short time span, strongly suggest that with further research efforts self-propelling particles may be applied for performing complex functions such as targeted drug or vaccine delivery, medical diagnostics and minimally invasive surgeries; thereby, revolutionizing the diagnosis and treatment of several diseases.[139-141] However, these catalytic nanomotors need H_2O_2 medium for propulsion, which poses a serious challenge to potential *in vivo* applications of such particles. Nanowires actuated by external magnetic fields appear to be a viable alternative as they do not require a "fuel" for propulsion, and cargo transportation abilities of such particles are being actively explored.[79-81] Other promising candidates for biomedical type applications are believed to be the recently developed ultrasound driven motors (since ultrasound is safe and is already extensively used in the field of medicine)[82,83,139] and bubble-propelled Al-Ga/Ti micromotors based on the water-splitting reaction.[76]

Some other areas where applicability of self-propelling particles has been explored include pumping and mixing of fluids in lab-on-chip devices by immobilizing such particles on the walls of the microfluidic channels (Fig. 1.9a),[58,142-145] motion-based chemical sensing by tracking changes in the speed of the particles in the presence of target analyte,[124,136] "writing" of surface microstructures achieved by localized deposition of material through magnetically-guided self-propulsion of particles,[146,147] nanotool-based drilling of biological cells by corkscrew-like movement of asymmetrically rolled-up catalytic nanotubes (Fig. 1.9b),[148] environmental remediation by selective capture of oil drops in water by superhydrophobized catalytic motors (Fig. 1.9c),[149] and in the area of microrobotics for performing minimally invasive procedures in medicine and surgeries[141,150].

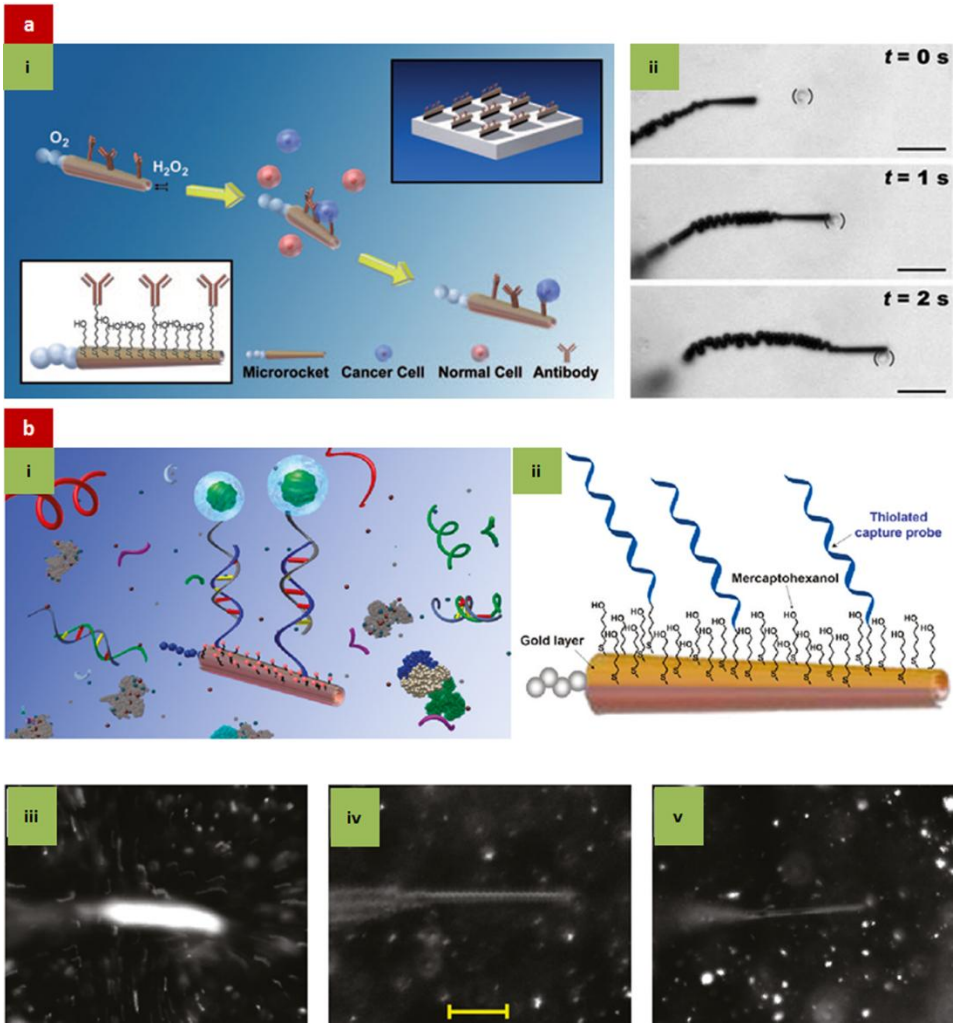

Figure 1.8 Proof-of-principle examples of applying autonomously propelling particles for selective isolation of cells and biomolecules from unprocessed media. (a) Cartoon (i) and time-lapse snapshots (ii) showing selective pick-up and transportation of cancer cell, out of a mixture of cells, using bubble propelled microtube rockets functionalized with antibodies (scale bar = 60 μm).[130] (b) Cartoon depicting the selective isolation of target nucleic acid from a raw biological sample using biologically modified microrockets (i), and surface chemistry involved in functionalization of the surface of the microtubes (ii). The selectivity of such functionalized microtubes is evident by comparing snapshot (iii) with snapshots (iv) and (v) – the capture of fluorescently tagged target DNA molecules is evident in (iii); whereas, mismatched and complementary DNA sequences are not captured by the microrocket as evident in (iv) and (v).[134]

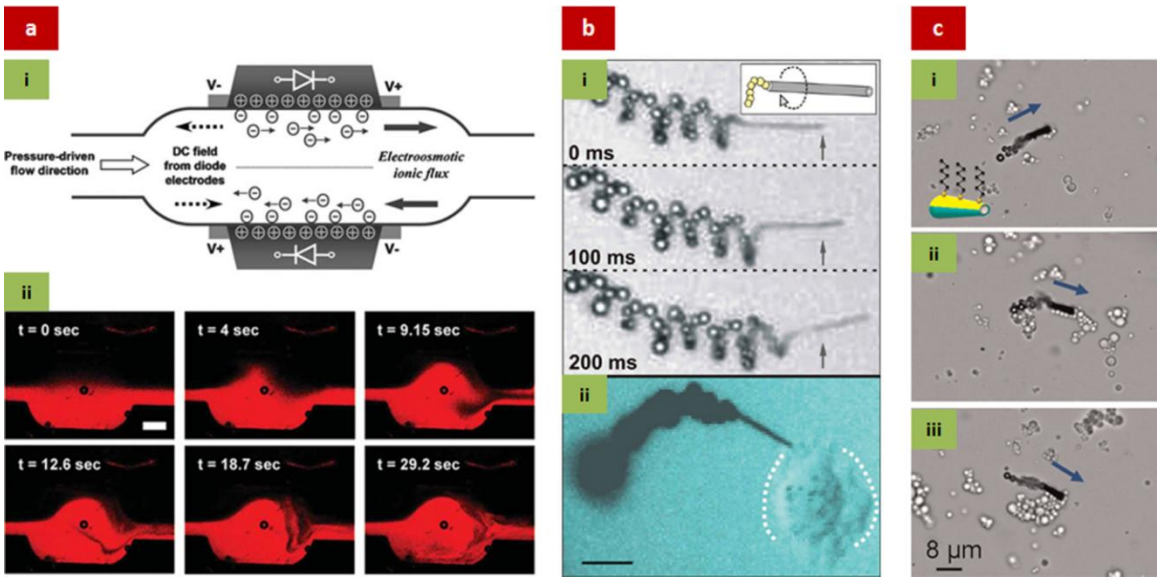

Figure 1.9 Examples of potential applications of self-propelling particles. (a) Diodes self-propel on water surface when freely suspended, but also can be applied for pumping/mixing fluids in microfluidic channels when immobilized on the channel walls. Mixing of fluid in a microfluidic channel by two oppositely oriented diodes has been illustrated in the schematic in (i) and the time-lapse images in (ii).[144] (b) Asymmetrically rolled-up catalytic nanotubes self-propel in H_2O_2 solution in a corkscrew-like trajectory as illustrated in the time-lapse images in (i), and can be applied as a "nanotool" for drilling into biological cells as depicted in (ii), scale bar = 10 μm.[148] (c) Alkanethiol-coated superhydrophobized catalytic nano/microscale motors ("microsubmarines") can pick-up oil drops while propelling in an oil-water emulsion with added H_2O_2 fuel, as shown in the time-lapse images (i), (ii) and (iii) at navigation times of 11, 53 and 70 s.[149]

1.5 Layout of this Dissertation

My graduate research was focused on exploring novel mechanisms for powering the self-propulsion of millimeter-sized particles in liquids. We developed three classes of self-propelling particles capable of harnessing chemical energy, electrical energy and metabolic action of live cells for propulsion at low Reynolds number. Chapter 2 presents the principles and results of hydrogel-based self-propelling particles that exhibit a unique pulsating motion in water over long periods of time. We proposed and verified their propulsion mechanism (based on the generation of a self-sustained cycle of surface tension gradient driven flows), and characterized and modeled the pulse interval and the distance propelled by these

particles. On the basis of the quantification of this mass-transfer driven motion, we constructed floaters of various designs programmed to move in stunningly regular sequence of translational and rotational steps, performing various "dances" and following complex trajectories. In Chapter 3, we have applied these hydrogel-based self-propelling particles for simultaneously breaking up and collecting the oil films floating on water. We found that the efficiency of oil collection by mobile absorbents was significantly higher compared to stationary ones, and believe that the same approach can be applied to intensify other mass-transfer processes involving fluid-particle systems as well.

The work presented in Chapter 4 describes biogenic or biocatalytic self-propelling particles that use yeast cells (immobilized in hydrogel or polyelectrolyte matrix) as catalyst to power their propulsion in glucose and hydrogen peroxide (H_2O_2) solution. We found that the motion of the yeast boat in H_2O_2 solution was very vigorous relative to its sluggish motion in glucose solution. We correlated the particle velocity in H_2O_2 solution to the phenomenon of bubble bursting and obtained reasonable agreement between the two. In Chapter 5, we introduce a novel technique of steering the diode-based self-propelling particles on water. The diodes, remotely powered by an external uniform AC electric field, were shuttled back and forth on water by modifying the wave symmetry of the applied AC field. We proposed and analyzed the electrokinetic mechanism behind diode rotation (based on the preference of the diode to remain forward-biased with respect to the field). We believe that this new principles of steering and controlling the direction of diode motion could find important applications in MEMs and microrobotics. Chapter 6 summarizes my graduate research and provides the outlook for extending this work.

1.6 References

1. Berg, H. C. and Anderson, R. A. Bacteria swim by rotating their flagellar filaments. *Nature* **245,** 380-382 (1973).

2. Blair, D. F. and Berg, H. C. Restoration of torque in defective flagellar motors. *Science* **242,** 1678-1681 (1988).

3. Lauga, E., Goldstein, R. E. Dance of the microswimmers. *Phys. Today* **65,** 30-35 (2012).

4. Carlier, M.-F. *et al*. Actin Depolymerizing Factor (ADF/Cofilin) Enhances the Rate of Filament Turnover: Implication in Actin-Based Motility. *J. Cell Biol.* **136,** 1307-1322 (1997).

5. Cameron, L. A., Giardini, P. A., Soo, F. S., Theriot, J. A. Secrets of actin-based motility revealed by a bacterial pathogen. *Nat. Rev. Mol. Cell. Biol.* **1,** 110-119 (2000).

6. Hess, H., Bachand, G. D., Vogel, V. Powering Nanodevices with Biomolecular Motors. *Chem. Eur. J.* **10,** 2110-2116 (2004).

7. Goel, A., Vogel, V. Harnessing biological motors to engineer systems for nanoscale transport and assembly. *Nat. Nanotechnol.* **3,** 465-475 (2008).

8. Purcell, E. M. Life at Low Reynolds-Number. *Am. J. Phys.* **45,** 3-11 (1977).

9. Kay, E. R., Leigh, D. A., Zerbetto, F. Synthetic Molecular Motors and Mechanical Machines. *Angew. Chem. Int. Edit.* **46,** 72-191 (2007).

10. Mallouk, T. E., Sen, A. Powering Nanorobots. *Sci. Am.* **300,** 72-77 (2009).

11. Wang, J. Can Man-Made Nanomachines Compete with Nature Biomotors? *ACS Nano* **3,** 4-9 (2009).

12. Mirkovic, T., Zacharia, N. S., Scholes, G. D., Ozin, G. A. Fuel for Thought: Chemically Powered Nanomotors Out-Swim Nature's Flagellated Bacteria. *ACS Nano* **4,** 1782-1789 (2010).

13. Ebbens, S. J., Howse, J. R. In pursuit of propulsion at the nanoscale. *Soft Matter* **6,** 726-738 (2010).

14. Sengupta, S., Ibele, M. E., Sen, A. Fantastic Voyage: Designing Self-Powered Nanorobots. *Angew. Chem. Int. Ed.* **51,** 8434-8445 (2012).

15. Browne, W. R., Feringa, B. L. Making molecular machines work. *Nat. Nanotechnol.* **1,** 25-35 (2006).

16. Scriven, L. E., Sternling, C. V. The Marangoni Effects. *Nature* **187,** 186-188 (1960).

17. Suciu, D. G., Smigelschi, O., Ruckenstein, E. Spreading of Liquids on Liquids. *J. Colloid Interf. Sci.* **33,** 520-528 (1970).

18. Bush, J. W. M., Hu, D. L. Walking on Water: Biolocomotion at the Interface. *Annu. Rev. Fluid Mech.* **38,** 339-369 (2006).

19. Nakata, S., Hayashima, Y. Spontaneous dancing of a camphor scraping. *J. Chem. Soc. Faraday Trans.* **94,** 3655-3658 (1998).

20. Nakata, S., Hayashima, Y. Spontaneous motion of a solid is sensitive to the pH of an aqueous phase. *Langmuir* **15,** 1872-1875 (1999).

21. Nakata, S., Kohira, M. I., Hayashima, Y. Mode selection of a camphor boat in a dual-circle canal. *Chem. Phys. Lett.* **322,** 419-423 (2000).

22. Nakata, S., Hayashima, Y., Ishii, T. Self-motion of a camphoric acid boat as a function of pH of aqueous solutions. *Colloids Surf. A* **182,** 231-238 (2001).

23. Hayashima, Y., Nagayama, M., Nakata, S. A camphor grain oscillates while breaking symmetry. *J. Phys. Chem. B* **105,** 5353-5357 (2001).

24. Kohira, M. I., Hayashima, Y., Nagayama, M., Nakata, S. Synchronized self-motion of two camphor boats. *Langmuir* **17,** 7124-7129 (2001).

25. Kitahara, H., Hiromatsu, S., Doi, Y., Nakata, S., Islam, M. R. Self-Motion of a Camphor Disk Coupled with Convection. *Phys. Chem. Chem. Phys.* **6,** 2409−2414 (2004).

26. Nakata, S., Murakami, M. Self-Motion of a Camphor Disk on an Aqueous Phase Depending on the Alkyl Chain Length of Sulfate Surfactants. *Langmuir* **26,** 2414-2417 (2010).

27. Suematsu, N. J. *et al*. Mode-Switching of the Self-Motion of a Camphor Boat Depending on the Diffusion Distance of Camphor Molecules. *J. Phys. Chem. C* **114,** 9876-9882 (2010).

28. Ikura, Y. S., Tenno, R., Kitahata, H., Suematsu, N. J., Nakata, S. Suppression and Regeneration of Camphor-Driven Marangoni Flow with the Addition of Sodium Dodecyl Sulfate. *J. Phys. Chem. B* **116,** 992−996 (2012).

29. Nakata, S. *et al*. Reciprocating Motion of a Self-Propelled Object on a Molecular Layer with a Local Minimum and a Local Maximum Isotherm. *J. Phys. Chem. C* **117,** 6346-6352 (2013).

30. Acree, W. E. Empirical expression for predicting surface tension of liquid mixtures. *J. Colloid Interf. Sci.* **101,** 575-576 (1984).

31. Gong, J. P., Matsumoto, S., Uchida, M., Isogai, N., Osada, Y. Motion of polymer gels by spreading organic fluid on water. *J. Phys. Chem.* **100,** 11092-11097 (1996).

32. Mitsumata, T., Ikeda, K., Gong, J. P., Osada, Y. Solvent-driven chemical motor. *Appl. Phys. Lett.* **73,** 2366-2368 (1998).

33. Bassik, N., Abebe, B. T., Gracias, D. H. Solvent Driven Motion of Lithographically Fabricated Gels. *Langmuir* **24,** 12158-12163 (2008).

34. Mitsumata, T., Ikeda, K., Gong, J. P., Osada, Y. Controlled motion of solvent-driven gel motor and its application as a generator. *Langmuir* **16,** 307-312 (2000).

35. Sharma, R., Chang, S.-T., Velev, O. D. Gel-based self-propelling particles get programmed to dance. *Langmuir* **28,** 10128-10135 (2012).

36. Luo, C., Li, H., Liu, X. C. Propulsion of microboats using isopropyl alcohol as a propellant. *J. Micromech. Microeng.* **18,** 067002 (2008).

37. Xiao, M., Cheng, M., Zhang, Y., Shi, F. Combining the Marangoni Effect and the pH-Responsive Superhydrophobicity–Superhydrophilicity Transition to Biomimic the Locomotion Process of the Beetles of Genus *Stenus*. *Small* **9,** 2509-2514 (2013).

38. Okawa, D., Pastine, S. J., Zettl, A., Frechet, J. M. J. Surface Tension Mediated Conversion of Light to Work. *J. Am. Chem. Soc.* **131,** 5396-5398 (2009).

39. Zhao, G., Pumera, M. Liquid−Liquid Interface Motion of a Capsule Motor Powered by the Interlayer Marangoni Effect. *J. Phys. Chem. B* **116,** 10960-10963 (2012).

40. Ismagilov, R. F., Schwartz, A., Bowden, N., Whitesides, G. M. Autonomous movement and self-assembly. *Angew. Chem. Int. Edit.* **41,** 652-654 (2002).

41. Vicario, J. *et al*. Catalytic molecular motors: fuelling autonomous movement by a surface bound synthetic manganese catalase. *Chem. Commun.* 3936-3938 (2005).

42. Gibbs, J. G., Zhao, Y. P. Autonomously motile catalytic nanomotors by bubble propulsion. *Appl. Phys. Lett.* **94,** 163104 (2009).

43. Dey, K. K., Senapati, K. K., Phukan, P., Basu, S., Chattopadhyay, A. Stable Magnetic Chemical Locomotive with Pd Nanoparticle Incorporated Ferromagnetic Oxide. *J. Phys. Chem. C* **115,** 12708–12715 (2011).

44. Mei, Y. F. *et al*. Versatile Approach for Integrative and Functionalized Tubes by Strain Engineering of Nanomembranes on Polymers. *Adv. Mater.* **20,** 4085-4090 (2008).

45. Manesh, K. M. *et al*. Template-Assisted Fabrication of Salt-Independent Catalytic Tubular Microengines. *ACS Nano* **4,** 1799-1804 (2010).

46. Mei, Y. F., Solovev, A. A., Sanchez, S., Schmidt, O. G. Rolled-up nanotech on polymers: from basic perception to self-propelled catalytic microengines. *Chem. Soc. Rev.* **40,** 2109-2119 (2011).

47. Sanchez, S., Solovev, A. A., Mei, Y., Schmidt, O. G. Dynamics of Biocatalytic Microengines Mediated by Variable Friction Control. *J. Am. Chem. Soc.* **132,** 13144–13145 (2010).

48. Sanchez, S. *et al*. The Smallest Man-Made Jet Engine. *Chem. Rec.* **11,** 367–370 (2011).

49. Wilson, D. A., Nolte, R. J. M., van Hest, J. C. M. Autonomous movement of platinum-loaded stomatocytes. *Nat. Chem.* **4,** 268–274 (2012).

50. Pantarotto, D., Browne, W. R., Feringa, B. L. Autonomous propulsion of carbon nanotubes powered by a multienzyme ensemble. *Chem. Commun.* 1533-1535 (2008).

51. Zhao, G., Wang, H., Khezri, B., Webster, R.D., Pumera, M. Influence of real-world environments on the motion of catalytic bubble-propelled micromotors. *Lab Chip* **13,** 2937–2941 (2013).

52. Zhao, G., Viehrig, M., Pumera, M. Challenges of the movement of catalytic micromotors in blood. *Lab Chip* **13,** 1930–1936 (2013).

53. Zhao, G., Sanchez, S., Schmidt, O. G., Pumera, M. Poisoning of bubble propelled catalytic micromotors: the chemical environment matters. *Nanoscale* **5,** 2909–2914 (2013).

54. Fournier-Bidoz, S., Arsenault, A. C., Manners, I., Ozin, G. A. Synthetic self-propelled nanorotors. *Chem. Commun.* 441-443 (2005).

55. Ozin, G. A., Manners, I., Fournier-Bidoz, S., Arsenault, A. Dream Nanomachines. *Adv. Mater.* **17,** 3011-3018 (2005).

56. Paxton, W. F. *et al*. Catalytic Nanomotors: Autonomous Movement of Striped Nanorods. *J. Am. Chem. Soc.* **126,** 13424–13431 (2004).

57. Wang, Y. *et al*. Bipolar electrochemical mechanism for the propulsion of catalytic nanomotors in hydrogen peroxide solutions. *Langmuir* **22,** 10451-10456 (2006).

58. Paxton, W. F. *et al*. Catalytically induced electrokinetics for motors and micropumps. *J. Am. Chem. Soc.* **128,** 14881–14888 (2006).

59. Kocherginsky, N. Acidic lipids, H^+-ATPases, and mechanism of oxidative phosphorylation. Physico-chemical ideas 30 years after P. Mitchell's Nobel Prize award. *Prog. Biophys. Mol. Biol.* **99,** 20-41 (2009).

60. Mano, N., Heller, A. Bioelectrochemical propulsion. *J. Am. Chem. Soc.* **127,** 11574-11575 (2005).

61. Pumera, M. Electrochemically powered self-propelled electrophoretic nanosubmarines. *Nanoscale* **2,** 1643-1649 (2010).

62. Mirkovic, T., Zacharia, N. S., Scholes, G. D., Ozin, G. A. Nanolocomotion – Catalytic Nanomotors and Nanorotors. *Small* **6,** 159-167 (2010).

63. Paxton, W. F., Sundararajan, S., Mallouk, T. E., Sen, A. Chemical Locomotion. *Angew. Chem. Int. Edit.* **45,** 5420–5429 (2006).

64. Golestanian, R., Liverpool, T. B., Ajdari, A. Propulsion of a molecular machine by asymmetric distribution of reaction products. *Phys. Rev. Lett.* **94,** 220801 (2005).

65. Golestanian, R., Liverpool, T. B., Ajdari, A. Designing phoretic micro- and nano-swimmers. *New J. Phys.* **9,** 126 (2007).

66. Ruckner, G., Kapral, R. Chemically Powered Nanodimers. *Phys. Rev. Lett.* **98,** 150603 (2007).

67. Córdova-Figueroa, U. M., Brady, J. F., Shklyaev, S. Osmotic propulsion of colloidal particles *via* constant surface flux. *Soft Matter* **9,** 6382-6390 (2013).

68. Pavlick, R. A., Sengupta, S., McFadden, T., Zhang, H., Sen, A. Polymerization-Powered Motor. *Angew. Chem. Int. Edit.* **50,** 9374–9377 (2011).

69. Howse, J. R. *et al*. Self-Motile Colloidal Particles: From Directed Propulsion to Random Walk. *Phys. Rev. Lett.* **99,** 048102 (2005).

70. Gangwal, S., Cayre, O. J., Bazant, M. Z., Velev, O. D. Induced-Charge Electrophoresis of Metallodielectric Particles. *Phys. Rev. Lett.* **100,** 058302 (2008).

71. Lavrentovich, O. D., Lazo, I., Pishnyak, O. P. Nonlinear electrophoresis of dielectric and metal spheres in a nematic liquid crystal. *Nature.* **467,** 947-950 (2010).

72. Chang, S. T., Paunov, V. N., Petsev, D. N., Velev, O. D. Remotely powered self-propelling particles and micropumps based on miniature diodes. *Nat. Mater.* **6,** 235-240 (2007).

73. Calvo-Marzal, P. *et al*. Propulsion of nanowire diodes. *Chem. Commun.* **46,** 1623-1624 (2010).

74. Loget, G., Kuhn, A. Propulsion of Microobjects by Dynamic Bipolar Self-Regeneration. *J. Am. Chem. Soc.* **132,** 15918–15919 (2010).

75. Loget, G., Kuhn, A. Electric field-induced chemical locomotion of conducting objects. *Nat. Commun.* **2,** 535 (2011).

76. Gao, W., Pei, A., Wang, J. Water-Driven Micromotors. *ACS Nano* **6,** 8432-8438 (2012).

77. Ghosh, A., Fischer, P. Controlled propulsion of artificial magnetic nanostructured propellers. *Nano Lett.* **9,** 2243–2245 (2009).

78. Dreyfus, R. *et al*. Microscopic artificial swimmers. *Nature* **437,** 862-865 (2005).

79. Petit, T., Zhang, L., Peyer, K. E., Kratochvil, B. E., Nelson, B. J. Selective Trapping and Manipulation of Microscale Objects Using Mobile Microvortices. *Nano Lett.* **12,** 156–160 (2012).

80. Zhang, L., Petit, T., Peyer, K. E., Nelson, B. J. Targeted Cargo Delivery Using a Rotating Nickel Nanowire. *Nanomed.-Nanotechnol.* **8,** 1074–1080 (2012).

81. Gao, W. *et al*. Cargo-Towing Fuel-Free Magnetic Nano-swimmers for Targeted Drug Delivery. *Small* **8,** 460–467 (2012).

82. Wang, W., Castro, L. A., Hoyos, M., Mallouk, T. E. Autonomous Motion of Metallic Microrods Propelled by Ultrasound. *ACS Nano* **6,** 6122-6132 (2012).

83. Kagan, D. *et al*. Acoustic Droplet Vaporization and Propulsion of Perfluorocarbon-Loaded Microbullets for Targeted Tissue Penetration and Deformation. *Angew. Chem. Int. Edit.* **51,** 7519–7522 (2012).

84. Kim, J. *et al*. Establishment of a fabrication method for a long-term actuated hybrid cell robot. *Lab Chip* **7,** 1504-1508 (2007).

85. Behkam, B., Sitti, M. Bacterial flagella-based propulsion and on/off motion control of microscale objects. *Appl. Phys. Lett.* **90,** 023902 (2007).

86. Soong, R. K. *et al*. Powering an inorganic nanodevice with a biomolecular motor. *Science* **290,** 1555-1558 (2000).

87. Brunner, C., Wahnes, C., Vogel, V. Cargo pick-up from engineered loading stations by kinesin driven molecular shuttles. *Lab Chip* **7,** 1263-1271 (2007).

88. Feynman, R. P. There's Plenty of Room at the Bottom. *Eng. Sci.* **23,** 22–36 (1960).

89. Ibele, M., Mallouk, T. E., Sen, A. Schooling Behavior of Light-Powered Autonomous Micromotors in Water. *Angew. Chem. Int. Edit.* **481,** 3308–3312 (2009).

90. Chaturvedi, N., Hong, Y., Sen, A., Velegol, D. Magnetic Enhancement of Phototaxing Catalytic Motors. *Langmuir* **26,** 6308-6313 (2010).

91. Hong, Y., Velegol, D., Chaturvedi, N., Sen, A. Biomimetic behavior of synthetic particles: from microscopic randomness to macroscopic control. *Phys. Chem. Chem. Phys.* **12,** 1423-1435 (2010).

92. Sen, A., Ibele, M., Hong, Y., Velegol, D. Chemo and phototactic nano/microbots. *Faraday Discuss. Phys.* **143,** 15-27 (2009).

93. Hong, Y., Blackman, N. M. K., Kopp, N. D., Sen, A., Velegol, D. Chemotaxis of nonbiological colloidal rods. *Phys. Rev. Lett.* **99,** 178103 (2007).

94. Baraban, L., Harazim, S. M., Sanchez, S., Schmidt, O. G. Chemotactic Behavior of Catalytic Motors in Microfluidic Channels. *Angew. Chem. Int. Edit.* **52,** 5552–5556 (2013).

95. Ebbens, S., Jones, R. A. L., Ryan, A. J., Golestanian, R., Howse, J. R. Self-assembled autonomous runners and tumblers. *Phys. Rev. E* **82,** 015304 (2010).

96. Baraban, L. *et al*. Transport of cargo by catalytic Janus micro-motors. *Soft Matter* **8,** 48-52 (2012).

97. Gao, W., Pei, A., Feng, X., Hennessy, C., Wang, J. Organized Self-Assembly of Janus Micromotors with Hydrophobic Hemispheres. *J. Am. Chem. Soc.* **135,** 998–1001 (2013).

98. Reinmüller, A., Schöpe, H. J., Palberg, T. Self-Organized Cooperative Swimming at Low Reynolds Numbers. *Langmuir* **29,** 1738-1742 (2013).

99. Palacci, J., Sacanna, S., Steinberg, A. P., Pine, D. J., Chaikin, P. M. Living Crystals of Light-Activated Colloidal Surfers. *Science* **339,** 936-940 (2013).

100. Hanczyz, M. M. *et al*. Fatty Acid Chemistry at the Oil-Water Interface: Self-Propelled Oil Droplets. *J. Am. Chem. Soc.* **129,** 9386-9391 (2007).

101. Banno, T., Kuroha, R., Toyota, T. pH-Sensitive Self-Propelled Motion of Oil Droplets in the Presence of Cationic Surfactants Containing Hydrolyzable Ester Linkages. *Langmuir* **28,** 1190-1195 (2012).

102. Nagai, K., Sumino, Y., Kitahata, H., Yoshikawa, K. Mode selection in the spontaneous motion of an alcohol droplet. *Phys. Rev. E* **71,** 065301 (2005).

103. Bekki, S., Vignes-Adler, M., Nakache, E., Adler, P. M. Solutal Marangoni effect: I. Pure interfacial transfer. *J. Colloid Interface Sci.* **140,** 492-506 (1990).

104. Bekki, S., Vignes-Adler, M., Nakache, E. Solutal Marangoni effect: II. Dissolution. *J. Colloid Interface Sci.* **152,** 314-324 (1992).

105. Gao, W., Sattayasamitsathit, S., Wang, J. Catalytically Propelled Micro-/Nanomotors: How Fast Can They Move?. *Chem. Rec.* **12,** 224–231 (2012).

106. Wang, J. Cargo-towing synthetic nanomachines: Towards active transport in microchip devices. *Lab Chip* **12,** 1944–1950 (2012).

107. Ebbens, S. J., Buxton, G. A., Alexeev, A., Sadeghia, A., Howse, J. R. Synthetic running and tumbling: an autonomous navigation strategy for catalytic nanoswimmers. *Soft Matter* **8,** 3077-3082 (2012).

108. Masoud, H., Bingham, B. I., Alexeev, A. Designing maneuverable micro-swimmers actuated by responsive gel. *Soft Matter* **8,** 8944-8951 (2012).

109. Wang, J., Manesh, K. M. Motion Control at the Nanoscale. *Small* **6,** 338–345 (2010).

110. Kline, T. R., Paxton, W. F., Mallouk, T. E., Sen, A. Catalytic nanomotors: Remote-controlled autonomous movement of striped metallic nanorods. *Angew. Chem. Int. Edit.* **44,** 744–746 (2005).

111. Solovev, A. A., Mei, Y., Urena, E. B., Huang, G., Schmidt, O. G. Catalytic Microtubular Jet Engines Self-Propelled by Accumulated Gas Bubbles. *Small* **5,** 1688–1692 (2009).

112. Laocharoensuk, R., Burdick, J., Wang, J. Carbon-nanotuble-induced acceleration of catalytic nanomotors. *ACS Nano* **2,** 1069-1075 (2008).

113. Burdick, J., Laocharoensuk, R., Wheat, P. M., Posner, J. D., Wang, J. Synthetic nanomotors in microchannel networks: Directional microchip motion and controlled manipulation of cargo. *J. Am. Chem. Soc.* **130,** 8164–8165 (2008).

114. Balasubramanian, S. *et al*. Thermal Modulation of Nanomotor Movement. *Small* **5,** 1569–1574 (2009).

115. Sanchez, S., Ananth, A. N., Fomin, V. N., Viehrig, M., Schmidt, O. G. Superfast Motion of Catalytic Microjet Engines at Physiological Temperature. *J. Am. Chem. Soc.* **133,** 14860–14863 (2011).

116. Calvo-Marzal, P. *et al*. Electrochemically-triggered motion of catalytic nanomotors. *Chem. Commun.* 45094–4511 (2009).

117. Hess, H., Clemmens, J., Qin, D., Howard, J., Vogel, V. Light-controlled molecular shuttles made from motor proteins carrying cargo on engineered surfaces. *Nano. Lett.* **1,** 235-239 (2001).

118. Solovev, A. A., Smith, E. J., Bof' Bufon, C. C., Sanchez, S., Schmidt, O. G. Light-Controlled Propulsion of Catalytic Microengines. *Angew. Chem. Int. Edit.* **50,** 10875–10878 (2011).

119. Sattayasamitsathit, S., Gao, W., Calvo-Marzal, P., Manesh, K. M., Wang, J. Simplified Cost-Effective Preparation of High-Performance Ag-Pt Nanowire Motors. *ChemPhysChem* **11,** 2802–2805 (2010).

120. Demirok, U. K., Laocharoensuk, R., Manesh, K. M., Wang, J. Ultrafast Catalytic Alloy Nanomotors. *Angew. Chem. Int. Edit.* **47,** 9349–9351 (2008).

121. Zacharia, N. S., Sadeq, Z. S., Ozin, G. A. Enhanced speed of bimetallic nanorod motors by surface roughening. *Chem. Commun.* **39,** 5856–5858 (2009).

122. Gao, W., Sattayasamitsathit, S., Orozo, J., Wang, J. Highly Efficient Catalytic Microengines: Template Electrosynthesis of Polyaniline/Platinum Microtubes. *J. Am. Chem. Soc.* **133,** 11862–11864 (2011).

123. Li, J. X. *et al*. Dynamics of catalytic tubular microjet engines: dependence on geometry and chemical environment. *Nanoscale* **3,** 5083-5089 (2011).

124. Kagan, D. *et al*. Chemical Sensing Based on Catalytic Nanomotors: Motion-Based Detection of Trace Silver. *J. Am. Chem. Soc.* **131,** 12082–12083 (2009).

125. Gao, W., Manesh, K. M., Hua, J., Sattayasamitsathit, S., Wang, J. Hybrid Nanomotor: A Catalytically/Magnetically Powered Adaptive Nanowire Swimmer. *Small* **7,** 2047–2051 (2011).

126. Solovev, A. A., Sanchez, S., Pumera, M., Mei, Y. F., Schmidt, O. G. Magnetic Control of Tubular Catalytic Microbots for the Transport, Assembly, and Delivery of Micro-objects. *Adv. Funct. Mater.* **20,** 2430-2435 (2010).

127. Sundararajan, S., Lammert, P. E., Zudans, A. W., Crespi, V. H., Sen, A. Catalytic motors for transport of colloidal cargo. *Nano Lett.* **8,** 1271–1276 (2008).

128. Sundararajan, S., Sengupta, S., Ibele, M. E., Sen, A. Drop-Off of Colloidal Cargo Transported by Catalytic Pt-Au Nanomotors via Photochemical Stimuli. *Small* **6,** 1479–1482 (2010).

129. Kagan, D. *et al*. Rapid Delivery of Drug Carriers Propelled and Navigated by Catalytic Nanoshuttles. *Small* **6,** 2741–2747 (2010).

130. Balasubramanian, S. *et al*. Micromachine-Enabled Capture and Isolation of Cancer Cells in Complex Media. *Angew. Chem. Int. Edit.* **50,** 4161–4164 (2011).

131. Gao, W., Farokhzad, O. C. Self-Propelled Microrockets to Capture and Isolate Circulating Tumor Cells. *Angew. Chem. Int. Edit.* **50,** 7220–7221 (2011).

132. Orozco, J. *et al*. Dynamic Isolation and Unloading of Target Proteins by Aptamer-Modified Microtransporters. *Anal. Chem.* **83,** 7962–7969 (2011).

133. Sanchez, S., Solovev, A. A., Schulze, S., Schmidt, O. G. Controlled Manipulation of Multiple Cells Using Catalytic Microbots. *Chem. Commun.* **47,** 698–700 (2011).

134. Kagan, D. *et al*. Functionalized Micromachines for Selective and Rapid Isolation of Nucleic Acid Targets from Complex Samples. *Nano Lett.* **11,** 2083–2087 (2011).

135. Campuzano, S. *et al*. Bacterial Isolation by Lectin-Modified Microengines. *Nano Lett.* **12,** 396–401 (2012).

136. Campuzano, S., Kagan, D., Orozco, J., Wang, J. Motion-driven sensing and biosensing using electrochemically propelled nanomotors. *Analyst* **136,** 4621–4630 (2011).

137. Kuralay, F. *et al*. Self-Propelled Carbohydrate-Sensitive Microtransporters with Built-In Boronic Acid Recognition for Isolating Sugars and Cells. *J. Am. Chem. Soc.* **134,** 15217-15220 (2012).

138. Wu, J. *et al*. Motion-based DNA detection using catalytic nanomotors. *Nat. Commun.* **1,** 36 (2010).

139. Wang, J., Gao, W. Nano/Microscale Motors: Biomedical Opportunities and Challenges. *ACS Nano* **6,** 5745-5751 (2012).

140. Patra, D. *et al*. Intelligent, self-powered, drug delivery systems. *Nanoscale* **5,** 1273-1283 (2013).

141. Nelson, B. J., Kaliakatsos, I. K., Abbott, J. J. Microrobots for Minimally Invasive Medicine. *Annu. Rev. Biomed. Eng.* **12,** 55-85 (2010).

142. Hong, Y., Diaz, M., Cordova-Figueroa, U. M., Sen, A. Light-Driven Titanium-Dioxide-Based Reversible Microfireworks and Micromotor/Micropump Systems. *Adv. Funct. Mater*. **20,** 1568-1576 (2010).

143. Solovev, A. A., Sanchez, S., Mei, Y., Schmidt, O. G. Tunable catalytic tubular micro-pumps operating at low concentrations of hydrogen peroxide. *Phys. Chem. Chem. Phys.* **13,** 10131-10135 (2011).

144. Chang, S. T., Beaumont, E., Petsev, D. N., Velev, O. D. Remotely powered distributed microfluidic pumps and mixers based on miniature diodes. *Lab Chip* **8,** 117-124 (2008).

145. Ibele, M. E., Wang, Y., Kline, T. R., Mallouk, T. E., Sen, A. Hydrazine fuels for bimetallic catalytic microfluidic pumping. *J. Am. Chem. Soc.* **129,** 7762-7763 (2007).

146. Manesh, K. M., Balasubramanian, S., Wang, J. Nanomotor-based 'writing' of surface microstructures. *Chem. Commun.* **46,** 5704-5706 (2010).

147. Manesh, K. M. *et al*. Nanomotor-based biocatalytic patterning of helical metal microstructures. *Nanoscale.* **5,** 1310-1314 (2013).

148. Solovev, A. A. *et al*. Self-Propelled Nanotools. *ACS Nano* **6,** 1751-1756 (2012).

149. Guix, M. *et al.* Superhydrophobic Alkanethiol-Coated Microsubmarines for Effective Removal of Oil. *ACS Nano* **6,** 4445-4451 (2012).

150. Fernandes, R., Gracias, D. H. Toward a miniaturized mechanical surgeon. *Mater. Today* **12,** 14-20 (2009).

CHAPTER 2

Gel-Based Self-Propelling Particles Get Programmed to Dance*

* Based on R. Sharma, S.-T. Chang and O. D. Velev, *Langmuir*, 2012, **28**, 10128-10135.

2.1 Introduction

A self-propelling particle moves on its own by converting energy from the environment (e.g., chemical, electrical, thermal) into mechanical motion with respect to the surrounding fluid. Self-propelling particles can be used in a broad spectrum of applications, such as targeted drug and vaccine delivery,[1] lab-on-a-chip devices (as microshuttles,[2-4] pumps or mixers,[5-7] and carriers of biomolecular libraries[1]), sensors for toxicity detection and medical diagnostics,[8,9] robotics,[10,11] and as starting models to mimic and understand the behavior of single and swarming microorganisms (e.g., chemotaxis, phototaxis, phagocytosis).[12-14]

The task of designing a self-propelling particle, a few millimeters or smaller in size, is not straightforward because as size decreases, effects such as Brownian collisions, viscous drag, and surface phenomena (diffusiophoresis, electrophoresis, thermophoresis, etc.) become dominant.[15] Scaling down motors and propellers to the microscale is complicated and they may not be as efficient as the corresponding larger analogues because of the limitations of the above mentioned viscous, thermal, and interfacial microscale effects; therefore, novel techniques of supplying power (or fuel) to such objects are required to facilitate their propulsion.

Several techniques for designing self-propelling particles have been explored.[16,17] These include bubble propulsion by the decomposition of a chemical "fuel" such as hydrogen peroxide,[12,18-20] application of external electric fields to remotely power the electrohydrodynamic motion of a miniature diode,[21,22] electroactive polymer gels,[13,23] self-electrophoresis by coupled redox reactions,[24-26] Marangoni effect by releasing a surface active substance on water,[27-31] diffusiophoresis due to concentration gradient over the particle surface,[32-34] harvesting self-oscillating reactions such as the Belousov-Zhabotinsky one,[35,36] and application of magnetic fields.[37,38] Some groups have also used intact living cells as "beast of burden",[39] or integrated biomolecular motors or enzymes with synthetic components to design a hybrid self-propelling particle.[40,41] Most of these particles show continuous translational motion. The particles that release a certain component stored onboard are only propelled for a short time period.

Here, we report a new class of gel-based self-propelling particles with periodic propulsion modes that may be designed to move in complex, multidirectional, pre-programmed trajectories. The particles are propelled by the Marangoni effect, where the gradient of a surface active compound leads to unbalanced interfacial tension stress and corresponding fluid motion.[42,43] The gel boats generate local concentration gradient and surface tension asymmetry (no external field such as electric or magnetic field is needed), and move autonomously. The most remarkable feature of these particles is that they exhibit a periodic (pulsating) motion for several hours unlike the continuous propulsion displayed by the self-propelling particles based on Marangoni effect reported earlier.[27-31] In the following sections we describe the experimental procedure for designing the gel-based floaters and discuss the reasons behind the pulsating nature of their motion. The pulse interval (time between two consecutive pulses) and the distance propelled in a pulse by these particles are characterized. These experimental data are correlated to scaling relationships for the ethanol release and the resulting interface-driven motion. On the basis of the quantification of the mass-transfer driven motion, we constructed floaters of various designs where the alcohol is released in different directions and at different rates. As a result, we report particles that move in stunningly regular sequence of translational and rotational steps, performing various "dances" and following complex trajectories.

2.2 Experimental Section

2.2.1 Materials

Plastic microbore tubing (Tygon), 0.040" ID × 0.070" OD, forming the particle shell, was purchased from Saint-Gobain (Akron, OH). Monomer acrylamide, cross-linker N,N'-methylenebisacrylamide, and initiator 2,2-dimethoxy-2-phenylacetophenone, for the synthesis of the polyacrylamide hydrogel, were purchased from Sigma (Milwaukee, WI). Sylgard 184 polydimethylsiloxane (PDMS) precursor and curing agent, for the synthesis of the PDMS plug, were purchased from Dow Corning (Midland, MI). Deionized (DI) water (18.2 MΩ.cm at 25 °C), was obtained from a Millipore Milli-Q Academic water purification system (Billerica, MA).

2.2.2 Construction of the Gel Boats

The cores of the gel-based self-propelling particles were cylinders of ethanol-infused polyacrylamide hydrogel contained in plastic tubing (Fig. 2.1). The ethanol-infused hydrogel was prepared by dissolving in ethanol-water solution the monomer acrylamide with the cross-linker N,N'-methylenebisacrylamide and the initiator 2,2-dimethoxy-2-phenylacetophenone in the ratio 1:0.1:0.01 by weight. The solution contained 11wt% of monomer. The percentage of ethanol in the solution determined the final concentration of the ethanol in the hydrogel (for example, mixing equal volumes of ethanol and water resulted in an ethanol concentration of ≈ 50 vol% in the hydrogel). The liquid mixture was injected into the microbore tubing, and cured under a UV lamp (Model B-100A, Black-Ray) for ~ 10 min. After curing, the tubing was trimmed to 5 mm length, and to facilitate asymmetric ethanol release from the particle, a 1 mm long PDMS plug was inserted at one end. This plug was fabricated by filling the PDMS precursor into plastic tubing before curing at 70 ^{o}C. The cured plug was squeezed from the template tubing using tweezers, cut to 1 mm length, and inserted in the gel boat. The assembled boats were then floated on the surface of the water in a plastic Petri dish (~ 14 cm diameter, Corning Life Sciences) by capillary forces, and their motion was recorded with a DSC-V1 Cyber-Shot digital camera (Sony). More complex particles could be constructed by inserting multiple gels plugs in the floaters and cutting and connecting their ends at various angles.

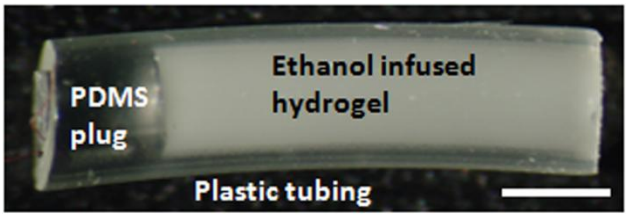

Figure 2.1 Photograph of a basic gel boat. One end of the "particle" is closed with a PDMS plug to block the mass-transfer. Scale bar = 1 mm.

2.3 Results and Discussion

The gel boats propel in a pulsating manner for more than three hours, unlike the continuous translational motion of previous "camphor boat" floaters moving by Marangoni effect. The order of magnitude of the pulse interval of the particles is 10 sec and that of the typical distance moved in each pulse is 1 cm (the precise value of these parameters varies with time, as discussed later). A typical trajectory of such a particle is illustrated in Figure 2.2a. The trajectory is likely related to the intrinsic curvature of the plastic tubing, as can be seen in Figure 2.1, or the asymmetry of the ethanol release profile at the end of the floater (cross-section of the end not being perfectly flat), leading to asymmetric push/pull forces. The corresponding plots of distance travelled in pulses and velocity profile of the gel boat are shown in Figure 2.2b. The intermittent rapid motion is quantified by the increase in the velocity and pulse distance, followed by the particle coming to rest, and this process keeps repeating.

2.3.1 Propulsion Mechanism

The gel-based particles float on the water suspended by the surface tension (when a particle is pushed below the water surface, it sinks to the bottom of the Petri dish as it is more dense than water). The two circular ends of the suspended gel boat are positioned below the air-water interface, as illustrated in Fig. 2.3. The release of ethanol from the hydrogel takes place beneath the water surface. As ethanol is less dense than water, it is carried to the surface by buoyancy. This results in ethanol concentration gradient at the surface, as the amount of ethanol spreading on the surface decreases with increasing distance from the open hydrogel end of the gel-based floater. The generated concentration gradient leads to surface tension asymmetry because the presence of ethanol lowers the surface tension of water.[44] Surface tension gradients result in interfacial flows towards the region with higher surface tension (or lower ethanol concentration), a phenomenon known as Marangoni effect.[27-31] The release of ethanol from only one end of the gel boats gives rise to surface tension gradient across the floaters. In summary, the imbalance of the horizontal component of the surface tension

across the floaters causes unidirectional propulsion of the gel boats away from the region having higher ethanol concentration, as depicted in Fig. 2.3.

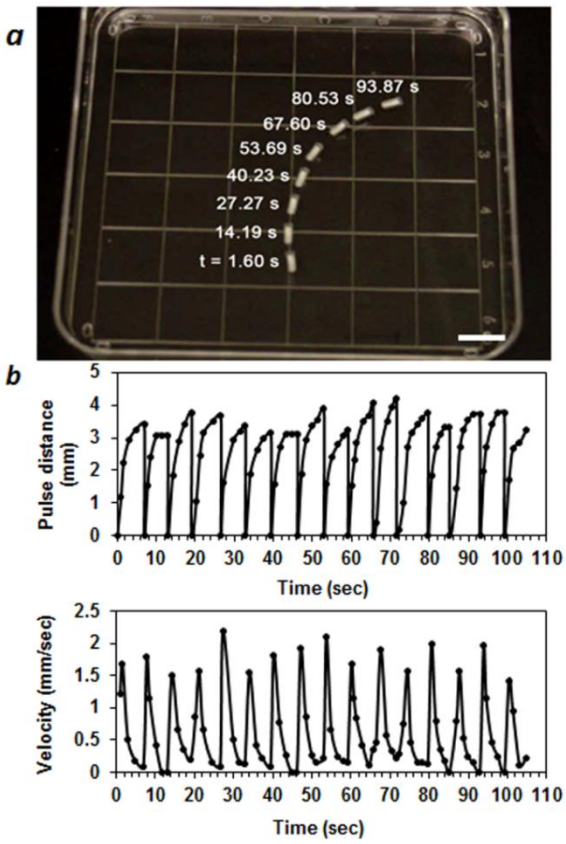

Figure 2.2 (a) Photograph of a typical trajectory of a basic gel-based particle in water (assembled from superimposed images). The curvature in the trajectory is a result of the intrinsic imperfections in the tubing and the hydrogel used to construct these floaters. (b) Plots of distance travelled in individual pulses and velocity profile of the particle versus time, corresponding to (a). These plots quantify the periodicity in the motion of the gel boat and similar data were used in interpreting the role of the mass-transfer effects. Scale bar = 1 cm.

The Marangoni effect alone can not explain the periodic motion, arising because of the disruption of the ethanol supply from the water flows below the surface. The emergence of the flows in the water phase generated by the propulsion of the gel boat seems to be the key to the periodic motion. As the largely submerged particle dragged by the surface tension

gradient begins moving, the flows of the liquid around and behind the moving particle disrupt the ethanol transport to the air-water interface by "swiping" away the ethanol plume released from the hydrogel. The disruption of the ethanol flux to the surface restores the surface tension symmetry across the floaters, and this in turn terminates the particles' propulsion. As the water and the gel boat come to rest, the ethanol transport towards the interface is initiated again at the open end of the particle and the process keeps repeating. Thus, the cycle of particle motion followed by rest is self-sustained and results in periodic propulsion of the gel-based floaters.

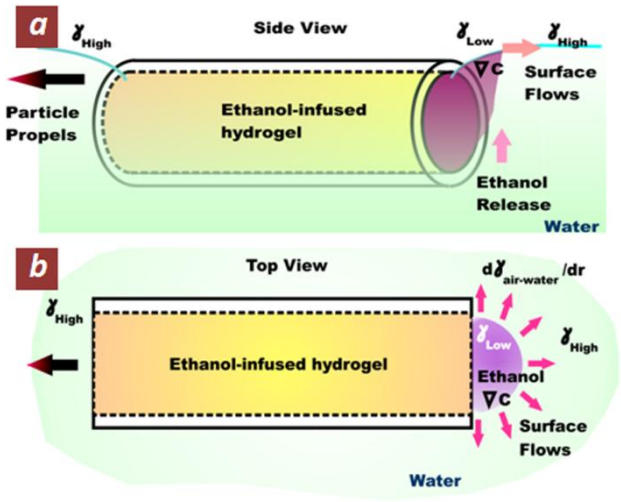

Figure 2.3 Schematic of the propulsion mechanism of the gel-based floaters. The particle is suspended at the air-water interface by the surface tension. The released ethanol travels upwards due to buoyancy and generates surface tension gradient. The asymmetry of surface tension across the floaters is the driving force behind the propulsion of the gel boats. (b) is the top-view of (a).

Our proposed mechanism for particle propulsion has broad similarity to the phenomenon of auto-oscillation of surface-tension from the release of surfactants below the water surface reported by Kovalchul et al.[45] Moreover, we verified our proposed mechanism by mixing a food dye in the gel medium to trace the ethanol release from the hydrogel and its

transport profile in water. The setup of this control experiment is illustrated in Figure 2.4a. The gel boat, (in this case with both its ends open to mass transfer), was placed on the bottom of the Petri dish inside the water. We observed continuous release of ethanol from the hydrogel, which was, however, disrupted periodically on its way upwards to the surface. As the released ethanol-enriched plume reached the water surface driven by buoyancy, surface tension gradient driven flows were generated. These flows perturbed the water in the Petri dish and consequently interrupted the transfer of ethanol to the interface, resulting in elimination of the surface tension gradient. In the absence of ethanol flow reaching the surface, the Marangoni effect stopped. This made possible the resumption of the ethanol transport to the surface, and the entire cycle recurred. Figure 2.4b presents an illustration of the sequence of phenomena during one such cycle of this experiment. As the immobile particle resided at the bottom of the Petri dish with ethanol being released from both ends, the flows at the air-water interface pulsated back and forth.

The periodic disruption of the propulsion of the floating gel self-propelling particles should be guided by the flow patterns as the ones observed above. This mechanism is physically different from that of the intermittent motion reported by Suematsu et al. for camphor boats,[27] which depends on the horizontal distance of diffusion of the molecules before reaching the water surface.[27] The pulsating motion of the gel-floaters described here, relies firstly on the buoyancy for the transport of released ethanol to the air-water interface and secondly on convective flows for interrupting this transport. The combination of these two effects imparts a unique periodic motion to these gel-based floaters. We have derived expressions for the motion of the gel-boats based on this proposed mechanism, as discussed later.

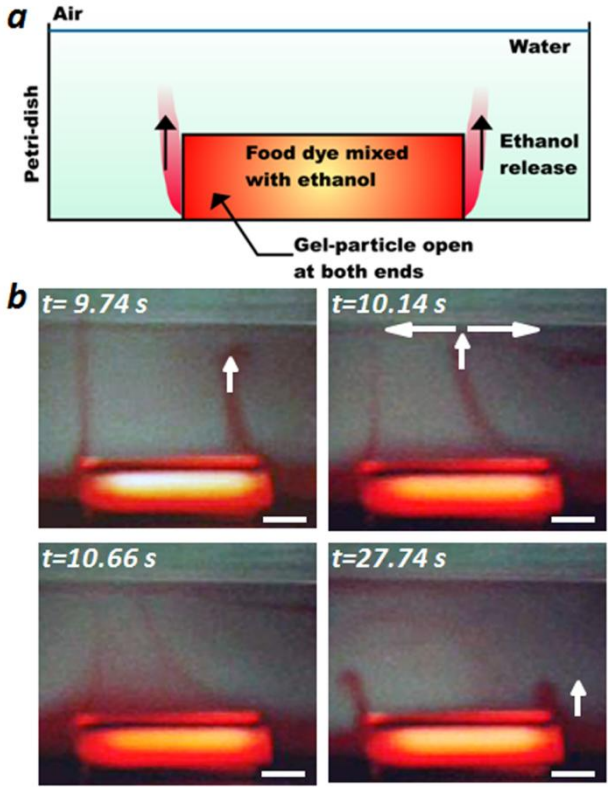

Figure 2.4 Control experiment where food dye is mixed with ethanol to trace its release from the hydrogel and the origin of the interfacial oscillations. The gel boat (open at both ends) is residing at the bottom of the Petri dish. (a) Schematic of the side-view of the experiment. (b) Experimental images of a cycle of ethanol release from the particle. Released ethanol travels upwards due to buoyancy. Flows generated by Marangoni effect impede ethanol supply to the surface, which in turn arrests the interfacial motion. This process is self-sustained and cyclical, as depicted by the arrows indicating ethanol release from the right end of the floater (for simplicity the release from the other end has not been depicted by arrows, but it demonstrates similar transient motion). Scale bars = 1 mm.

2.3.2 Quantification of the Ethanol Release from the Hydrogel

We calculated the rate of ethanol release from the gel boat by treating it as a cylinder with one end open to mass transfer and uniform initial ethanol concentration (Fig. 2.5). When the particle is floated on water, the ethanol concentration in the vicinity of the open end of the cylinder is assumed to be zero, because buoyancy carries the released ethanol to the surface and does not let it accumulate near the floater. The bulk flows generated in water during

particle propulsion also disperse the ethanol released from the hydrogel. The ethanol concentration profile in this cylinder (with uniform initial concentration and boundary condition of zero concentration at its one open end), as a function of time, is given by,[46]

$$C = \frac{4C_0}{\pi}\sum_{n=0}^{\infty}\frac{(-1)^n}{(2n+1)}e^{-D(2n+1)^2\pi^2 t/4l^2}\cos\frac{(2n+1)\pi x}{2l} \qquad (2.1)$$

where C_0 is the initial concentration of ethanol in the gel (7.9×10^{-2} g/cm^3 for 10% ethanol by volume and 39.5×10^{-2} g/cm^3 for 50% ethanol by volume), l is the length of the gel body (4 mm) excluding the PDMS plug, d is the inner diameter of the particle (1 mm), D is the ethanol-water counter-diffusion coefficient (1.1×10^{-9} m^2/s for 10% ethanol by volume and 0.5×10^{-9} m^2/s for 50% ethanol by volume)[47], and x is the distance from the insulated circular end of the cylinder.

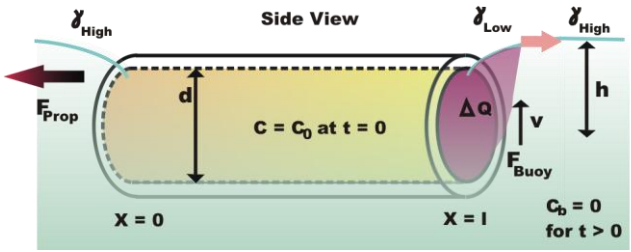

Figure 2.5 Schematic illustrating the parameters used in the expressions for the approximate relations between ethanol release and pulse interval and distance. The floater was modeled as a cylinder, having uniform initial ethanol concentration C_0, with one end open to mass-transfer. The bulk concentration of ethanol C_b was assumed to be negligible (zero) at the open end, based on the propulsion mechanism. ΔQ = ethanol released from the hydrogel for a pulse, F_{buoy} = buoyancy force, v = upward velocity of ethanol, h = distance travelled by ethanol to reach the water surface, l = length of the particle, d = inner diameter of the particle, γ = surface tension of ethanol-water mixture, F_{prop} = net horizontal component of the force on the gel boat due to the asymmetry of surface tension across its length.

We integrated this concentration profile over the length of the cylinder to obtain the total amount of ethanol Q contained in the hydrogel at any time t, given by,

$$Q = \frac{2C_0 l d^2}{\pi} \sum_{n=0}^{\infty} \frac{(-1)^n}{(2n+1)^2} e^{-D(2n+1)^2 \pi^2 t/4l^2} \sin \frac{(2n+1)\pi l}{2l} \tag{2.2}$$

We use the ethanol-water counter-diffusion coefficient because as ethanol is released from the hydrogel, water diffuses into the gel because of osmosis (hydrogel has higher affinity for water than for ethanol).[48] Counter-diffusion of water also decreases the ethanol concentration in the gel with time. Using eqn (2.2), the net amount of ethanol released from the gel-based floater in between two consecutive pulses, ΔQ, can be obtained by,

$$\Delta Q = Q(t_n) - Q(t_{n+1}) \tag{2.3}$$

where t_n is the time at which the n^{th} pulse occurs. We analyzed the digital movies of the experiment on a frame-by-frame basis to obtain the intervals t_1, t_2, t_3, …, t_n, t_{n+1} at which the particle pulsates, and by using eqn 2.3 calculated the ΔQ for each pulse. We plotted ΔQ versus time for gel boats with 10% and 50% ethanol by volume in the hydrogel, and obtained that ~ 0.3 µg (the ΔQ value at which the plots terminate, indicating negligible particle motion) is the minimum amount of ethanol needed by these gel boats to propel in water by overcoming the viscous drag (Fig. 2.6).

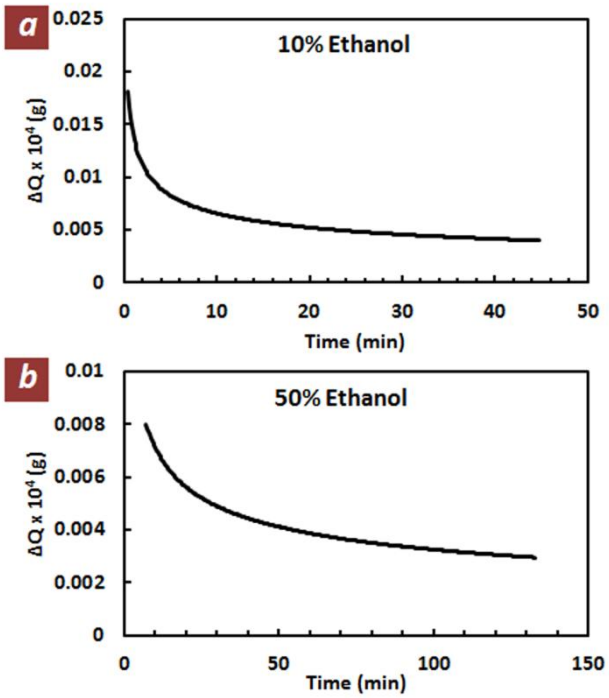

Figure 2.6 Plots of ΔQ versus time for gel boats with (a) 10% and (b) 50% initial ethanol concentration (by volume) in the gel.

2.3.3 Evaluation of the Pulse Interval Duration

We derive below a few scaling relationships allowing to quantify the motion of the boats. We correlated the pulse interval (time between two consecutive pulses) of the gel boat to the amount of ethanol released between two sequential pulses, ΔQ. We expect that the buoyancy force F_{buoy} on the released ethanol will be proportional to the density difference between the ethanol plume and the surrounding fluid $\Delta\rho$, which in turn is proportional to the amount of ethanol released between two successive pulses, that is, ΔQ (Fig. 2.5).

$$F_{buoy} \propto \Delta\rho \propto \Delta Q \tag{2.4}$$

The time, Δt, needed for the released ethanol to reach the water surface (approximated as the pulse interval) is given by

$$\Delta t = \frac{h}{v} \tag{2.5}$$

where *h* is the depth below the surface at which the ethanol release takes place, and *v* is the speed with which the ethanol is transported towards the air-water interface (Fig. 2.5). We assume that the ethanol transport towards the surface takes place under steady-state rise, i.e., the buoyancy force is balanced by the drag force acting on the ethanol plume. This drag force then would be proportional to the upward velocity *v* of the ethanol plume assuming that the ethanol transport takes place in the laminar regime;[49] therefore, *v* is proportional to the buoyancy, and

$$v \propto F_{buoy} \tag{2.6}$$

$$\Delta t \propto \frac{h}{F_{buoy}} \propto \frac{h}{\Delta Q} \tag{2.7}$$

On the basis of relation (2.7), we approximate the pulse interval Δt of the gel-based floaters as,

$$\Delta t = \frac{k_1}{\Delta Q} \tag{2.8}$$

where k_1 is a fitting parameter. In short, the pulse interval was assumed inversely proportional to ΔQ because as the concentration of the released ethanol decreases, the buoyancy carrying it towards the surface also decreases; hence, the time taken by the ethanol to reach the water surface (or pulse interval) increases.

2.3.4 Evaluation of the Distance Propelled in a Pulse

The distance *d'* travelled by the gel-based particle in a pulse is proportional to the propulsive force F_{prop} acting on the gel boat, which in turn may be correlated to the surface tension difference, $\Delta\gamma$, across its two ends (Fig. 2.5) as follows,

$$d' \propto F_{prop} \propto \Delta\gamma \propto \frac{\Delta\gamma}{\Delta Q}\Delta Q \tag{2.9}$$

Assuming that the surface tension of the ethanol-water mixture can be approximated as a sum of the surface tensions of ethanol and water weighted according to their mole fractions in the mixture,[50] we have

$$\gamma = x_e \gamma_e + (1 - x_e)\gamma_w \tag{2.10}$$

$$\frac{d\gamma}{dC} = \frac{d\gamma}{d\left(x_e \frac{N}{V}\right)} = \frac{d\gamma}{\frac{N}{V} dx_e} = \frac{V}{N}(\gamma_e - \gamma_w) = \text{constant} \tag{2.11}$$

where γ_e, γ_w and γ are the surface tensions of ethanol, water and ethanol-water mixture, respectively, x_e is the mole fraction of ethanol, C is the ethanol concentration, N is the total number of moles and V is the total volume of the solution. From eqns (2.9) & (2.11), we express the distance moved by the particle in a pulse as,

$$d' = k_2 \ \Delta Q \tag{2.12}$$

where k_2 is a fitting proportionality coefficient. In short, the release of ethanol at higher concentration in the gel results in larger surface tension gradient across the floaters; hence, the distance propelled by them in a pulse is also larger.

The results of the fitting of the expressions approximating the pulse interval and distance, eqns (2.8) & (2.12), to the experimental data for a floater comprising of 10% and 50% initial ethanol concentration in the hydrogel, using k_1 and k_2 as fitting parameters, are shown in Fig. 2.7. The obtained values of the fitting parameters k_1 and k_2 are different for floaters with 10% and 50% ethanol concentration in the hydrogel. The higher magnitude of k_1 for the case of 10% ethanol in the hydrogel is because it will take more time for a given ΔQ amount of ethanol (released from the hydrogel) to accumulate on the surface in this case relative to 50% ethanol in the hydrogel. Similarly, higher magnitude of k_2 for the case of 50% ethanol in the hydrogel is obtained because for a given ΔQ amount of ethanol released from the hydrogel, the distance propelled by the particle will be larger relative to 10% ethanol in the hydrogel because of more rapid rate of ethanol transport to the surface. Given the length of the experiments and the complexity in processing of the data, we find the agreement between the results and the scaling expressions reasonable. The simple relations derived for the pulse interval and distance appear to describe well the pulsed Marangoni motion and thus they can be used for predicting the trends in the parameters of the oscillatory motion. The pulse interval is increasing with time because the concentration of the released ethanol (and the ethanol concentration in the gel) decreases with time, due to ethanol-water counter-

diffusion. A decrease in the ethanol concentration increases the pulse interval, as discussed above. The distance propelled in pulses decreases with time because the concentration of the released ethanol decreases with time.

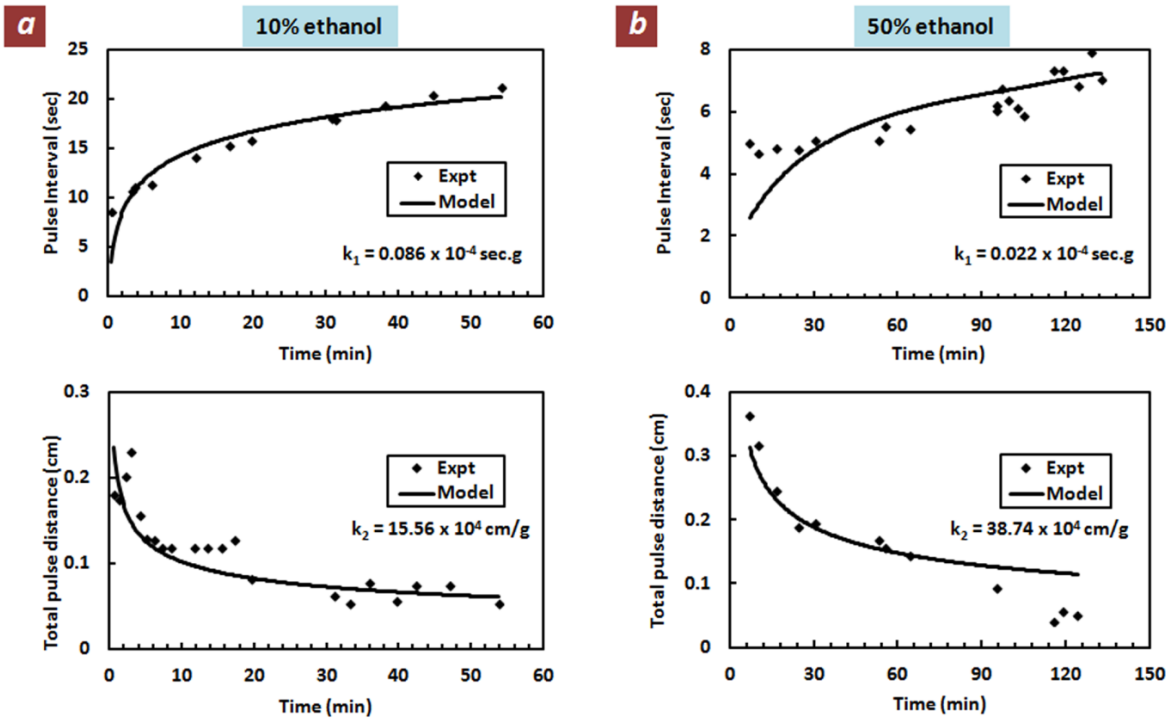

Figure 2.7 Experimental data of the pulse interval (Δt) and total distance (d') propelled in each pulse, fitted to eqns (2.8) and (2.12), respectively, for floaters with (a) 10% and (b) 50% vol. initial ethanol concentration in the gel. The obtained values of the fitting parameters have also been shown.

2.3.5 Programing the Particle Translational and Rotational Motion

The analysis of the ways in which the mass transport through the gel controls the periodicity and the length of the periodic particle propulsion allowed us to construct prototypes of particles with remarkably complex modes of motion, moving in pre-programmed trajectories. This was achieved by having multiple release sites and/or directing the ethanol release

sideways. The simplest example tested was a two-compartment particle, where two hydrogels separated by a PDMS plug in the center of the tubing were infused with different concentrations of ethanol, 50% and 10% (Figure 2.8a & b). The ethanol is thus released at different rates from the two opposing open ends of the microtubing. The difference in the release rate resulted in a particle that performed a remarkably regular pattern of three-step forward one-step back "dancing" (Figure 2.8c).

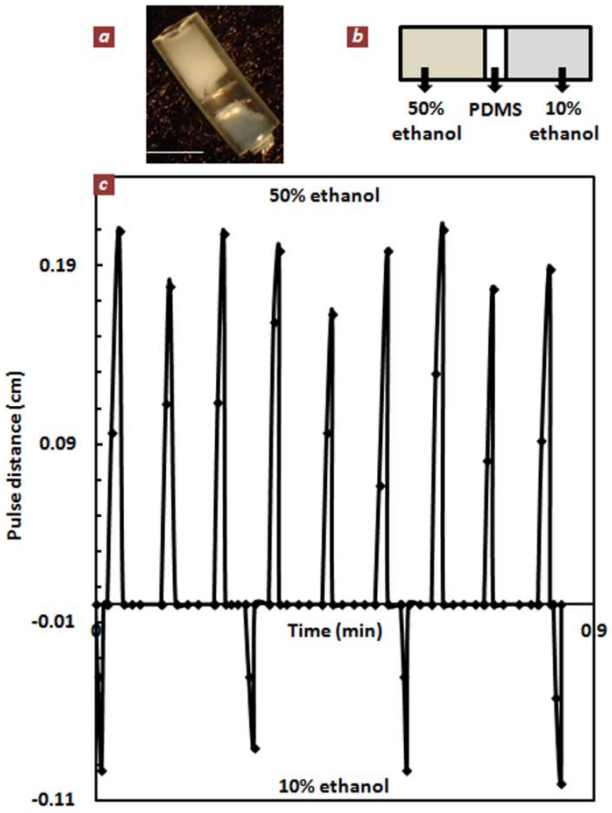

Figure 2.8 (a) Snapshot and (b) schematic of a particle consisting of a 50% and a 10% ethanol hydrogel separated with a PDMS plug, scale bar = 2 mm. (c) Pulse distance versus time plot for this gel-boat (negative pulses represent motion in opposite direction). The positive pulses are driven by the 50% ethanol hydrogel.

We measured the pulse intervals as well as the corresponding pulse distances, and independently predicted the nature of motion assuming that the Marangoni propulsion modes driven by the two ends of the particle are largely uncorrelated (eqns 2.8 & 2.12). The predicted motion was found to be in good correspondence with the experimental results shown in Figure 2.8c. The expressions derived predicted the ratio of pulse intervals for the pulses originating from the 50% and 10% ethanol ends to be 0.25, where the experimentally obtained ratio was 0.35. Similarly, the ratio of pulse distance for pulses originating from the 50% and 10% ethanol ends was estimated to be 2.49 from the expressions, where the one observed in experiments was 2.16. Table 2.1 compares the pulse intervals and the distances corresponding to the pulses from the two ends, obtained from the experiments and the relations derived. The agreement between the quantitative predictions and experiments suggests that we can program the motion of these gel-boats by adjusting the parameters such as the concentration of ethanol in the hydrogel, length of the hydrogel, and others. In more general view, it opens the ability to create a vastly diverse class of novel particles that can be designed to perform intricately complex trajectories. We illustrate this capability with a few examples below.

Table 2.1 Experimental and model-based data for the pulse intervals and the pulse distances, corresponding to the pulses originating from the two ends of a particle consisting of a 50% ethanol hydrogel at one end and a 10% ethanol hydrogel at the other.

	Expt. (50%)	Model (50%)	Expt. (10%)	Model (10%)	Expt. Ratio (50%:10%)	Predicted Ratio (50%:10%)
Pulse Interval	**5.83**	**3.76**	**16.54**	**14.83**	**0.35**	**0.25**
Distance	**0.19**	**0.23**	**0.09**	**0.09**	**2.16**	**2.49**

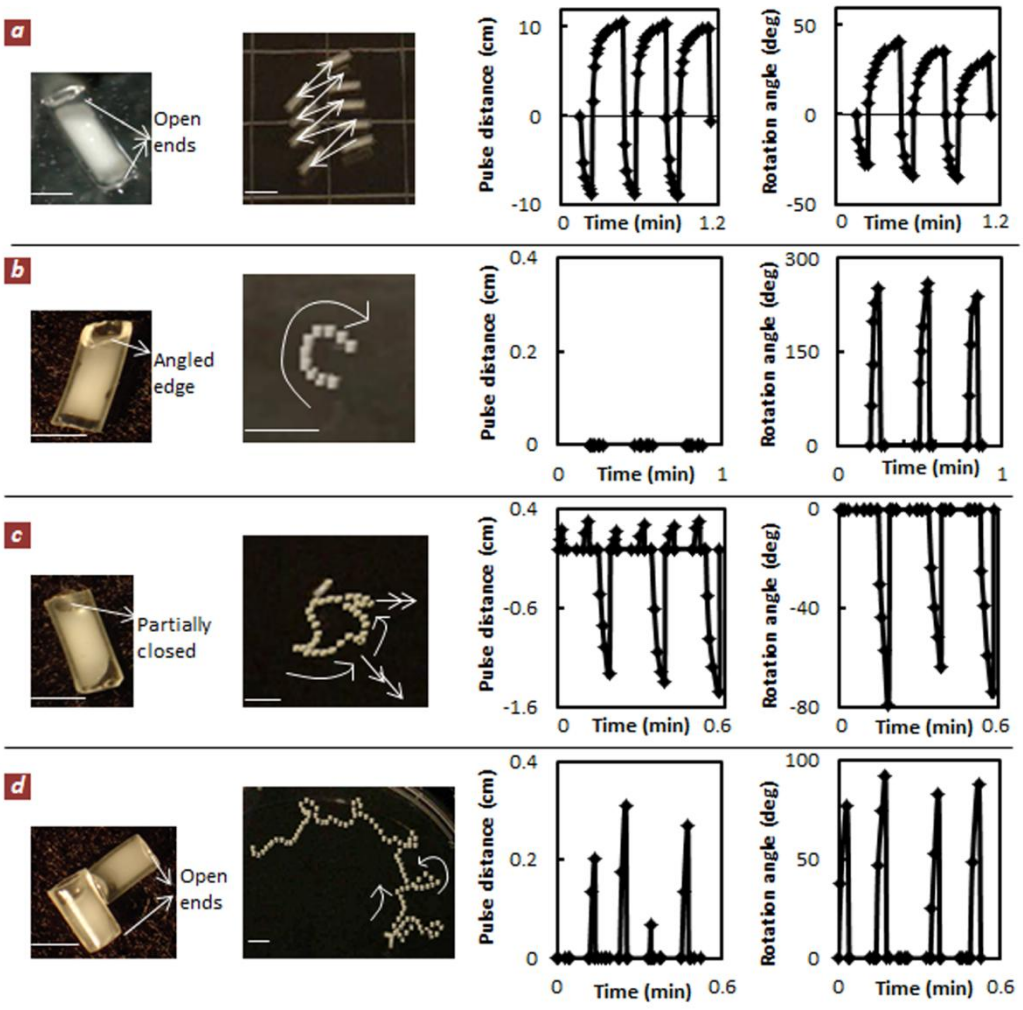

Figure 2.9 Snapshot, trajectory, plots of pulse distance and rotation angle against time for floaters with (a) both ends open, (b) one end open and angled, (c) one end open and the other partially closed, and (d) two particles attached together in an "L-shape". Scale bars in particle snapshots = 2 mm, Scale bars in the trajectories overlay images = 1 mm.

The pattern of particle motion could be readily changed by making minor alterations in the design of the floaters. A few different particle designs were tested, and the corresponding trajectories observed along with the plots of pulse distance and rotation angle versus time are tabulated in Figure 2.9. A symmetric particle open at both ends evenly pulsates back and forth (Fig. 2.9a), whereas a particle with one end partially closed with a

PDMS plug pulsates back and forth asymmetrically, with the frequency and pulse distance differing in the two directions. The partially closed from one end particle in Figure 2.9c performs a long jump in one direction followed by two small jumps in the opposite direction, resembling the steps in a tango dance (note the difference between these steps and the ones of the two-gel particle in Fig. 2.8c). Similarly, placing the hydrogel closer to one edge of the tubing but away from the other also causes asymmetry in the forward and backward pulses. Additionally, cutting the edges of the particles at an angle imparts a rotational component into their motion. Depending on the angle at the edge, either the translational component of motion dominates (Fig. 2.9a & c), or the rotational component dominates as in the particle that periodically swirls around, shown in Fig. 2.9b. Attaching together two particles into an "L-shape" also introduces a rotational element into the particle's motion (Fig. 2.9d). This is because in addition to generating Marangoni effect, the two attached particles act as rudders[51] with respect to each other. Thus, an L-shaped particle's trajectory constitutes a large circle with periodic small swirls over a larger area of the water surface. The relations for the pulse interval and distance and the making of the "dancing" particles reported above are first steps towards the design of pulsed floaters that can travel in even more complex programmed trajectories than the ones illustrated in Figure 2.9.

2.4 Conclusions

We present gel-based self-propelling floaters that exhibit unique pulsating motion in water over long times. We investigated the mechanism behind their propulsion and found that the reason for the pulsating mode of their motion is a recurring cycle of surface tension gradient driven flows followed by a disruption of the ethanol flux to the surface. These particles are simple, inexpensive and easy to make. We have used ethanol as a "fuel" to power the propulsion of gel boats in our experiments but other surface active substances (that are less dense than water) such as methanol, acetone, or isopropanol can also be used. The amount of the surface active substance in the hydrogel determines the duration of motion. These particles propel for long period of time, for example, gel boats with 50% ethanol (by volume) in the hydrogel kept propelling for more than two hours. We characterized the motion of

these floaters by deriving scaling relationship for their pulse interval and the distance propelled by them in a pulse. These expressions were in agreement with the experimental results. Furthermore, introducing variations in the design of the floaters significantly alters their nature of motion (resulting in periodic rotational motion, asymmetric back and forth pulsation, or a combination of both).

A limitation of the design of such self-propelling particles based on Marangoni effect is that the propulsion lasts only as long as the "fuel" (surface active substance) is available. This limitation can be overcome by loading such particles with a catalyst that can generate the surface active substance on its own but does not get consumed in the process. For example, we have used yeast cells as catalyst for powering the propulsion of novel "biogenic" floaters, as described in Chapter 4.

These self-propelling boats can find potential applications in lab-on-a-chip devices as shuttles for cargo transportation, as sensors for detecting the presence of toxins in water bodies or the presence of certain biomolecules in the field of medical diagnostics. These applications demand functionalization of these floaters to enable them to respond to external stimuli in the environment. Our work presented here is an initial step in the design of early prototypes of such devices capable of performing these complex functions.

2.5 Acknowledgements

We are grateful to Dr. Sejong Kim for providing advice and experimental help. This study was supported by grant from the US National Science Foundation (CBET 0828900), and Basic Science Research Program through the National Research Foundation of Korea (NRF) funded by the Ministry of Education, Science and Technology (grant no. 2011-0004871).

2.6 References

1. Kagan, D. *et al.* Rapid Delivery of Drug Carriers Propelled and Navigated by Catalytic Nanoshuttles. *Small* **6,** 2741-2747 (2010).

2. Burdick, J., Laocharoensuk, R., Wheat, P. M., Posner, J. D., Wang, J. Synthetic nanomotors in microchannel networks: Directional microchip motion and controlled manipulation of cargo. *J. Am. Chem. Soc.* **130,** 8164-8165 (2008).

3. Solovev, A. A., Sanchez, S., Pumera, M., Mei, Y. F., Schmidt, O. G. Magnetic Control of Tubular Catalytic Microbots for the Transport, Assembly, and Delivery of Micro-objects. *Adv. Funct. Mater.* **20,** 2430-2435 (2010).

4. Sundararajan, S., Sengupta, S., Ibele, M. E., Sen, A. Drop-Off of Colloidal Cargo Transported by Catalytic Pt-Au Nanomotors via Photochemical Stimuli. *Small* **6,** 1479-1482 (2010).

5. Ibele, M. E., Wang, Y., Kline, T. R., Mallouk, T. E., Sen, A. Hydrazine fuels for bimetallic catalytic microfluidic pumping. *J. Am. Chem. Soc.* **129,** 7762-7763 (2007).

6. Chang, S. T., Beaumont, E., Petsev, D. N., Velev, O. D. Remotely powered distributed microfluidic pumps and mixers based on miniature diodes. *Lab Chip* **8,** 117-124 (2008).

7. Hong, Y. Y., Diaz, M., Cordova-Figueroa, U. M., Sen, A. Light-Driven Titanium-Dioxide-Based Reversible Microfireworks and Micromotor/Micropump Systems. *Adv. Funct. Mater.* **20,** 1568-1576 (2010).

8. Campuzano, S., Kagan, D., Orozco, J., Wang, J. Motion-driven sensing and biosensing using electrochemically propelled nanomotors. *Analyst* **136,** 4621-4630 (2011).

9. Yang, W., Misko, V. R., Nelissen, K., Kongd, M., Peeters, F. M. Using self-driven microswimmers for particle separation. *Soft Matter* **8,** 5175-5179 (2012).

10. Frutiger, D. R., Kratochvil, B. E.; Vollmers, K.; Nelson, B. J. Magmites - Wireless resonant magnetic microrobots. *IEEE Int. Conf. Robot.* **2008**, *1-9*, 1770-1771.

11. Fernandes, R., Gracias, D. H. Toward a miniaturized mechanical surgeon. *Mater. Today* **12,** 14-20 (2009).

12. Ismagilov, R. F., Schwartz, A.; Bowden, N.; Whitesides, G. M. Autonomous movement and self-assembly. *Angew. Chem. Int. Edit.* **41,** 652-654 (2002).

13. Kwon, G. H. *et al*. Biomimetic Soft Multifunctional Miniature Aquabots. *Small* **4,** 2148-2153 (2008).

14. Hong, Y. Y., Velegol, D., Chaturvedi, N., Sen, A. Biomimetic behavior of synthetic particles: from microscopic randomness to macroscopic control. *Phys. Chem. Chem. Phys.* **12,** 1423-1435 (2010).

15. Purcell, E. M. Life at Low Reynolds-Number. *Am. J. Phys.* **45,** 3-11 (1977).

16. Mirkovic, T., Zacharia, N. S., Scholes, G. D., Ozin, G. A. Fuel for Thought: Chemically Powered Nanomotors Out-Swim Nature's Flagellated Bacteria. *ACS Nano* **4,** 1782-1789 (2010).

17. Ebbens, S. J., Howse, J. R. In pursuit of propulsion at the nanoscale. *Soft Matter* **6,** 726-738 (2010).

18. Vicario, J. *et al.* Catalytic molecular motors: fuelling autonomous movement by a surface bound synthetic manganese catalase. *Chem. Commun.* 3936-3938 (2005).

19. Mei, Y. F., Solovev, A. A., Sanchez, S., Schmidt, O. G. Rolled-up nanotech on polymers: from basic perception to self-propelled catalytic microengines. *Chem. Soc. Rev.* **40,** 2109-2119 (2011).

20. Gibbs, J. G., Zhao, Y. P. Autonomously motile catalytic nanomotors by bubble propulsion. *Appl. Phys. Lett.* **94,** 163104 (2009).

21. Chang, S. T., Paunov, V. N., Petsev, D. N., Velev, O. D. Remotely powered self-propelling particles and micropumps based on miniature diodes. *Nat. Mater.* **6,** 235-240 (2007).

22. Calvo-Marzal, P. *et al.* Propulsion of nanowire diodes. *Chem. Commun.* **46,** 1623-1624 (2010).

23. Osada, Y., Okuzaki, H., Hori, H. A polymer gel with electrically driven motility. *Nature* **355,** 242-244 (1992).

24. Mano, N., Heller, A. Bioelectrochemical propulsion. *J. Am. Chem. Soc.* **127,** 11574-11575 (2005).

25. Wang, Y. *et al.* Bipolar electrochemical mechanism for the propulsion of catalytic nanomotors in hydrogen peroxide solutions. *Langmuir* **22,** 10451-10456 (2006).

26. Pumera, M. Electrochemically powered self-propelled electrophoretic nanosubmarines. *Nanoscale* **2,** 1643-1649 (2010).

27. Suematsu, N. J. *et al.* Mode-Switching of the Self-Motion of a Camphor Boat Depending on the Diffusion Distance of Camphor Molecules. *J. Phys. Chem. C* **114,** 9876-9882 (2010).

28. Mitsumata, T., Ikeda, K., Gong, J. P., Osada, Y. Solvent-driven chemical motor. *Appl. Phys. Lett.* **73,** 2366-2368 (1998).

29. Bassik, N., Abebe, B. T., Gracias, D. H. Solvent Driven Motion of Lithographically Fabricated Gels. *Langmuir* **24,** 12158-12163 (2008).

30. Nagai, K., Sumino, Y., Kitahata, H., Yoshikawa, K. Mode selection in the spontaneous motion of an alcohol droplet. *Phys. Rev. E* **71,** 065301 (2005).

31. Luo, C., Li, H., Liu, X. C. Propulsion of microboats using isopropyl alcohol as a propellant. *J. Micromech. Microeng.* **18,** 067002 (2008).

32. Golestanian, R., Liverpool, T. B., Ajdari, A. Propulsion of a molecular machine by asymmetric distribution of reaction products. *Phys. Rev. Lett.* **94,** 220801 (2005).

33. Volpe, G., Buttinoni, I., Vogt, D., Kummerer, H.-J., Bechinger, C. Microswimmers in patterned environments. *Soft Matter* **7,** 8810-8815 (2011).

34. Liu, W. *et al.* Ultrafast nanotube based diffusiophoresis nanomotors. *Appl. Phys. Lett.* **96,** 053114 (2010).

35. Yoshida, R. Self-Oscillating Gels Driven by the Belousov-Zhabotinsky Reaction as Novel Smart Materials. *Adv. Mater.* **22,** 3463-3483 (2010).

36. Maeda, S., Hara, Y., Sakai, T., Yoshida, R., Hashimoto, S. Self-walking gel. *Adv. Mater.* **19,** 3480-3484 (2007).

37. Dreyfus, R. *et al.* Microscopic artificial swimmers. *Nature* **437,** 862-865 (2005).

38. Fischer, P., Ghosh, A. Magnetically actuated propulsion at low Reynolds numbers: towards nanoscale control. *Nanoscale* **3,** 557-563 (2011).

39. Weibel, D. B. *et al.* Microoxen: Microorganisms to move microscale loads. *P. Natl. Acad. Sci. USA* **102,** 11963-11967 (2005).

40. Soong, R. K. *et al.* Powering an inorganic nanodevice with a biomolecular motor. *Science* **290,** 1555-1558 (2000).

41. Pantarotto, D., Browne, W. R., Feringa, B. L. Autonomous propulsion of carbon nanotubes powered by a multienzyme ensemble. *Chem. Commun.* 1533-1535 (2008).

42. Scriven, L. E., Sternling, C. V. Marangoni Effects. *Nature* **187,** 186-188 (1960).

43. Suciu, D. G., Smigelschi, O., Ruckenstein, E. Spreading of Liquids on Liquids. *J. Colloid Interf. Sci.* **33,** 520-528 (1970).

44. Vazquez, G., Alvarez, E., Navaza, J. M. Surface Tension of Alcohol + Water from 20 to 50 ^{o}C. *J. Chem. Eng. Data* **40,** 611-614 (1995).

45. Kovalchuk, V. I., Kamusewitz, H., Vollhardt, D., Kovalchuk, N. M. Auto-oscillation of surface tension. *Phys. Rev. E* **60,** 2029-2036 (1999).

46. Carslaw, H. S., Jaeger, J. C. in *Conduction of Heat in Solids*, Oxford Press, London 1959, Ch. 3.

47. Zhang, L., Wang, Q., Liu, Y. C., Zhang, L. Z. On the mutual diffusion properties of ethanol-water mixtures. *J. Chem. Phys.* **125,** 104502 (2006).

48. Anderson, J. L., Malone, D. M. Mechanism of osmotic flow in porous membranes. *Biophys. J.* **14,** 957-982 (1974).

49. Bird, R. B., Stewart, W. E., Lightfoot, E. N. in *Transport Phenomena*, Wiley, Singapore 1960, Ch. 2.

50. Acree, W. E. Empirical expression for predicting surface tension of liquid mixtures. *J. Colloid Interf. Sci.* **101,** 575-576 (1984).

51. Qiao, L., Xiao, D., Lu, F. K., Luo, C. Control of the radial motion of a self-propelled microboat through a side rudder. *Transducers* 1448-1451 (2011).

CHAPTER 3

Engine-Payload Self-Propelling Absorbing Particles for Highly Efficient Collection of Oil from Water Surfaces*

* Based on R. Sharma, L. D'Costa and O. D. Velev, *in preparation for Nature*

3.1 Introduction

A self-propelling particle uses energy (such as chemical, thermal, electrical, etc.) from its environment for propulsion by generating local field asymmetry.[1-5] The self-propelling particles have been a subject of intense fundamental interest as they pose a number of basic problems regarding the mechanism of motion and the evolution of ensembles of interacting and communicating objects. They have also been a subject of fascination and inspiration, as their dynamics resembles the motion of many biological species. However, for some time they have played the role of a "solution looking for a problem," in the light of potential applications that have been envisioned for such motile objects.[6,7] We present a novel approach of collecting thin films of oil on water by using self-propelling absorbent particles. Previous research on oil collection focuses on synthesis of suspended passive absorbents.[8-19] We demonstrate a new class of gel-based self-propelling floaters moving by Marangoni effect, and having an absorbent head. These actively mobile particles are extremely effective in collecting oil film from a surface by a rapid convective-diffusive mechanism. The results could pave the way to radical intensification of many chemical engineering processes where presently immobile or suspended particles absorb and process a certain component by passive diffusion. The general theoretical results will be applicable not only to self-propelling interfacial floaters, but also to osmotically-driven bulk catalytic particles.

Accidental oil spills on water are a major societal concern because of environmental degradation.[20,21] The oil tends to form thin films that spread over large areas. The majority of the presently used absorbents rely on natural drifting (driven by air or water currents) to move around and collect the oil film floating on the water surface. This is an inefficient way of cleaning up oil spills as it is limited by the diffusion of oil towards the absorbent. Novel solutions need to be formulated urgently for dealing with such oil spills. Some of the recent more elaborate oil clean-up strategies involve incorporating magnetic components into the absorbent particles to enable their steering using external magnets to track the oil spill on water.[22-24] Also, it has been demonstrated recently that superhydrophobized nano/microscale motors ("microsubmarines") propelling in hydrogen peroxide solution can attach oil drops over their surfaces.[25]

The new oil-collecting self-propelling particles described here demonstrate a novel application of the fundamental technique of motion at liquid surfaces. We describe a class of simple and efficient engine-payload particles whose active propulsion drastically intensifies the process of oil film disruption and absorption, and point the way towards optimization of many other interfacial or bulk collection and catalysis processes. The components of the first prototype of self-propelling oil-collecting floaters are illustrated in Figure 3.1a. The "engine" is made up of polyacrylamide hydrogel infused with a surface-active substance contained in a small piece of plastic tubing. We used solutions of ethanol or sodium dodecyl sulfate (SDS) as "propellant" infused into the hydrogel "engine". The propulsion of an "engine"-only particle driven by the release of a surface-active substance from a hydrogel has been analyzed and characterized by us in a recent paper.[26] The "payload" is a commercial oil-absorbent material (hydrophobic nonwoven composed of polypropylene) that collects and stores the oil as the particle propels. The polydimethylsiloxane (PDMS) plug in between the absorbent and the hydrogel prevents the penetration of SDS/ethanol into the absorbent section. To demonstrate and characterize the performance of these particles, mineral oil (dyed with Oil Red O) was poured on water in a plastic Petri dish. The oil spreads in a thin layer covering the water surface. The assembled particles were floated on the surface of this water by capillary forces where they immediately begin to propel due to a self-sustained cycle of Marangoni effect driven flows.[26] A typical trajectory of such oil-assimilating particles is illustrated in Figure 3.1b. As the particle propels, two concurrent effects occur – oil film disruption at the hydrogel end and absorption at the other end.

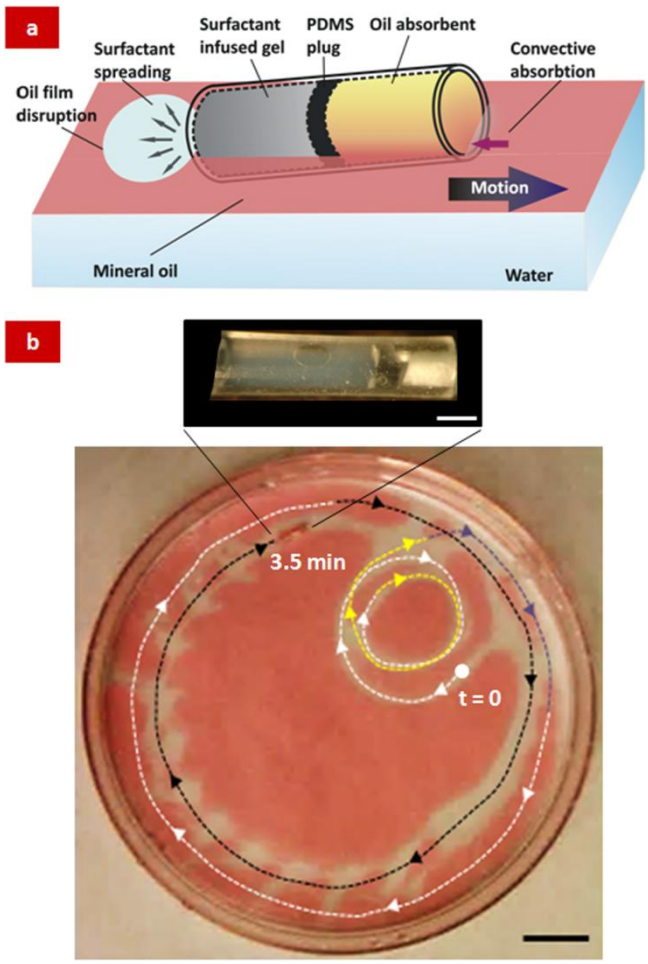

Figure 3.1 (a) Schematic illustrating the composition and working principle of an oil-collecting self-propelling particle floating at the air-water interface. (b) Snapshot of the oil-covered water surface after 3.5 min of releasing the self-propelling oil collector illustrating the trajectory of particle movement (scale bar = 2 cm) and photograph of an "engine-payload" particle (scale bar = 1.5 mm).

3.2 Experimental Section

3.2.1 Particle Assembly

The ethanol-infused polyacrylamide gel was crosslinked within the microbore tubing (0.050" × 0.090" OD) as previously described by us in ref. 26. Additionally, 0.1 g/ml of SDS (Sigma-Aldrich, Milwaukee, WI) was added to the hydrogel precursor solution prior to curing. After curing, the tubing was trimmed to 8 mm length. A 1 mm long PDMS plug (preparation

described in ref. 26) was pushed further into the tubing with tweezers making space for the oil-absorbent. The vacant space was then stuffed with ~ 1 mg of oil-absorbent, obtained from New Pig Inc. (Tipton, PA). The ratio of the lengths of the hydrogel and absorbent was ~ 5:2 within the 8 mm tubing. Mobile particles without absorbent, used in the control experiments, comprise of the surfactant infused hydrogel within the 8 mm tubing with one end sealed with a 1 mm long PDMS plug. Stationary absorbent "control" particles consist of only the absorbent within the 8 mm tubing.

Particles comprising of ethanol infused agarose gel were assembled as follows. The agarose gel was prepared by mixing agar powder (Acros Organics), 2% by weight, with DI water heated over a hot plate. The solution was then allowed to cool down to room temperature and during this process (before gelation) an equal volume of ethanol was added to it to obtain 50% v/v ethanol-water mixture in the hydrogel. A 1 mm long PDMS plug was inserted at one end of an 8 mm long piece of microbore tubing, and pushed further into the tubing with a tweezer to divide the interior of the tubing into two chambers of 5 mm and 2 mm lengths. Oil-absorbent (1-2 mg) from New Pig was filled into the 2 mm chamber using tweezers, and the other end was filled with the agarose gel by simply inserting the open end of the tubing vertically into the hydrogel.

In the simplified particle design, one corner of a 4 mm × 8 mm rectangular absorbent sheet was wetted with 2 µl of 50% v/v ethanol-water solution containing 21.5 mM surfactant. The sheets were then left to dry before floating them on water. We tested three different surfactants - sodium dodecyl sulfate, sodium tetradecyl sulfate and sodium hexadecyl sulfate (Sigma-Aldrich, Milwaukee, WI). The magnetically responsive self-propelling sheet was prepared by incorporating Fe_2O_3 nanoparticles (Sigma Aldrich, Milwaukee, WI) on a 5 × 8 mm rectangular absorbent sheet. 4 µl of 50% v/v ethanol-water solution containing 21.5 mM STS was pipetted on one edge of the sheet, and 4 µl of a suspension of Fe_2O_3 nanoparticles (comprising of 0.16 g of nanoparticles per ml of 50% v/v ethanol-water solution) was pipetted on the other edge. The sheet was then left to dry before floating it on water.

All experiments were performed in a 14.6 cm diameter Petri dish containing 60 ml deionized water (obtained from a Millipore Milli-Q Academic water purification system, Billerica, MA) with 60 µl of light mineral oil (Sigma-Aldrich, Milwaukee, WI), dyed with 2.6 mg/ml of Oil Red O (Sigma-Aldrich, Milwaukee, WI), floating on the surface.

3.3 Results and Discussion

3.3.1 Characterization of Oil Film Dispersion

The recorded experimental movies were analyzed to quantify the change in the area of oil coverage by monitoring the number of pixels representing the dye colored area over time. Control experiments were performed with moving particles without absorbent and stationary particles with absorbent (details in Section 3.2). The obtained plots of oil coverage as a function of time are shown in Figure 3.2a. The magnitude of oil film dispersion, measured by the decrease in the count of red colored pixels, is much larger for the mobile particles (with or without absorbent) compared to the stationary ones. The release of the surface-active material from the hydrogel end of the mobile particles leads to dispersion of the oil film due to Marangoni effect driven spreading of the surfactant. The surface pressure of the surfactant adsorption monolayer causes compression of the oil layer over the water surface. The extent of oil dispersion depends on the surface tension, solubility/volatility and overall spreading dynamics of the surface-active agent released. For example, when only ethanol was used as "propellant" (by incorporating an ethanol infused agarose gel as "engine", details in Section 3.2), the degree of oil film dispersion was significantly reduced since ethanol is miscible in water as well as volatile, causing compressed oil film to rapidly re-spread (Fig. 3.2b). SDS, on the other hand, has lower solubility in water and is non-volatile. Therefore, spreading of SDS contracts the oil film more than the spreading of ethanol. The oil dispersion propensities of other sodium n-alkyl sulfate homologues are discussed below.

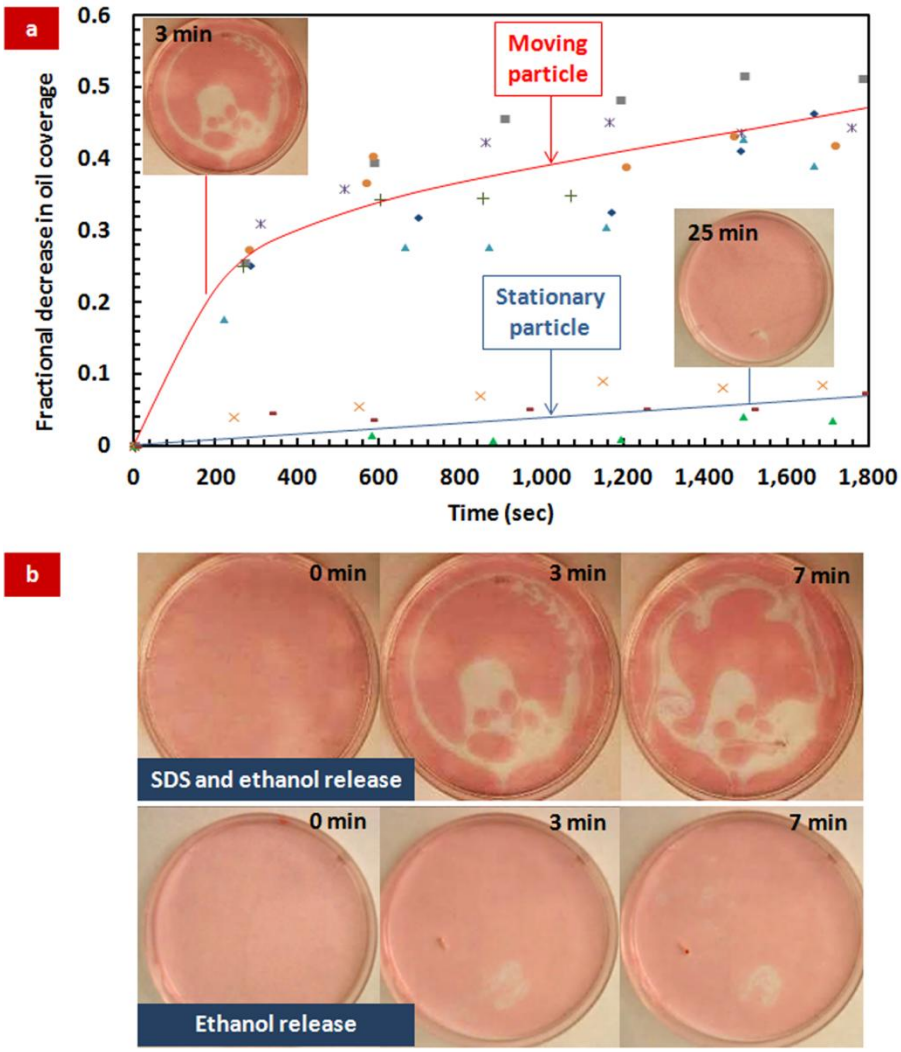

Figure 3.2 (a) Fractional decrease in the area of oil spread on water with time for self-propelling particles compared to that observed for stationary particles. Lines fitted to the data points are to guide the eye. Snapshots of the oil coverage on water for the two particle types have been shown as insets for comparison – the decrease in oil film area for a moving particle in 3 min is much greater than that for a stationary particle in 25 min. (b) Snapshots of the Petri dish surface illustrating oil dispersion by particles releasing SDS versus particles releasing ethanol.

3.3.2 Characterization of Oil Absorption

In addition to dispersion, these self-propelling particles are also simultaneously collecting the oil into the absorbent "payload" head. The rate of absorption is dependent on the diffusive and convective transport of oil to the absorbent.

$$\frac{\partial C}{\partial t} = -v.\nabla c + D\nabla^2 c \tag{3.1}$$

where C is the oil concentration in the absorbent, v is the particle velocity, D is the diffusivity of oil in the absorbent, t is the time and ∇c is the gradient of oil across the absorbent. Assuming that the convective term is dominant for a mobile particle and that the local oil concentration outside the particle remains constant, the following exponential correlation between the oil weight absorbed, W, and the distance moved in oil, d, is obtained

$$\frac{\partial C}{\partial t} = -v.\nabla c \Rightarrow \frac{\partial C}{\partial t} = -v\frac{\partial c}{\partial r} = kv(C_o - C) \Rightarrow C = C_o(1-e^{-k.d}) \Rightarrow W = W_o(1-e^{-k.d}) \tag{3.2}$$

where C_o is the oil concentration outside the particle, W_o is the maximum oil weight that can be collected by the working section of the particle and k (assumed constant) represents the inverse of the effective distance over which the oil concentration gradient exists. The derived weight-distance correlation suggests that for a hypothetical particle moving with constant velocity, the rate of oil collection would increase with increasing particle velocity (Fig. 3.3). In our experiments, the nature of particle motion is periodic and the type of surfactant used as well as its rate of release determines the particle velocity. Therefore, the distance propelled by the particles in a given time indirectly represents the rate/type of surfactant released from the particles. Typical plot of particle velocity in oil, illustrating the periodicity in its motion, and the plot of cumulative distance travelled in oil (obtained by analyzing the frames of the experimental movies) have been shown in Fig. 3.4.

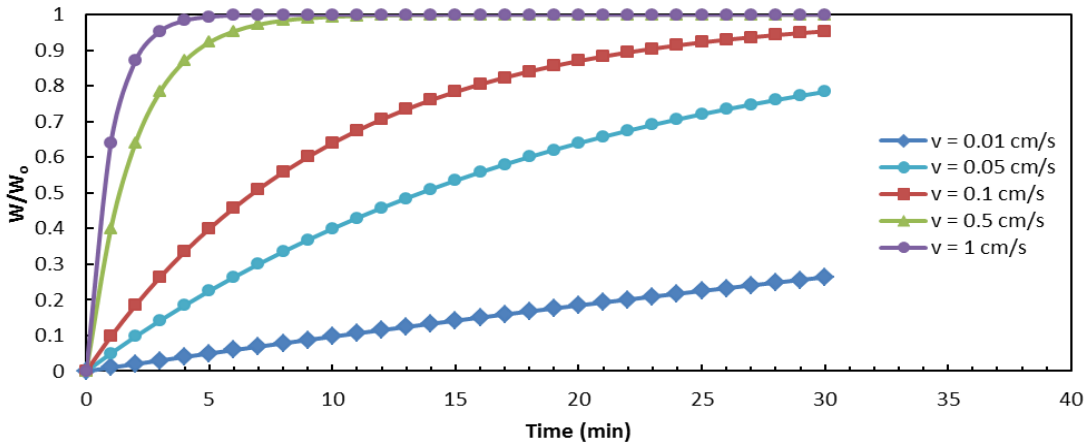

Figure 3.3 Theoretical plots of the weight-distance correlation for a particle moving with constant velocity.

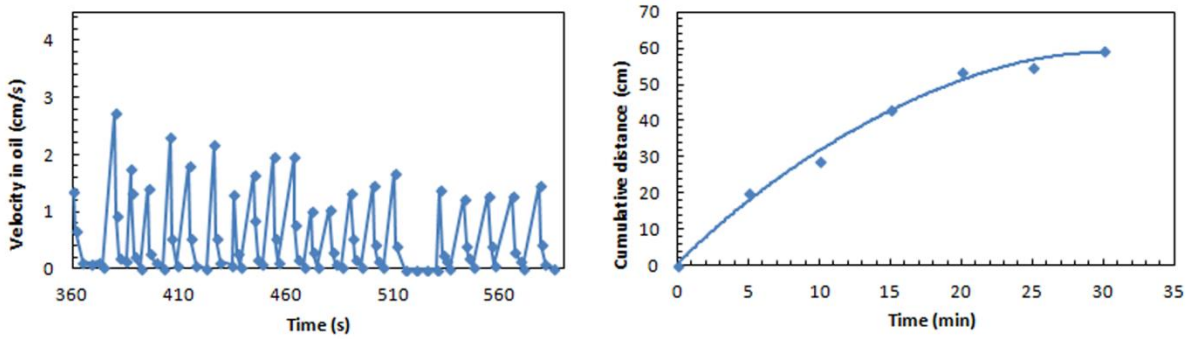

Figure 3.4 Typical plots of the velocity profile and distance travelled in oil for a particle releasing SDS and ethanol.

The experimental data of weight gain over time (obtained by periodically weighing the particle in an analytical balance during the experiment) are plotted in Figure 3.5. Stationary absorbents rely on diffusion and natural drifting for gathering the oil spread over large area on the water surface. The data in Fig. 3.5 clearly show that the mobile oil-absorbing particles are more effective collectors compared to stationary absorbents of similar size due to additional contribution of convective oil flux in the former case. The weight gain

data of the mobile oil-collecting particles were fitted with the weight-distance correlation above. W_o was obtained experimentally to be ~ 4.2 mg and k, used as the fitting parameter, was estimated to be 0.017 cm^{-1}. The values of both W_o and k would depend on the type and amount of absorbent in the particle head, and are expected to be higher for more efficient absorbents. Mobile absorbent-containing particles moving on clean water surface did not show an increase in weight over time. Mobile particles without absorbent showed a minimal increase in weight due to collection of some oil by capillarity.

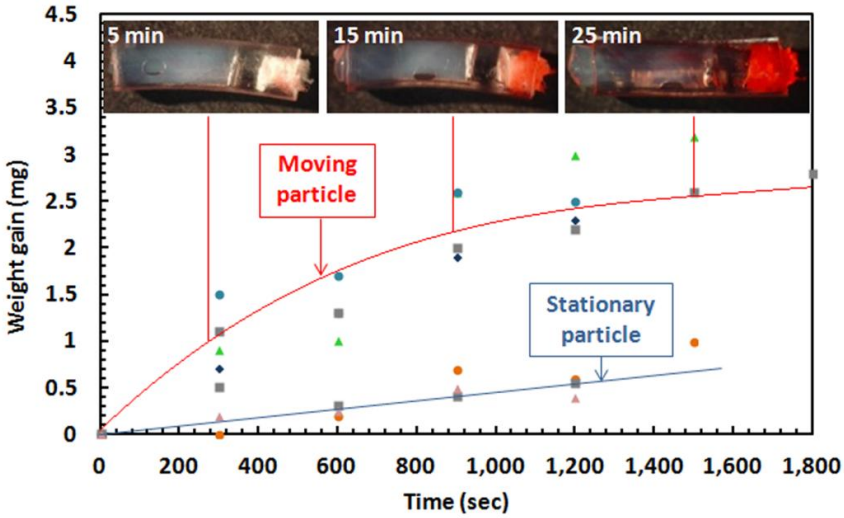

Figure 3.5 Weight gain over time for self-propelling oil-collecting particles compared to that observed for stationary particles. Line fitted to the data of mobile absorbing particles is obtained from the derived weight-distance correlation, whereas the line fitted to the data of stationary particles is for guiding the eye. Time-lapse snapshots of a mobile oil-collecting particle have been shown as insets after 5, 15 and 25 min of propulsion (note the increasing color intensity as the absorbent head becomes saturated with oil).

3.3.3 Simplifying Particle Design: Mobile Absorbent Sheets

This technique can be developed further by designing new, simple and inexpensive particles of practical value. One extremely simple way of achieving this is by infusing a small amount of surfactant into one side of an absorbent sheet, a few millimeters in size, cut out from a roll

of oil-collecting material (Fig. 3.6a). The absorbent sheets formed in this way self-propel vigorously on the water surface. Their trajectory depends on the sheet's shape and the direction of infusion. A few examples of the rotational-translational trajectories of such propellers are shown in Fig. 3.6b. Their mode of operation and efficiency depend on the type of surfactant. Fig. 3.6a & b illustrate the degree of oil dispersion and absorption by microsheets releasing SDS, sodium tetradecyl sulfate (STS) and sodium hexadecyl sulfate (SHS) as means of propulsion on water (details in Section 3.2). The sheet velocity decreases with increasing (surfactant's) alkyl chain length. The slower motion of absorbent sheets propelled by higher molecular weight homologues is probably a result of the slowing rate of surfactant diffusion from absorbent onto water surface with increasing hydrophobicity or chain length. The efficiency of oil dispersion by the sheets (Fig. 3.7) is dependent on two factors – the rate of release of surfactant molecules from absorbent into water (decreases with increasing chain length) and the surface pressure of the surfactant monolayer (increases with increasing chain length).

The structure of the surfactant film also varies among the homologues as with increasing chain length the surfactant molecules form ordered, tightly packed, liquid-like monolayer at the air-liquid interface due to hydrophobic interactions between the alkyl chains.[27] The difference in the pattern of surfactant spreading was even more distinct when these homologous surfactants were directly pipetted over the oil covered water surface. We pipetted 2 µl of the surfactant solution, used for wetting the absorbent sheets, directly over the oil covered water surface. Figure 3.8 compares the decrease in oil coverage by surfactant spreading for these control experiments. As can be seen in Fig. 3.8, the extent of spreading in terms of the area increases with increasing alkyl chain length due to greater surface pressure of longer chain length homologues. It is interesting to note that in the case of ethanol or SDS, the spread film collapses back quickly and almost completely. This tendency diminishes with increasing alkyl chain length, as in the cases of C14 and C16 surfactants the film only partially collapses back. Also, the time it takes for the spread surfactant film to collapse increases with increasing chain length of the surfactant. This trend suggests that with increasing alkyl chain length, the surfactant film at the air-liquid interface becomes more

incompressible or liquid-like due to hydrophobic interactions between the alkyl chains. Due to the decreasing rates of surfactant release from absorbent with increasing alkyl chain length, the nature of oil film dispersion by the surfactant infused absorbent sheets (Fig. 3.6a & b) is quite different from that observed when the surfactant is directly pipetted over the air-water interface (Fig. 3.8).

Distances propelled by the surfactant-driven absorbent sheets have been quantified in Figure 3.9. Since the sheets propel due to the process of spreading, distance travelled is representative of the process of surfactant release and spreading. This explains the correspondence between the trend of plots in Fig. 3.6a and Fig. 3.9. Also, there is correspondence between the total distance propelled (Fig. 3.9) and the amount of oil absorbed (Fig. 3.6a) in the case of SDS and STS driven sheets, in agreement with the weight-distance correlation; whereas, in the case of SHS driven sheet, oil collection is predominantly diffusion-driven.

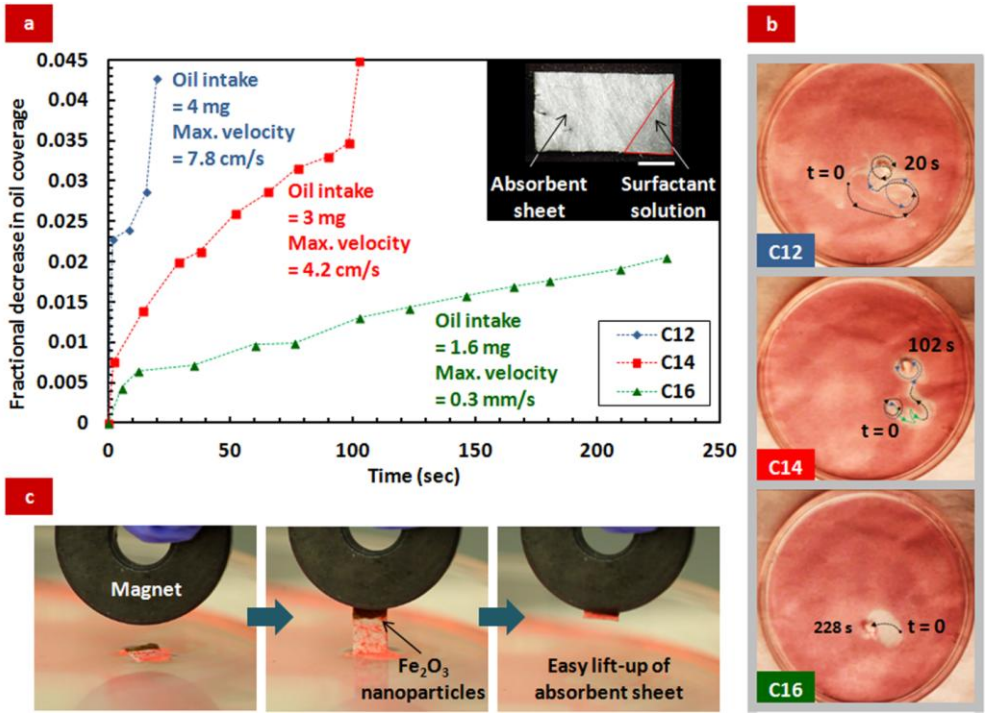

Figure 3.6 (a) Fractional decrease in oil coverage vs. time for absorbent sheets (inset at top right corner, scale bar = 2 mm) propelled with sodium dodecyl sulfate (C12), sodium tetradecyl sulfate (C14) and sodium hexadecyl sulfate (C16). Total amount of oil absorbed and maximum propulsion velocity for each case have also been listed. (b) Snapshots of the Petri dish surface at the end of the motion for C12, C14 and C16 driven absorbent sheets showing the trajectories of sheet movement. (c) Snapshots demonstrating pick-up of an absorbent sheet, incorporated with iron oxide nanoparticles, using a magnet.

The dimensions of these oil-gathering particles can be easily scaled up or down and their shape can be optimized. The addition of a magnetic component into the self-propelling absorbent sheets (details in Section 3.2) could enable easy pick-up of the sheets out of water using a magnet after the oil is collected (as exemplified in Fig. 3.6c), which can also be used for magnetically compressing the stored oil out of the particle mass. Moreover, such particles can be designed using multiple combinations of oil absorbent matrix and surface-active material. Novel oil sorbents, that are being tested and developed actively by numerous research groups,[8-19,21-24] can be mobilized to create self-propelling particles.

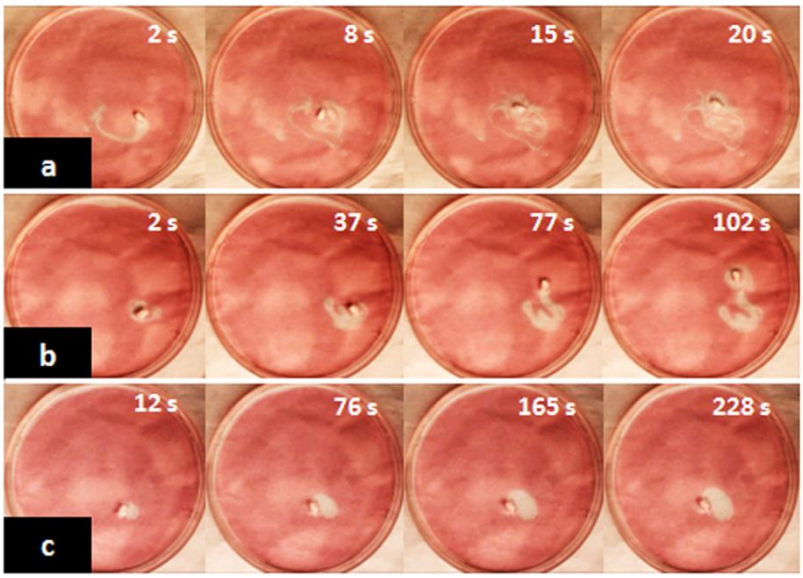

Figure 3.7 Snapshots of the Petri dish surface illustrating the differences between the dispersion of the oil film by absorbent sheets driven by (a) SDS, (b) STS and (c) SHS.

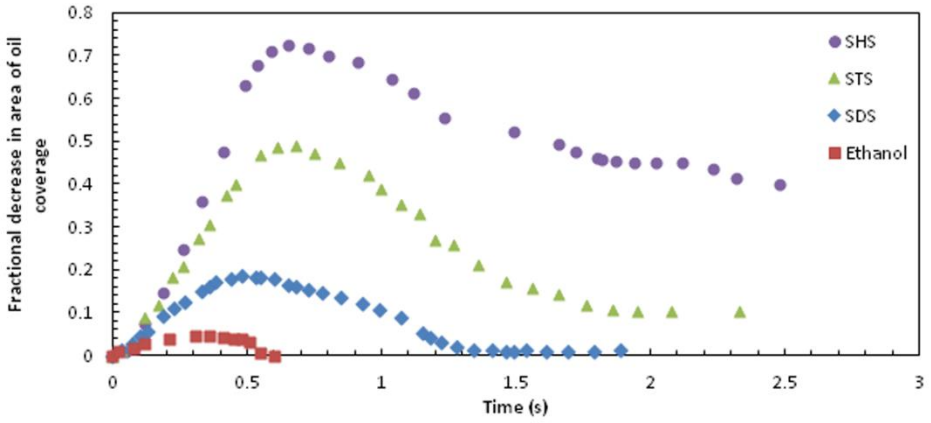

Figure 3.8 Plots showing the decrease in the area of oil spread on water due to spreading of three members of the homologous series of sodium n-alkyl sulfates, SDS, STS and SHS, dissolved in 50% v/v ethanol-water solution and the spreading of just the 50% v/v ethanol-water solution. Positive slope represents surfactant film spreading (compression of oil film) and negative slope represents its collapse (re-spreading of oil film).

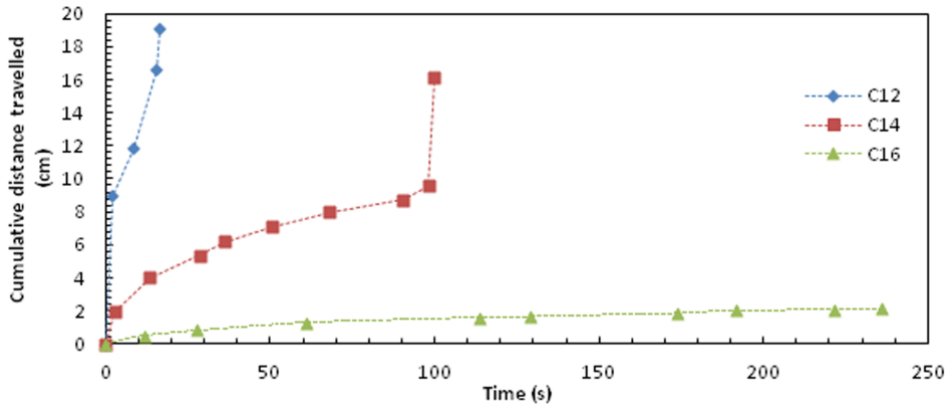

Figure 3.9 Plot comparing the distance propelled in oil by absorbent sheets driven by spreading of three members of the homologous series of sodium n-alkyl sulfates (SDS, STS, SHS) dissolved in 50% v/v ethanol-water solution.

3.4 Conclusions

In conclusion, we have demonstrated that the incorporation of oil absorbents into autonomously moving particles radically enhances the rate of oil absorption and dispersion relative to the currently used immobile absorbents. While the benefits and disadvantages of applying chemical dispersants for dealing with oil spills are still being debated,[28] the simple approach described here demonstrates the potential of self-propelling particles to drastically increase the speed and efficiency of a number of engineering processes requiring rapid transport of a solute or phase to a solid absorbent and/or catalyst. For example, asymmetric catalytic particles propel osmotically by generating a concentration gradient of reaction products around them.[29,30] We believe such self-propelling catalytic particles can accelerate the rate of a reaction to a greater extent relative to passive catalysts, owing to enhanced (convective) flux of reactants towards them.

3.5 Acknowledgements

We thank the NCSU Office of Undergraduate Research for providing research grant to Lisa D'Costa. The useful discussions with Dr. Dimiter Petsev (UNM) are gratefully acknowledged.

3.6 References

1. Mallouk, T. E., Sen, A. Powering Nanorobots. *Sci. Am.* **300,** 72-77 (2009).

2. Wang, J. Can Man-Made Nanomachines Compete with Nature Biomotors? *ACS Nano* **3,** 4-9 (2009).

3. Mirkovic, T., Zacharia, N. S., Scholes, G. D., Ozin, G. A. Fuel for Thought: Chemically Powered Nanomotors Out-Swim Nature's Flagellated Bacteria. *ACS Nano* **4,** 1782-1789 (2010).

4. Ebbens, S. J., Howse, J. R. In pursuit of propulsion at the nanoscale. *Soft Matter* **6,** 726-738 (2010).

5. Sengupta, S., Ibele, M. E., Sen, A. Fantastic Voyage: Designing Self-Powered Nanorobots. *Angew. Chem. Int. Ed.* **51,** 8434-8445 (2012).

6. Wang, J., Gao, W. Nano/Microscale Motors: Biomedical Opportunities and Challenges. *ACS Nano* **6,** 5745-5751 (2012).

7. Patra, D. *et al*. Intelligent, self-powered, drug delivery systems. *Nanoscale* **5,** 1273-1283 (2013).

8. Oh, Y. S., Maeng, J., Kim, S. J. Use of microorganism-immobilized polyurethane foams to absorb and degrade oil on water surface. *Appl. Microbiol. Biotechnol.* **54,** 418-423 (2000).

9. Ono, T., Sugimoto, T., Shinkai, S., Sada, K. Lipophilic polyelectrolyte gels as super-absorbent polymers for nonpolar organic solvents. *Nat. Mater.* **6,** 429-433 (2007).

10. Yuan, J. *et al.* Superwetting nanowire membranes for selective absorption. *Nat. Nanotechnol.* **3,** 332-336 (2008).

11. Gui, X. *et al.* Carbon Nanotube Sponges. *Adv. Mater.* **22,** 617-621 (2010).

12. Choi, S. J. *et al.* A Polydimethylsiloxane (PDMS) Sponge for the Selective Absorption of Oil from Water. *ACS Appl. Mater. Interfaces* **3,** 4552-4556 (2011).

13. Korhonen, J. T., Kettunen, M., Ras, R. H. A., Ikkala, O. Hydrophobic Nanocellulose Aerogels as Floating, Sustainable, Reusable, and Recyclable Oil Adsorbents. *ACS Appl. Mater. Interfaces* **3,** 1813-1816 (2011).

14. Cheng, M. *et al.* A Functionally Integrated Device for Effective and Facile Oil Spill Cleanup. *Langmuir* **27,** 7371-7375 (2011).

15. Diego-Taboada, A. *et al.* Sequestration of edible oil from emulsions using new single and double layered microcapsules from plant spores. *J. Mater. Chem.* **22,** 9767-9773 (2012).

16. Carmody, O., Frost, R., Xi, Y., Kokot, S. Adsorption of hydrocarbons on organo-clays - Implications for oil spill remediation. *J. Colloid Interf. Sci.* **305,** 17-24 (2007).

17. Lei, W., Portehault, D., Liu, D., Qin, S., Chen, Y. Porous boron nitride nanosheets for effective water cleaning. *Nat. Commun.* **4,** 1777 (2013).

18. Shang, Y. *et al.* An *in situ* polymerization approach for the synthesis of superhydrophobic and superoleophilic nanofibrous membranes for oil-water separation. *Nanoscale* **4,** 7847-7854 (2012).

19. Zhang, X., Li, Z., Liu, K., Jiang, L. Bioinspired Multifunctional Foam with Self-Cleaning and Oil/Water Separation. *Adv. Funct. Mater.* **23,** 2881-2886 (2013).

20. Machlis, G. E., McNutt, M. K. Scenario-Building for the Deepwater Horizon Oil Spill. *Science* **329,** 1018-1019 (2010).

21. Adebajo, M. O., Frost, R. L., Kloprogge, J. T., Carmody, O., Kokot, S. Porous Materials for Oil Spill Cleanup: A Review of Synthesis and Adsorbing Properties. *J. Porous Mat.* **10,** 159-170 (2003).

22. Zhu, Q., Tao, F., Pan, Q. Fast and Selective Removal of Oils from Water Surface via Highly Hydrophobic Core-Shell Fe_2O_3@C Nanoparticles under Magnetic Field. *ACS Appl. Mater. Interfaces* **2,** 3141-3146 (2010).

23. Thanikaivelan, P., Narayanan, N. T., Pradhan, B. K., Ajayan, P. M. Collagen based magnetic nanocomposites for oil removal applications. *Sci. Rep.* **2,** 230 (2012).

24. Calcagnile, P. *et al.* Magnetically Driven Floating Foams for the Removal of Oil Contaminants from Water. *ACS Nano* **6,** 5413-5419 (2012).

25. Guix, M. *et al.* Superhydrophobic Alkanethiol-Coated Microsubmarines for Effective Removal of Oil. *ACS Nano* **6,** 4445-4451 (2012).

26. Sharma, R., Chang, S. T., Velev, O. D. Gel-Based Self-Propelling Particles Get Programmed To Dance. *Langmuir* **28,** 10128-10135 (2012).

27. Varga, I., Meszaros, R., Gilanyi, T. Adsorption of Sodium Alkyl Sulfate Homologues at the Air/Solution Interface. *J. Phys. Chem. B* **111,** 7160-7168 (2007).

28. Schrope, M. Researchers debate oil-spill remedy. *http://www.nature.com/news/researchers-debate-oil-spill-remedy-1.12267#/ref-link-3* (2013).

29. Córdova-Figueroa, U. M., Brady, J. F., Shklyaev, S. Osmotic propulsion of colloidal particles *via* constant surface flux. *Soft Matter* **9,** 6382-6390 (2013).

30. Golestanian, R., Liverpool, T. B., Ajdari, A. Propulsion of a molecular machine by asymmetric distribution of reaction products. *Phys. Rev. Lett.* **94,** 220801 (2005).

CHAPTER 4

Biocatalytic Self-Propelling Particles

4.1 Introduction

A drawback in the design of Marangoni effect driven self-propelling particles, described in Chapters 2 and Chapter 3, is that their motion is dependent on the amount of fuel (surface-active material) present in the gel. This limitation can be overcome by loading these particles with a catalyst that can power their motion but does not get consumed in the process. With this objective in mind, we designed "hybrid" biogenic or biocatalytic particles composed of both live and synthetic elements, where live cells are employed as catalyst for generating chemical concentration gradient across the particles to facilitate their propulsion (the particles act as bio-reactors).

We have utilized yeast cells as catalyst to provide energy for propulsion to these particles through two different processes of glucose fermentation and hydrogen peroxide (H_2O_2) decomposition. Glucose and H_2O_2, which act as fuel in these processes, are present outside the particle. Therefore, these yeast boats can propel as long as glucose or hydrogen peroxide is available in their surroundings, in principle, by harvesting energy from the catalytic activity of yeast cells. Although synthetic catalysts[1-7] and isolated enzymes[8,9] have been used previously for propelling objects in liquids, in our knowledge such biocatalytic particles that use intact live cells for catalysis have not been reported previously.

4.2 Experimental Section

We tested various configurations of yeast boats (Figure 4.1). The boats contained yeast packed near one end of an intact or half-cut 5-7 mm long, 0.050" ID × 0.090" OD, Tygon microbore tubing (Saint-Gobain). Yeast (Fleischmann's active dry yeast) was immobilized within the hydrogel (polyacrylamide, agarose and alginate) or layers of polyelectrolyte before being packed into the tubing.[10-12] Polyacrylamide hydrogel precursor solution was prepared by mixing monomer acrylamide, cross-linker N,N'-Methylenebisacrylamide and initiator 2,2-Dimethoxy-2-Phenylacetophenone (Sigma) in deionized (DI) water in the ratio 1:0.1:0.01 by weight. The solution contained 11% w/w of monomer. Agarose gel precursor solution contained 1% w/w agarose (Acros Organics) in deionized (DI) water heated over a hot plate. Yeast was mixed with the uncured gel solution and filled into the tubing prior to gelation by

10 min UV treatment (Model B-100A, Black-Ray) in the case of polyacrylamide gel or cooling in the case of agarose gel. Yeast was immobilized in alginate gel by firstly hydrating it in 0.1 M pH 7 phosphate buffer to prepare 10% w/w yeast suspension. This suspension was mixed with equal volume of a solution of 4% w/w sodium alginate (Fluka Biochemika) in DI water. This solution was pipetted drop-wise into a solution of 1.5% w/w calcium chloride (Acros Organics) in DI water to (instantly) form beads of alginate gel with immobilized yeast, that were packed into the tubing. We also immobilized yeast with solutions of 5%, 10% and 20 % w/w polyelectrolyte (Poly-styrene sulfonic acid sodium salt or PSS (Polysciences) and Poly-dimethyldiallylammonium chloride or polyDADMAC (Sigma)) in DI water. This was done by either mixing yeast directly with polyelectrolyte solutions or by layer-by-layer injection of yeast and polyelectrolyte solutions into the tubing. In Fig. 4.1d & g, one end of the tubing was closed with a gel plug (agarose, polyacrylamide or alginate gel of same composition as that used for immobilizing yeast), and in Fig 4.1g the other end of the tubing was closed with a polydimethylsiloxane (PDMS) plug which prevents any mass-transfer from taking place. PDMS plug was fabricated by filling the Sylgard 184 PDMS precursor (Dow Corning) into the plastic tubing before curing at 70 ^{o}C. The cured plug was squeezed from the template tubing using tweezers, cut to 1 mm length, and inserted in the yeast boat. In Fig. 4.1e a film of polystyrene latex microspheres 0.72 and 8.7 μm diameter (Interfacial Dynamics Corp.) was deposited on the yeast-end of the tubing by dip-coating. Experiments were carried out in solutions of 0-3% w/w H_2O_2 (Topical solution USP) in DI water or in a solution of 0.8 M glucose (Sigma) in DI water. DI water (18.2 MΩ.cm at 25 °C), was obtained from a Millipore Milli-Q Academic water purification system (Billerica, MA). We varied different parameters such as the amount of yeast, concentration of glucose, cross-linking ratio of hydrogels in our experiments to optimize the motion of biocatalytic particles. These results have been discussed in the following sections along with the details on such parameters.

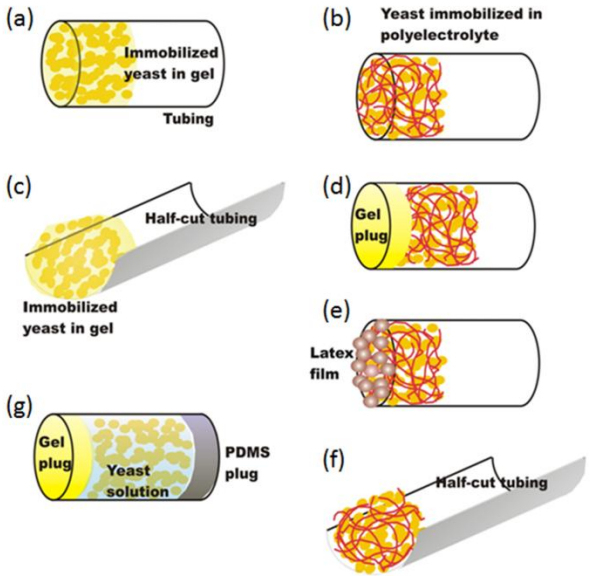

Figure 4.1 Schematic showing different designs of biocatalytic particles. Yeast immobilized using hydrogel or polyelectrolyte matrix is contained at one edge of intact or half-cut plastic tubing in (a)-(f). In (d) and (e), one end of the tubing is plugged with a gel plug or latex film. In (g), yeast suspension in water is encapsulated within the tubing with PDMS and hydrogel plugs at its ends.

4.3 Results and Discussion

4.3.1 Glucose Fermentation

Yeast catalyzes the breakdown of glucose in order to obtain energy (metabolism), producing ethanol and carbon-dioxide as by-products.

$$C_6H_{12}O_6 \xrightarrow{Yeast} 2\ C_2H_5OH + 2\ CO_2 \uparrow$$

The process of fermentation by yeast has been employed immensely for the production of bread and alcoholic beverages. We hypothesized that particles comprising of yeast cells could propel in glucose solution by harvesting energy from the process of fermentation (Figure 4.2a). Release of ethanol from one end of the particle would lead to surface tension asymmetry across it as ethanol lowers the surface tension of water, causing a net propulsion force to act on the particle due to Marangoni effect.[13-14]

In the case of configurations illustrated in Fig. 4.1a & c we did not observe satisfactory particle motion possibly due to additional diffusion limitation to mass-transfer

offered by the hydrogel plug;[15-17] whereas for the configuration in Fig. 4.1b, we observed rupturing of the polyelectrolyte matrix that we believe is caused due to the pressure build-up from CO_2 generation. In the case of Fig. 4.1g, when we mixed glucose with the yeast solution within the tubing, we observed bubble formation (along with propulsion of the particle by diffusion of generated ethanol out of the hydrogel) that eventually forced the hydrogel plug out of the tubing. Whereas, when we added glucose to the solution surrounding the particle, we observed development of bubbles near the hydrogel end of the tubing that finally pushed the hydrogel out and we did not observe substantial particle motion. Similarly, for the configurations illustrated in Fig. 4.1d & e, we found that the gel plug and the latex film were not rigid enough to hold the yeast inside the tubing against the pressure build-up by CO_2 generation. We overcame these issues by using the configuration in Fig. 4.1f. We did not observe rupturing of the polyelectrolyte matrix in this design because the pressure build-up by CO_2 generation was relatively low as the tubing was half-cut and open to the surrounding air. Figure 4.2b is the cumulative distance versus time plot of a yeast boat (comprising of 0.4 mg baker's yeast immobilized with 0.4 mg of a solution of 10% w/w PolyDADMAC in DI water in a half-cut tubing, as shown in Fig. 4.2a) moving in a solution of 0.8 M glucose in DI water. The average speed of the yeast boat during the latter 5 hrs of the total of 10 hrs spent in glucose solution is 10 μm/s. This velocity magnitude is of the same order as that observed when the particle was floated in just water (no glucose). The insignificant propulsion force on the particle could be due to multiple factors such as the slow rate of the glucose fermentation process,[18] small amount of yeast present in the particle (0.4 mg), and high viscosity of 0.8 M glucose solution.[19] We overcome some of these limiting factors inhibiting the particle motion by using H_2O_2 as a medium for propulsion in place of glucose, as discussed in the following section.

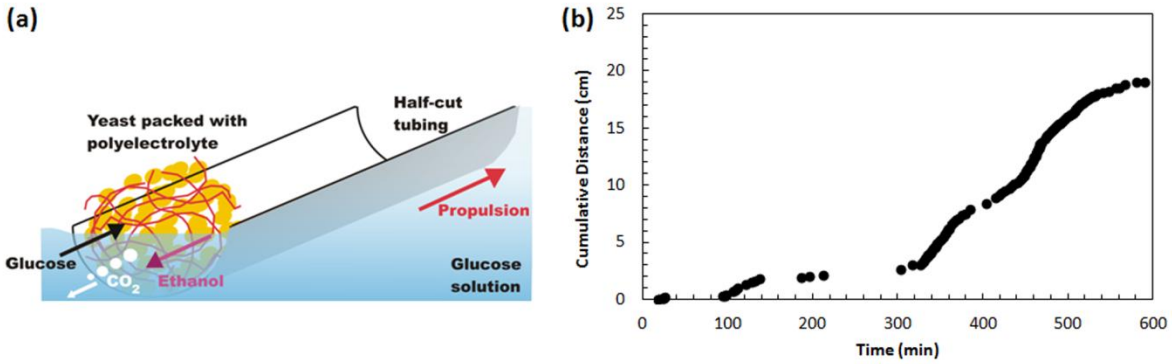

Figure 4.2 (a) Schematic showing the propulsion mechanism of a yeast boat in glucose solution. Fermentation of glucose releases ethanol which propels the particle by Marangoni effect. (b) Plot of cumulative distance versus time of a yeast boat, design similar to that in (a), propelling in glucose solution.

4.3.2 Hydrogen Peroxide Decomposition

Yeast catalyzes the decomposition of hydrogen peroxide (H_2O_2) into water and oxygen as H_2O_2 is toxic to yeast.

$$2H_2O_2 \xrightarrow{Yeast} 2H_2O + O_2 \uparrow$$

This process is very vigorous - one molecule of catalase enzyme can decompose ~10^5 molecules of H_2O_2 per second.[20-21] We hypothesized that yeast in the particle would convert H_2O_2 present in its surroundings into water and oxygen. In addition to the recoil from bubble release, bursting of the generated O_2 bubbles near one end of the particle would also result in its propulsion due to spreading of the thin film around the bubbles as the film ruptures and collapses,[22] as illustrated in Figure 4.3.

Since H_2O_2 is toxic to yeast, we tested the viability of yeast cells in H_2O_2 solution by staining them with fluorescein diacetate (FDA) dye. No reduction in fluorescent intensity of cells was observed after two hours in H_2O_2 solution (Figure 4.4a), indicating that the cell were still viable; whereas significant reduction in fluorescence occurred after letting the cells stay in H_2O_2 solution for a week (Figure 4.4b), compared to glucose solution (Figure 4.4c). Redox titration studies were performed to test for the rate of decomposition of H_2O_2 solution

by the yeast boat using potassium permanganate as an oxidizing agent. We found that the decrease in H_2O_2 concentration over a period of four hours was only ~6% (Figure 4.4c).

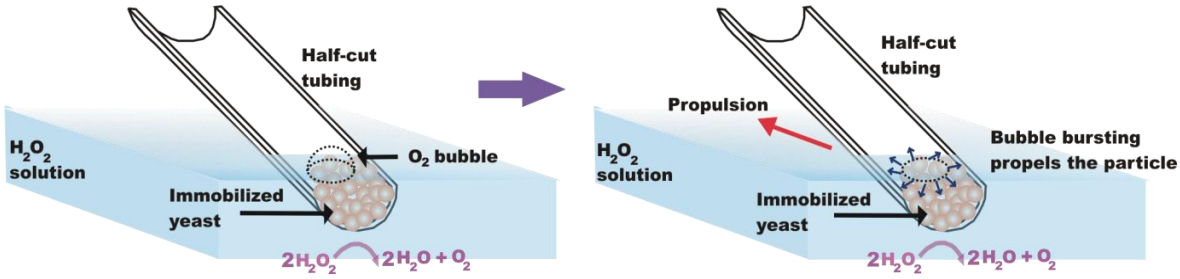

Figure 4.3 Schematic illustrating the propulsion mechanism of a yeast boat in hydrogen peroxide solution based on the bursting of oxygen bubbles at one end of the particle containing immobilized yeast cells.

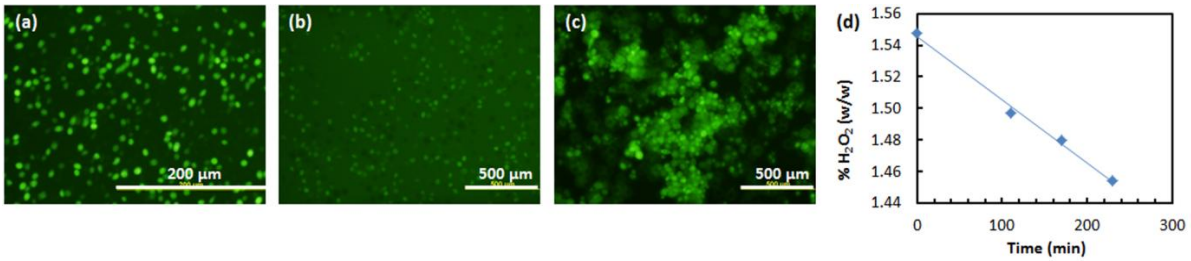

Figure 4.4 Fluorescent intensity is an indicator of cell viability. Yeast cells are still viable after remaining in H_2O_2 solution for 2 hrs (a). There is a significant decrease in viability after 1 week in H_2O_2 solution (b), but the cells are still viable after 1 week in glucose solution (c). (d) Plot illustrating the rate of H_2O_2 decomposition with time due to propulsion of the yeast boat.

The plots of cumulative distance versus time for yeast boats (comprising of 0.4 mg baker's yeast immobilized with 0.3 mg of a solution of 10% w/w PSS in DI water in a half-cut tubing, as shown in Fig. 4.1f) in 3% and 1.5% w/w H_2O_2 solutions, are presented in Figure 4.5a. The average speed of yeast boat in 3% H_2O_2 solution is 0.45 mm/s, whereas in 1.5% H_2O_2 solution it is 0.19 mm/s. The speed of the yeast boat is an order of magnitude

higher in H_2O_2 solution compared to glucose solution for the same amount of yeast present in the yeast boat. This is because the rate of H_2O_2 decomposition by yeast is faster compared to the rate of glucose fermentation and the viscosity of H_2O_2 solution is lower than the viscosity of glucose solution. We can see from the plots in Figure 4.5a that the motion is short-lasting in H_2O_2 solution. In 3% H_2O_2, motion lasted for about 3 min and in 1.5% H_2O_2 for 6 min. This is because the polyelectrolyte packing cannot withstand the high rate of bubble generation and eventually ruptures. Particle stability was higher with the configuration illustrated in Figure 4.1c comprising of yeast immobilized within alginate gel (composition described in the Experimental Section), where we observed propulsion for more than 2 hours as shown in Fig. 4.5b. Due to the additional diffusion limitation to mass-transport offered by the hydrogel, the average speed of the particle with this design was smaller than the case when yeast was immobilized with polyelectrolytes.

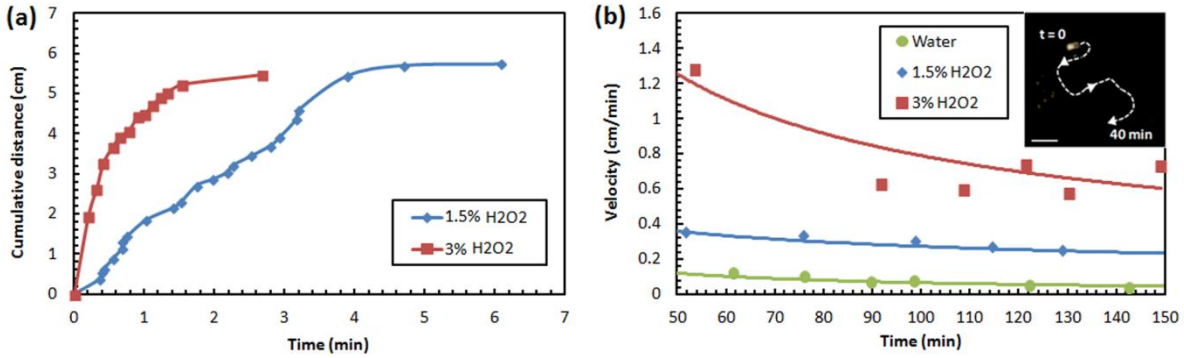

Figure 4.5 (a) Plot of cumulative distance versus time of yeast boats, design similar to that in Fig. 4.1f, propelling in 1.5% and 3% w/w H_2O_2 solutions. (b) Plot of velocity against time of yeast boats, design similar to that in Fig. 4.1c, propelling in water and H_2O_2 solutions (1.5% and 3% w/w). Inset shows the trajectory of such a yeast boat in 1.5% w/w H_2O_2 solution (scale bar = 1 cm).

Based on the propulsion mechanism of the yeast boat in H_2O_2 solution, we correlated its velocity *v* to the process of bubble-bursting as,

$$v = \alpha \times r \times f \tag{4.1}$$

where *r* is the radius of the generated oxygen bubbles, f is the frequency of bubble bursting and α is the proportionality constant. We obtained *v*, *r* and *f* as a function of time by analyzing the frames of the experimental movies of particle propulsion. The product of *r* and *f* was fitted to the particle velocity data (Figure 4.6a) and α, used as a fitting parameter, was estimated to be 0.74. This is a reasonable value as it implies that the particle moves an average distance of 0.74 cm when a bubble of 1 cm radius bursts. When surfactant (sodium dodecyl sulfate or SDS) was added to H_2O_2 solution, the generated oxygen bubbles were smaller in size and stable (did not burst). This severely inhibited particle propulsion – particle was slowly drifted forwards by the growing tail of released bubbles behind it as shown in Figure 4.6b, which reminds of the propulsion of a *Listeria* bacterium by the polymerization and cross-linking of actin protein into a comet-like tail behind the bacterium.[23,24]

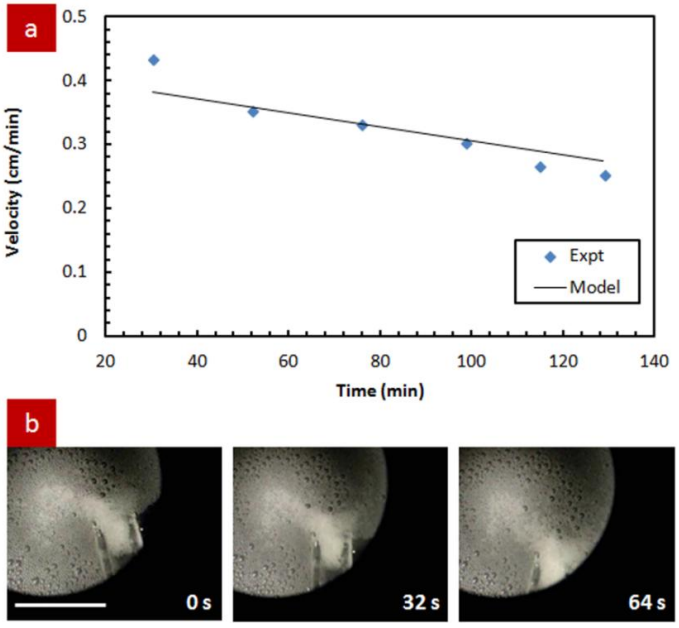

Figure 4.6 (a) Plot of velocity against time of a particle comprising of yeast immobilized in alginate gel, design similar to that in Fig. 4.1c, propelling in 1.5% w/w H_2O_2 solution. The experimental data is fitted with the product of bubble size and frequency of bubble bursting using eqn (4.1). (b) Snapshots showing the propulsion of a yeast boat in 1.5% w/w H_2O_2 solution due to a growing tail of released oxygen bubbles that are stable due to the addition of SDS (1 mM) into H_2O_2 solution (scale bar = 5 mm).

4.4 Conclusions

In this chapter, we have presented biocatalytic self-propelling particles that employ yeast cells for catalyzing the processes of glucose fermentation or hydrogen peroxide decomposition, which provides them with the energy for propulsion. We tested several particle designs to optimize the stability and propulsion of the yeast boats. We found that the particle motion in glucose solution was much slower compared to that in H_2O_2 solution due to the rapid rate of H_2O_2 decomposition and lower viscosity of H_2O_2 solution. Such catalytic self-propelling particles can be made to propel for long durations by replenishing the "fuel" in their surrounding medium, unlike the on-board fuel driven particles. Our work is the first demonstration of employing live cells directly as catalysts for generation of motion. Using intact live cells directly is a far simpler alternative to isolating enzymes from live cells and integrating them with synthetic components for catalysis driven propulsion. We believe our research will stimulate further exploration of novel catalyst-fuel combinations for development of such particles.

Both Marangoni effect driven and biocatalytic self-propelling particles exhibit powered random motion, as their motion trajectories are unpredictable. The next chapter of this dissertation is focused on the diode based self-propelling particles, whose direction of motion can be precisely controlled by remote steering, in contrast to the particles described in the previous chapters.

4.5 References

1. Ismagilov, R. F., Schwartz, A., Bowden, N., Whitesides, G. M. Autonomous movement and self-assembly. *Angew. Chem. Int. Edit.* **41,** 652-654 (2002).

2. Vicario, J. *et al*. Catalytic molecular motors: fuelling autonomous movement by a surface bound synthetic manganese catalase. *Chem. Commun.* 3936-3938 (2005).

3. Gibbs, J. G., Zhao, Y. P. Autonomously motile catalytic nanomotors by bubble propulsion. *Appl. Phys. Lett.* **94,** 163104 (2009).

4. Mei, Y. F. *et al*. Versatile Approach for Integrative and Functionalized Tubes by Strain Engineering of Nanomembranes on Polymers. *Adv. Mater.* **20,** 4085-4090 (2008).

5. Manesh, K. M. *et al*. Template-Assisted Fabrication of Salt-Independent Catalytic Tubular Microengines. *ACS Nano* **4,** 1799-1804 (2010).

6. Mei, Y. F., Solovev, A. A., Sanchez, S., Schmidt, O. G. Rolled-up nanotech on polymers: from basic perception to self-propelled catalytic microengines. *Chem. Soc. Rev.* **40,** 2109-2119 (2011).

7. Dey, K. K., Senapati, K. K., Phukan, P., Basu, S., Chattopadhyay, A. Stable Magnetic Chemical Locomotive with Pd Nanoparticle Incorporated Ferromagnetic Oxide. *J. Phys. Chem. C* **115,** 12708–12715 (2011).

8. Sanchez, S., Solovev, A. A., Mei, Y., Schmidt, O. G. Dynamics of Biocatalytic Microengines Mediated by Variable Friction Control. *J. Am. Chem. Soc.* **132,** 13144–13145 (2010).

9. Pantarotto, D., Browne, W. R., Feringa, B. L. Autonomous propulsion of carbon nanotubes powered by a multienzyme ensemble. *Chem. Commun.* 1533-1535 (2008).

10. Svaldo-Lanero, T. *et al*. Morphology, mechanical properties and viability of encapsulated cells. *Ultramicroscopy* **107,** 913-921 (2007).

11. Mei, L.-H., Yao, S.-J. Cultivation and modelling of encapsulated *Saccharomyces cerevisiae* in NaCS-PDMDAAC polyelectrolyte complexes. *J. Microencapsul.* **19,** 397-405 (2002).

12. Behera, S., Mohanty, R. C., Ray, R. C. Comparative study of bio-ethanol production from mahula (*Madhuca latifolia* L.) flowers by *Saccharomyces cerevisiae* and *Zymomonas mobilis*. *Appl. Energ.* **87,** 2352-2355 (2010).

13. Scriven, L. E., Sternling, C. V. The Marangoni Effects. *Nature* **187,** 186-188 (1960).

14. Suciu, D. G., Smigelschi, O., Ruckenstein, E. Spreading of Liquids on Liquids. *J. Colloid Interf. Sci.* **33,** 520-528 (1970).

15. Yankov, D. Diffusion of glucose and maltose in polyacrylamide gel. *Enzyme Microb. Tech.* **34,** 603-610 (2004).

16. Zhang, T., Fang, H. H. P. Effective Diffusion Coefficients of Glucose in Artificial Biofilms. *Environ. Technol.* **26,** 155-160 (2005).

17. Estapé, D., Gòdia, F., Solà, C. Determination of glucose and ethanol effective diffusion coefficients in Ca-alginate gel. *Enzyme Microb. Tech.* **14,** 396-401 (1992).

18. van den Brink, J. *et al*. Dynamics of Glycolytic Regulation during Adaptation of *Saccharomyces cerevisiae* to Fermentative Metabolism. *Appl. Environ. Microbiol.* **74,** 5710-5723 (2008).

19. Bui, A. V., Nguyen, M. H. Prediction of viscosity of glucose and calcium chloride solutions. *J. Food Eng.* **62,** 345-349 (2004).

20. Wang, Y. *et al*. Bipolar electrochemical mechanism for the propulsion of catalytic nanomotors in hydrogen peroxide solutions. *Langmuir* **22,** 10451-10456 (2006).

21. Aydemir, T., Kuru, K. Purification and partial characterization of catalase from chicken erythrocytes and the effect of various inhibitors on enzyme activity. *Turk. J. Chem.* **27,** 85-97 (2003).

22. Bird, J. C., de Ruiter, R., Courbin, L., Stone, H. A. Daughter bubble cascades produced by folding of ruptured thin films. *Nature* **465,** 759-762 (2010).

23. Carlier, M.-F. *et al*. Actin Depolymerizing Factor (ADF/Cofilin) Enhances the Rate of Filament Turnover: Implication in Actin-Based Motility. *J. Cell Biol.* **136,** 1307-1322 (1997).

24. Cameron, L. A., Giardini, P. A., Soo, F. S., Theriot, J. A. Secrets of actin-based motility revealed by a bacterial pathogen. *Nat. Rev. Mol. Cell. Biol.* **1,** 110-119 (2000).

CHAPTER 5

Remote Steering of Self-Propelling Microcircuits by Modulated Electric Field*

* Based on R. Sharma and O. D. Velev, *in preparation for Adv. Funct. Mater.*

5.1 Introduction

The science of complex functional particles is expanding rapidly towards new types of motile and self-propelling particles.[1-6] These particles carry a certain amount of propellant material, or convert the chemical or field energy from their environment into controlled directional motion. Novel techniques for propelling particles, a few millimeters or smaller in size, are being actively explored.[7-27] It can be hypothesized that in the not-so-distant future this research evolution will result in new types of "smart" particles that could move on their own, sense their environment and respond in highly specific ways.[28-37]

We have demonstrated previously a new class of self-propelling particles based on miniature semiconductor diodes powered by a global uniform alternating (AC) electric field.[38] The millimeter-sized diodes, floating on water, rectify the voltage induced between their electrodes. The resulting particle-localized electroosmotic (EO) flux propels them in the direction of either the cathode or the anode depending on their surface charge (Figure 5.1a). Interestingly, diode velocity was found to be independent of diode size and field frequency, which implies that they can be powered by contactless radio and microwave emitters. We also demonstrated that such self-propelling diodes exhibit complex functionalities. For example, light emission along with propulsion was displayed by light-emitting diodes (LEDs), whereas a rotor ring with diodes attached on its periphery exhibited rotational motion by harnessing the external uniform AC electric field. Similarly, diodes immobilized on the walls of microfluidic channels were shown to pump and mix liquids.[39] Recently semiconductor diode nanowires, synthesized by membrane template growth route, have also been propelled by the principle of AC electric field rectification.[40] These motile particles suggest rudimentary solutions to problems facing self-propelling microdevices, including harvesting power from external sources for propulsion and potential for a range of additional functions.

The next step in this direction is developing means of steering the moving microdevices. As illustrated in Figure 5.1b, rotating the orientation of the diode by 180^{o} reverses the direction of its motion (as the direction of counterionic flux near diode surface reverses).[38] In this work, we present a novel technique that allows us to remotely rotate the

orientation of the self-propelling diode, thereby steering it back and forth on-demand. The diodes rotate and reverse their direction of motion when a DC component (wave asymmetry) is introduced into the AC signal. This new principle of compounded AC+DC signal driven manipulation of the direction of motion of self-propelling diodes offers a first demonstration of the precise control of the motion and position of the swimming microdevices.

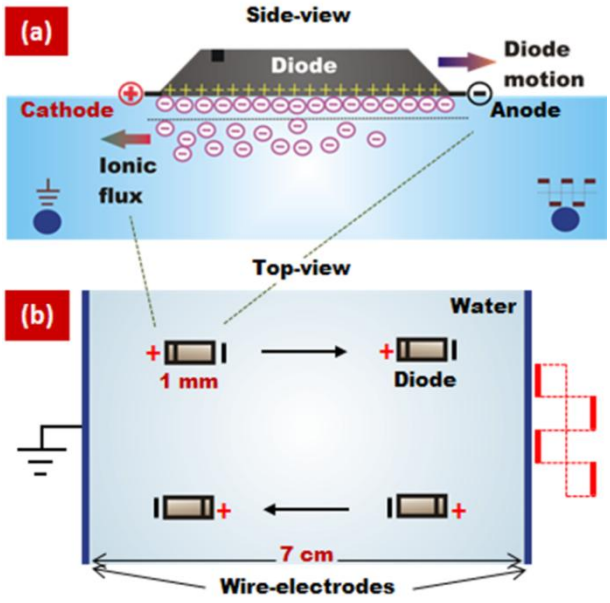

Figure 5.1 (a) Schematic illustrating the mechanism of self-propulsion of a diode, floating on water, due to electroosmosis near its surface powered by the DC potential drop across the diode. (b) DC potential drop across the diode results from the rectification of an external uniform AC electric field applied through the wire-electrodes across the Petri dish. Reversal in the orientation of the diode reverses its direction of motion as the direction of ionic flux near its surface reverses.

5.2 Experimental Section

The experiments were carried out in a plastic Petri dish of dimensions 9 cm x 9 cm x 1.5 cm in depth, with two thin wire electrodes at its bottom on opposite ends separated by a gap of 7 cm. Deionized (DI) water (18.2 MΩ cm at 25 °C), was obtained from a Millipore Milli-Q Academic water purification system (Billerica, MA). Silicon switching microdiodes (1.3 mm

× 0.9 mm × 0.65 mm, part number 1N4448HWTDICT-ND, Digi-Key Co.) were floated on the surface of DI water contained in the Petri dish, suspended by surface-tension. Square wave AC signal (800 V peak-to-peak, 1 kHz) was supplied to the wire-electrodes from a function generator (Agilent, 33120 A) and amplifier (Trek, PZD 700), and was monitored using an oscilloscope and a digital multimeter. Wave symmetry (duty cycle) was changed digitally from the function generator. Diode motion was observed under Olympus SZ-61 optical microscope and recorded with Sony DSC-V1 Cyber-Shot digital camera. The control experiment at the IEP of Petri dish was performed by lowering the pH of DI water to 5 by addition of HCl and the control experiment at the IEP of diode surface was performed by increasing the pH of DI water to 6.4 by addition of NaOH.

5.3 Results and Discussion

5.3.1 Effect of a Constant DC Field on Diode Motion

In our experimental setup, the millimeter-sized diode is freely floating over the water surface contained in a Petri dish and the electric field is applied through the two wire-electrodes across the bottom of the Petri dish surface (Fig. 5.1).When a uniform external AC field is applied to the electrodes, the self-propelling diode experiences only an alignment torque.[38,41] However, when a DC component is introduced into the external AC signal, rotational torque acts on the diode when the DC field across the diode is parallel with respect to the DC field across the wire-electrodes. We can relate this effect and think of it in terms of dipole-dipole interactions. The normalized energy of interaction, W, between the dipoles u_1 and u_2 in two parallel planes (Fig. 5.2) can be estimated by

$$\frac{w}{\left(\frac{u_1 u_2}{4\pi\varepsilon_0 \varepsilon r^3}\right)} = W = \cos\phi \tag{5.1}$$

where w is the interaction energy, ε_0 is the vacuum permittivity, ε is the relative permittivity of the medium, r is the separation distance between the two dipoles and ϕ is the rotation angle.[42] The two dipoles prefer to orient anti-parallel in relation to each other as the dipole-dipole interaction energy is minimized in this case, whereas the interaction energy is

maximum (unfavorable) when they align parallel to each other (Fig. 5.2). Similarly, the diode prefers to align such that the DC field across it is oriented anti-parallel to the external DC field. This phenomenon is observed because the DC potential drop across the diode always points in the direction of its anode (as illustrated in Fig. 5.1a) and hence, is dependent on the orientation of the diode. On the contrary, an isotropic material such as a piece of plastic would not show a preference for one orientation over other as the direction of DC potential drop across it will be independent of its orientation (drawing analogy to dipole-dipole interactions, the lower energy configuration in Fig. 5.2 will be unattainable for a plastic piece). We can also interpret this effect as the tendency of a diode to align itself in forward bias with respect to the field, as its polarizability is higher in this orientation.

A DC component can be introduced into an AC signal by changing the wave symmetry, also called duty cycle (Fig. 5.3a). Although application of DC fields provides an effective tool, in principle, for controlling the direction of diode motion, EO flows originating near the Petri dish surface (Fig. 5.3b) significantly affect the diode motion by drifting it forwards or backwards depending on the direction of external DC field, which is undesirable. These unwanted EO flows can be overcome by adjusting the pH of the liquid to the isoelectric point of the Petri dish surface. However, such fine tuning of the experimental conditions greatly limits the applicability of this technique.

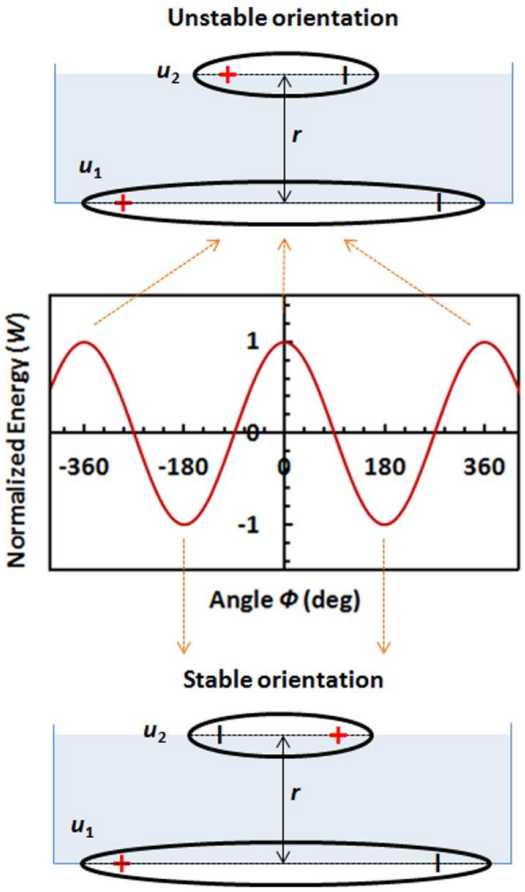

Figure 5.2 Dipoles u_1 and u_2 in two different planes prefer to orient anti-parallel with respect to each other as the dipole-dipole interaction energy is minimized in this case, whereas the interaction energy is maximized when they align parallel to each other. Similarly, a diode floating over the water surface prefers to orient such that the DC field across it is anti-parallel with respect to the DC field across the wire-electrodes.

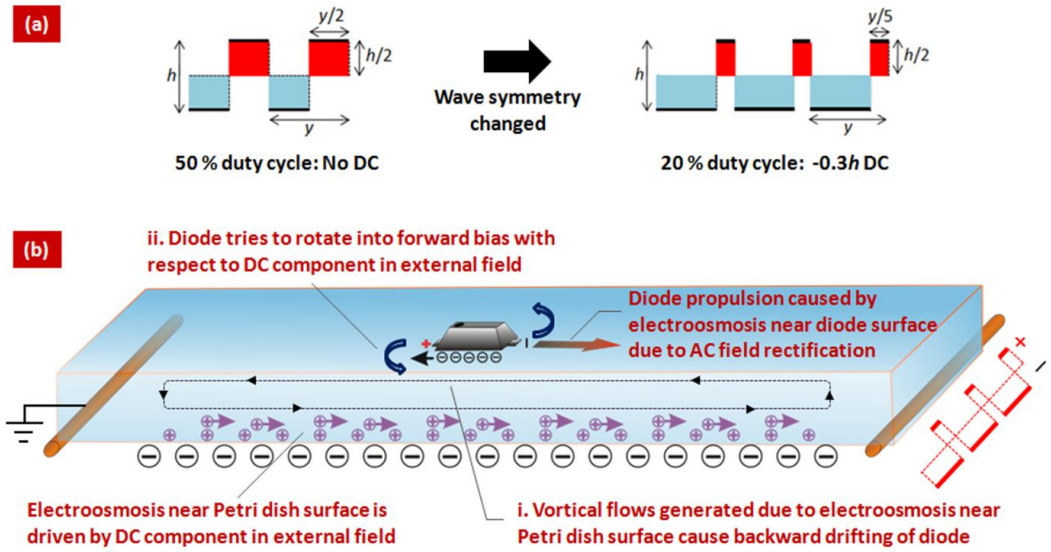

Figure 5.3 (a) A perfectly symmetric square wave has a duty cycle of 50% and there is no DC component present. When its duty cycle is changed to, for example, 20% - wave symmetry changes such that the signal is positive for 20% of the time in a cycle. Consequently, there is a net DC component present in this signal given by the time-average of the positive and negative components of the AC cycle = $[(y/5)\times(h/2) - (4y/5)\times(h/2)]/y = -0.3h$, as shown in the schematic. (b) Introduction of a DC component into the AC signal leads to two additional effects on a self-propelling diode – i. flows generated in the liquid due to electroosmosis near the Petri dish surface cause forward/backward drifting of the diode depending on the direction of the external DC field, ii. diode rotates to position itself in forward bias with respect to the external DC field (when it is oriented in reverse bias initially), which can also be interpreted as the tendency of the DC field/dipole across the diode to align itself anti-parallel with respect to the DC field/dipole across the wire-electrodes.

5.3.2 Effect of a Short-Lasting DC Field on Diode Motion

An alternative approach to induce rotational torque on the diode, while eliminating the undesirable effects of a constant external DC component, is to apply the DC field for only a short duration. This was implemented by transmitting the input signal through a capacitor before it reaches the wire electrodes (Fig. 5.4), since a capacitor tends to block the DC component in the signal as it charges (Fig. 5.5). For the short duration during which the capacitor charges, the diode responds to the external DC field as expected (Fig. 5.5a). It has a

tendency to orient/remain in forward bias with respect to the field, as explained in Fig. 5.2. Since the applied DC signal lasts for only a couple of seconds, its direct effect on the diode is temporary and does not alter the overall nature of diode motion except for the minor deviation observed during the short period when the capacitor is charging. However, once the external DC component is eliminated by the capacitor, there is an indirect effect of the applied DC pulse on the diode resulting from the counterion redistribution across the wire-electrodes (Fig. 5.5b). Counterion redistribution occurs during the applied DC pulse. After the DC component is removed, the field originating from the redistributed counterions, which is opposite in direction to the short-duration external DC field, influences the diode motion. The tendency of diode rotation is determined by its preference to be aligned such that the DC field across it is anti-parallel in relation to the counterionic field. As expected, the diode rotates when it is in reverse bias with respect to the counterionic field. Using this approach, introduction of short-duration DC pulses (caused due to charging of capacitor) allowed us to shuttle the self-propelling diode back and forth on the water surface on-demand as shown in Fig. 5.6, while overcoming the perturbation in diode motion from EO flows arising near the Petri dish surface.

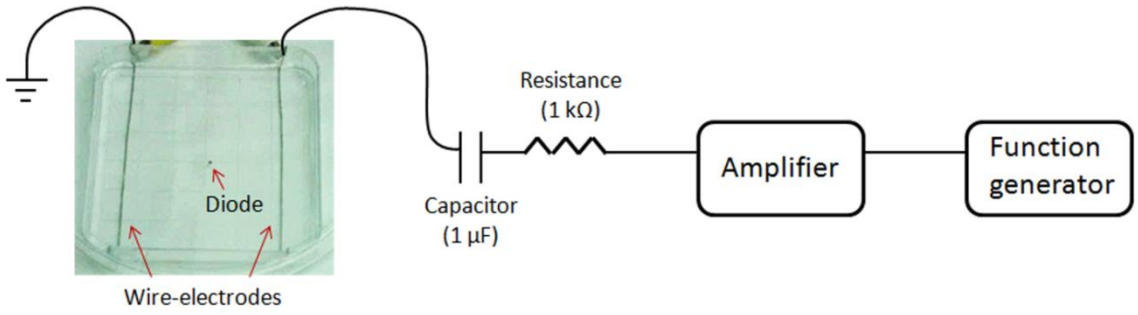

Figure 5.4 Experimental setup used for applying short-duration DC component to the wire-electrodes along with the AC signal. Capacitor blocks the DC component in the signal as it charges.

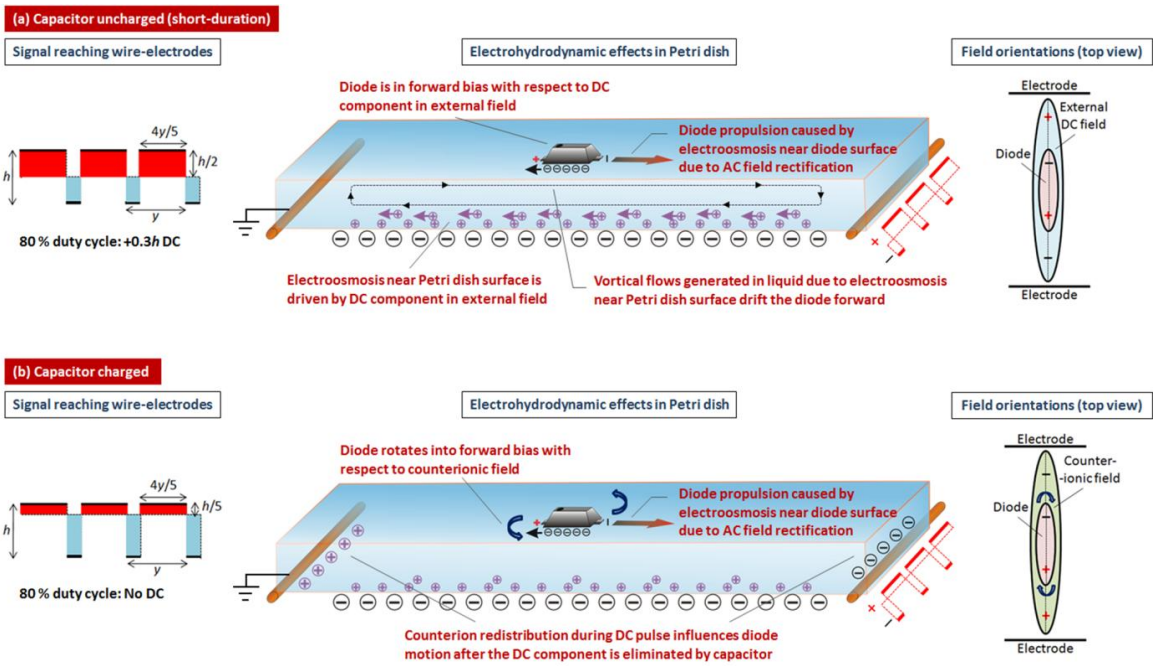

Figure 5.5 Schematic illustrating the nature of diode motion when a short-duration DC field is applied by blocking the DC component introduced into the AC signal through charging of a capacitor. (a) As the capacitor charges, self-propelling diode is affected by the external DC field. Since capacitor charging takes only a couple of seconds, these effects cause only a momentary perturbation in the diode motion. (b) Once the external DC component is eliminated by the capacitor, diode motion is influenced by the resulting counterion redistribution across the wire-electrodes. Diode tries to orient in forward bias with respect to the counterionic field, which is opposite in direction to the short-lasting external DC field.

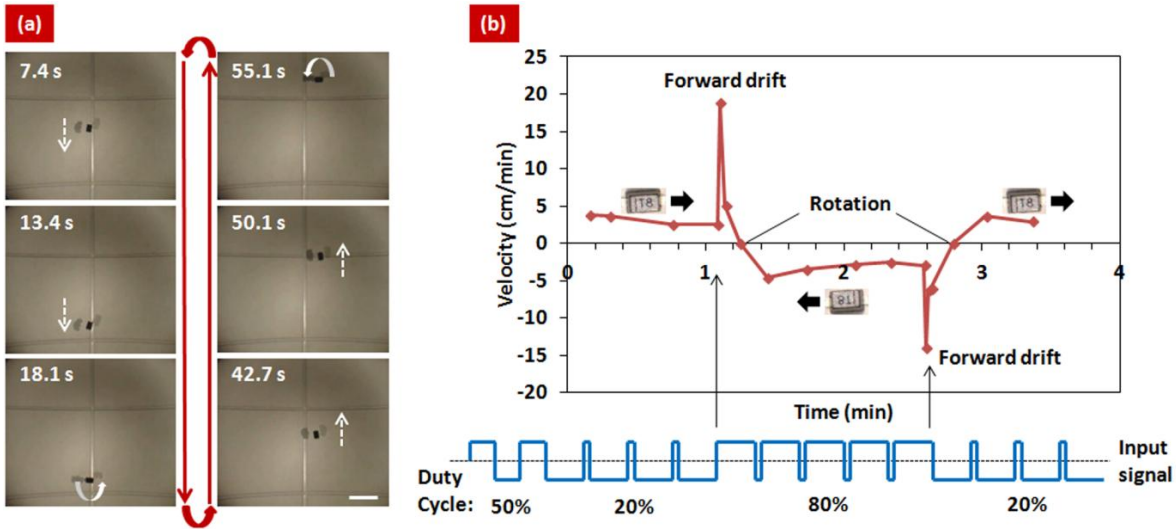

Figure 5.6 (a) Time-lapse snapshots of a millimeter-sized diode shuttling back and forth on water on-demand by introducing a short-duration DC component into the applied AC signal (scale bar = 5 mm). (b) Typical plot of velocity against time of a diode shuttling back and forth, along with a cartoon of the applied input signal (which is different from the signal reaching the wire-electrodes after passing through a capacitor, shown in Fig. 5.5 & 5.7). Rapid increase in diode velocity on changing the signal symmetry results from the short-lasting electroosmotic flows in the Petri dish while the capacitor charges, following which the diode rotates due to the resulting counterion redistribution.

When the same experiment was repeated with a piece of plastic, no rotation was observed as it is an isotropic material and therefore does not exhibit a preference for one orientation over another in the presence of the counterionic field. The plastic piece only drifts forwards-backwards driven by the short-lasting EO flows arising near the Petri dish surface during capacitor charging, which also affect the diode as illustrated in Fig. 5.5a. When the pH of water was lowered to the isoelectric point (IEP) of the Petri dish, rapid acceleration of the diode was not observed prior to rotation due to suppression of these EO flows. Rotation was still observed as counterion redistribution across the wire-electrodes still takes place. Similarly, when the pH was increased to the IEP of diode surface, diode self-propulsion was selectively inhibited in the absence of net ionic flux near the diode surface,[38] while it continued to respond to the short-duration DC field and the resulting counterion redistribution.

Interestingly, for the same sequential change in the duty cycle (wave symmetry) of the input signal, the initial magnitude of the DC voltage reaching the wire-electrodes for the case when the input signal was transmitted through a capacitor was twice the magnitude of the (constant) DC voltage for the case when capacitor was not used (Fig. 5.7). Table 5.1 summarizes the response of a self-propelling diode to a sequence of duty cycle change applied with and without a capacitor in the circuit, and compares the two cases.

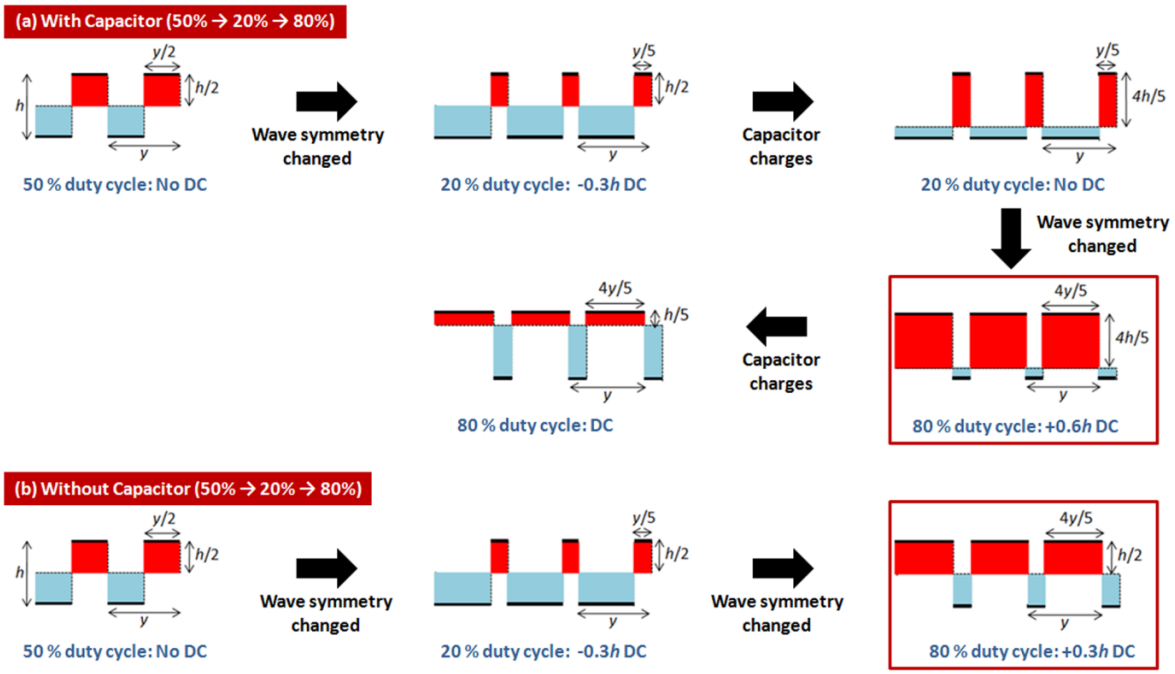

Figure 5.7 Schematic comparing the (cartoon of) signal reaching the wire-electrodes when the duty cycle of the input signal is changed from 50% → 20% →80% for the cases when (a) the signal passes through a capacitor before reaching the wire-electrodes and (b) the signal directly reaches the wire-electrodes. When the duty cycle is changed from 20% →80%, the initial magnitude of the DC voltage across the wire-electrodes in case (a) is twice the magnitude of the (constant) DC voltage in case (b).

Table 5.1 Summary of diode motion on water when the duty cycle of the AC signal is changed from 50% → 20% → 80% for with capacitor (short-duration DC) and without capacitor (constant DC) cases.

	Without capacitor		With capacitor	
50%	Propulsion		Propulsion	
20%	Tries to rotate (tilts) while drifting backwards		(i) Short-duration: tilts and stops (ii) Aligns and keep propelling ---->	
80%	Aligns again while drifting forwards		(i) Short-duration: forward drift (ii) Rotates and propels in opposite direction ---->	

5.3.3 Theoretical Estimations of Forces on Diode

Additionally, we have made back-of-the-envelope estimates of the rotational force acting on the diode from the counterion redistribution, and compared it to the alignment force and drag force experienced by the diode. Drawing analogy to the dipole-dipole interactions (Fig. 5.2), rotational torque on the diode was approximated by assuming it to be a finite dipole experiencing the field from the dipole resulting from counterion redistribution across the wire-electrodes. The orientation of the dipole across the diode with respect to the dipole across the wire-electrodes due to counterion redistribution has been shown in Fig. 5.8. The charge in the dipole u_1 across the wire electrodes resulting from counterionic redistribution was obtained from the Guoy-Chapman theory as[43]

$$q_1 = A \times \left(-\sqrt{8\varepsilon RTn_o} \sinh\left(\frac{vF\varphi_p}{2RT} \right) \right) = \pm 6.45 \times 10^{-7}\,\mathrm{C} \tag{5.2}$$

where q_1 is the charge in dipole u_1, A is the Petri dish surface area (49 cm^2), ε is the permittivity of water (7.1×10^{-10} F m^{-1}), R is the gas constant (8.31 C V K^{-1} mol^{-1}), T is the temperature (298 K), n_o is the ion concentration (1×10^{-7} mol L^{-1}), v is the valency of ions (1), F is Faraday's constant (96.5×10^3 C mol^{-1}) and ϕ_p is the zeta potential of the Petri dish surface (assumed 100 mV). The electric field of dipole u_1 at a distance z is given by

$$E_1 = \frac{u_1}{4\pi\varepsilon z^3} = \frac{q_1 d_1}{4\pi\varepsilon z^3} \tag{5.3}$$

where d_1 is the charge separation in dipole u_1 (7 cm) and z is the distance between the dipole u_1 and the diode (~0.5 cm). The rotational torque τ by the field E_1 on the dipole across the diode, u_2, can be approximated as

$$\tau = u_2 \times E_1 = (q_2 . d_2) \times E_1 = (q_2 d_2) E_1 \sin 10^o = F_r (d_2/2) \tag{5.4}$$

where q_2 is the charge and d_2 is the charge separation (= diode length, ~1 mm) in dipole u_2, and F_r is the rotational force on the diode from the torque τ. Solving this equation, we obtain

$$F_r = 1.41\times q_2 \times 10^7 \text{ F V}^2\text{m}^{-1} \tag{5.5}$$

At steady-state, the rotational force on the diode, calculated above, will be balanced by the opposing drag force (F_d) and alignment force (F_a).

$$F_r = F_d + F_a \tag{5.6}$$

Drag force, F_d, on the diode can be estimated by approximating it to be a cylinder of length d_2 (1 mm) and diameter D (0.9 mm) moving transversely in the liquid with velocity u (1.78 mm s^{-1}) as[44]

$$F_d = \frac{4\pi\mu u d_2}{\ln\left(\frac{7.4\mu}{Du\rho}\right)} = 1.46\times10^{-8}\text{ N} \tag{5.7}$$

where μ is the viscosity (10^{-3} Pa s) and ρ is the density (10^3 kg m^{-3}) of water. Similarly, alignment force, F_a, on the diode can be estimated by approximating it to be an ellipsoid of semimajor axes $a>b>c$ as[41]

$$F_a = \frac{\tau_a}{d_2/2} \approx \frac{4\pi a^3}{3d_2}\left[\frac{\varepsilon}{\ln(2a/b)-1}\right] E^2 \sin\left(2\times10^{^\circ}\right) = 8\times10^{-9}\text{ F V}^2\text{m}^{-1} \tag{5.8}$$

where τ_a is the alignment torque on the diode (0.38×10^{-11} F V^2) and E is the external electric field after the DC component in the signal is removed by the capacitor (2 V_{peak} mm^{-1}). Substituting the estimated values of F_a and F_d in eqn (5.6), we obtain the charge in the diode dipole to be

$$q_2 = \pm 1.6 \times 10^{-15} \text{C} \tag{5.9}$$

We can separately estimate the charge in the diode dipole, based on its capacitance C specified by the manufacturer (3 pF), as

$$q_{d1} = C \cdot V = \pm 2.4 \times 10^{-11} \text{C} \tag{5.10}$$

where V is the potential drop across the diode after the DC component in the signal is removed by the capacitor (8 V). We can also estimate the charge near the diode surface, q_{d2}, based on the Guoy-Chapman theory as[43]

$$q_{d2} = A \times \left(-\sqrt{8\varepsilon RTn_o} \sinh\left(\frac{vF\varphi_d}{2RT} \right) \right) = \pm 1.3 \times 10^{-10} \text{C} \tag{5.11}$$

where A is the diode surface area (~1 mm^2) and ϕ_d is the zeta potential of the diode surface (assumed 100 mV). Since the actual charge in the diode dipole (eqns 5.10 & 5.11) is much larger (by orders of magnitude) than the charge required for the rotational force to balance the drag and alignment forces (eqn 5.9) - the actual rotational force on the diode must be large enough to overcome the drag and alignment forces. This supports our hypothesis that diode rotation is caused due to the rotational torque by counterionic field.

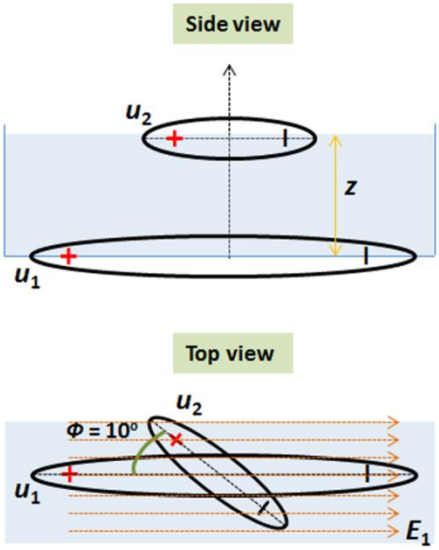

Figure 5.8 Schematic illustrating the orientation of the dipole across the diode (u_2) with respect to the dipole across the wire-electrodes due to counterion redistribution (u_1). z is the separation between the two dipoles and E_1 is the field from the dipole u_1.

5.3.4 Sideways Diode Motion

We also observed that when the applied duty cycle change does not completely rotate the diode, the diode exhibits sideways motion as shown in Fig. 5.9a. When the rotational torque acting on the diode does not fully overcome the alignment torque and the viscous drag, diode rotates only partially. Interestingly, we have observed sideways motion in multiple directions for a given orientation of a partially rotated diode. Few motion trajectories observed during sideways diode motion are shown in Fig. 5.9b. We believe such complex motion pattern is an outcome of two effects – 1. reactive propulsive force (from the counterion flux near diode surface) and 2. rotational torque (from the counterion redistribution across wire-electrodes) acting simulataneously on the diode. Further work needs to be done to understand how each of the various electrohydrodynamic effects taking place in the Petri dish influences the direction of sideways motion when the diode partially rotates. This would enable additional level of control on the precise direction of diode motion without using a four-electrode setup.

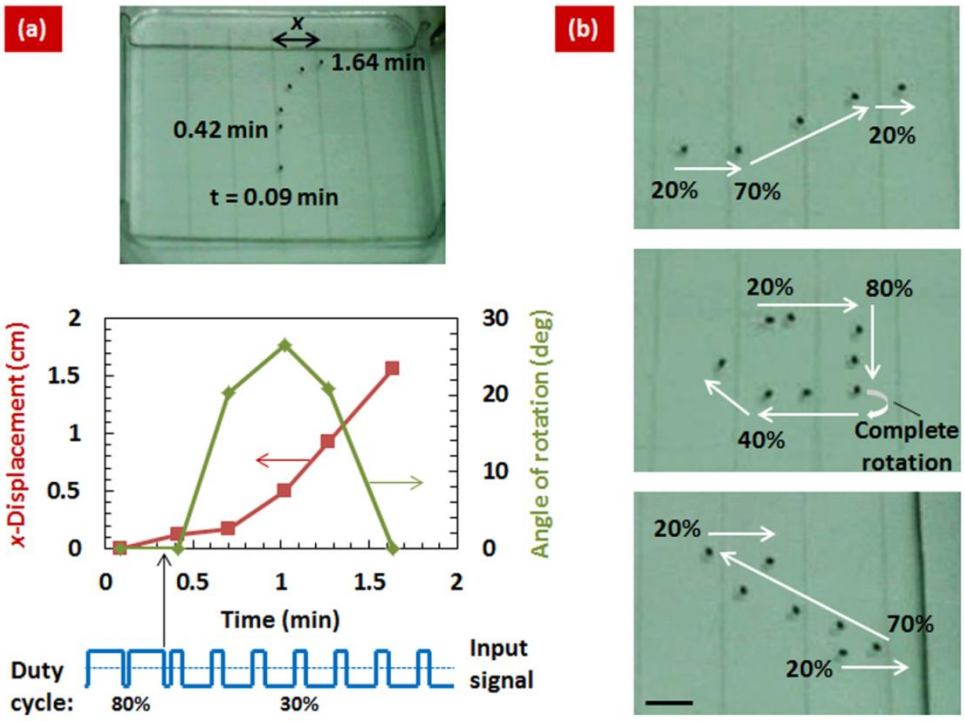

Figure 5.9 (a) Photograph of a trajectory of a self-propelling diode moving sideways (assembled from superimposed images), along with a plot of its *x*-displacement and angle of rotation versus time, when the duty cycle of the applied AC signal was changed from 80% → 30% as shown in the cartoon of the input signal. (b) Photographs of some of the trajectories observed during sideways diode motion (assembled from superimposed images).

5.4 Conclusions

We discovered and successfully implemented a technique that allows simple and effective on-demand steering of the self-propelling diodes by means of remotely controlling the parameters of the AC electric field. Application of short-lasting DC fields induces counterionic redistribution that can be used to remotely rotate the diode, while eliminating the undesirable fluid flows present during the application of constant DC fields. This new principle of duty cycle modulation driven precise control of the direction of motion of self-propelling microdevices is a first step towards the development of "intelligent" particles that can perform practical functions in the fields of MEMs and micro-robotics.

5.5 References

1. Mallouk, T. E., Sen, A. Powering Nanorobots. *Sci. Am.* **300,** 72-77 (2009).

2. Wang, J. Can Man-Made Nanomachines Compete with Nature Biomotors? *ACS Nano* **3,** 4-9 (2009).

3. Mirkovic, T., Zacharia, N. S., Scholes, G. D., Ozin, G. A. Fuel for Thought: Chemically Powered Nanomotors Out-Swim Nature's Flagellated Bacteria. *ACS Nano* **4,** 1782-1789 (2010).

4. Ebbens, S. J., Howse, J. R. In pursuit of propulsion at the nanoscale. *Soft Matter* **6,** 726-738 (2010).

5. Sengupta, S., Ibele, M. E., Sen, A. Fantastic Voyage: Designing Self-Powered Nanorobots. *Angew. Chem. Int. Ed.* **51,** 8434-8445 (2012).

6. Browne, W. R., Feringa, B. L. Making molecular machines work. *Nat. Nanotechnol.* **1,** 25-35 (2006).

7. Dreyfus, R. *et al*. Microscopic artificial swimmers. *Nature* **437,** 862-865 (2005).

8. Wang, W., Castro, L. A., Hoyos, M., Mallouk, T. E. Autonomous Motion of Metallic Microrods Propelled by Ultrasound. *ACS Nano* **6,** 6122-6132 (2012).

9. Sharma, R., Chang, S.-T., Velev, O. D. Gel-based self-propelling particles get programmed to dance. *Langmuir* **28,** 10128-10135 (2012).

10. Loget, G., Kuhn, A. Electric field-induced chemical locomotion of conducting objects. *Nat. Commun.* **2,** 535 (2011).

11. Loget, G., Kuhn, A. Propulsion of Microobjects by Dynamic Bipolar Self-Regeneration. *J. Am. Chem. Soc.* **132,** 15918–15919 (2010).

12. Kohira, M. I., Hayashima, Y., Nagayama, M., Nakata, S. Synchronized self-motion of two camphor boats. *Langmuir* **17,** 7124-7129 (2001).

13. Masoud, H., Bingham, B. I., Alexeev, A. Designing maneuverable micro-swimmers actuated by responsive gel. *Soft Matter* **8,** 8944-8951 (2012).

14. Solovev, A. A. *et al*. Self-Propelled Nanotools. *ACS Nano* **6,** 1751-1756 (2012).

15. Gao, W., Pei, A., Wang, J. Water-Driven Micromotors. *ACS Nano* **6,** 8432-8438 (2012).

16. Bassik, N., Abebe, B. T., Gracias, D. H. Solvent Driven Motion of Lithographically Fabricated Gels. *Langmuir* **24,** 12158-12163 (2008).

17. Okawa, D., Pastine, S. J., Zettl, A., Frechet, J. M. J. Surface Tension Mediated Conversion of Light to Work. *J. Am. Chem. Soc.* **131,** 5396-5398 (2009).

18. Gao, W., Sattayasamitsathit, S., Manesh, K. M., Weihs, D., Wang, J. Magnetically Powered Flexible Metal Nanowire Motors. *J. Am. Chem. Soc.* **132,** 14403-14405 (2010).

19. Ismagilov, R. F., Schwartz, A., Bowden, N., Whitesides, G. M. Autonomous movement and self-assembly. *Angew. Chem. Int. Edit.* **41,** 652-654 (2002).

20. Gibbs, J. G., Zhao, Y. P. Autonomously motile catalytic nanomotors by bubble propulsion. *Appl. Phys. Lett.* **94,** 163104 (2009).

21. Sanchez, S., Solovev, A. A., Mei, Y., Schmidt, O. G. Dynamics of Biocatalytic Microengines Mediated by Variable Friction Control. *J. Am. Chem. Soc.* **132,** 13144–13145 (2010).

22. Pantarotto, D., Browne, W. R., Feringa, B. L. Autonomous propulsion of carbon nanotubes powered by a multienzyme ensemble. *Chem. Commun.* 1533-1535 (2008).

23. Kwon, G. H. *et al*. Biomimetic Soft Multifunctional Miniature Aquabots. *Small* **4,** 2148-2153 (2008).

24. Yoshida, R. Self-Oscillating Gels Driven by the Belousov-Zhabotinsky Reaction as Novel Smart Materials. *Adv. Mater.* **22,** 3463-3483 (2010).

25. Fischer, P., Ghosh, A. Magnetically actuated propulsion at low Reynolds numbers: towards nanoscale control. *Nanoscale* **3,** 557-563 (2011).

26. Kay, E. R., Leigh, D. A., Zerbetto, F. Synthetic molecular motors and mechanical machines. *Angew. Chem. Int. Ed.* **46,** 72-191 (2007).

27. Wang, Y. *et al.* Directional and Path-Finding Motion of Polymer Hydrogels Driven by Liquid Mixing. *Langmuir* **28,** 11276-11280 (2012).

28. Wang, J., Gao, W. Nano/Microscale Motors: Biomedical Opportunities and Challenges. *ACS Nano* **6,** 5745-5751 (2012).

29. Patra, D. *et al*. Intelligent, self-powered, drug delivery systems. *Nanoscale* **5,** 1273-1283 (2013).

30. Kagan, D. *et al*. Rapid Delivery of Drug Carriers Propelled and Navigated by Catalytic Nanoshuttles. *Small* **6,** 2741–2747 (2010).

31. Solovev, A. A., Sanchez, S., Pumera, M., Mei, Y. F., Schmidt, O. G. Magnetic Control of Tubular Catalytic Microbots for the Transport, Assembly, and Delivery of Micro-objects. *Adv. Funct. Mater.* **20,** 2430-2435 (2010).

32. Hong, Y., Diaz, M., Cordova-Figueroa, U. M., Sen, A. Light-Driven Titanium-Dioxide-Based Reversible Microfireworks and Micromotor/Micropump Systems. *Adv. Funct. Mater.* **20,** 1568-1576 (2010).

33. Campuzano, S., Kagan, D., Orozco, J., Wang, J. Motion-driven sensing and biosensing using electrochemically propelled nanomotors. *Analyst* **136,** 4621–4630 (2011).

34. Yang, W., Misko, V. R., Nelissen, K., Kongd, M., Peeters, F. M. Using self-driven microswimmers for particle separation. *Soft Matter* **8,** 5175-5179 (2012).

35. Frutiger, D. R., Kratochvil, B. E.; Vollmers, K.; Nelson, B. J. Magmites - Wireless resonant magnetic microrobots. *IEEE Int. Conf. Robot.* **2008***, 1-9*, 1770-1771.

36. Hong, Y., Velegol, D., Chaturvedi, N., Sen, A. Biomimetic behavior of synthetic particles: from microscopic randomness to macroscopic control. *Phys. Chem. Chem. Phys.* **12,** 1423-1435 (2010).

37. Guix, M. *et al.* Superhydrophobic Alkanethiol-Coated Microsubmarines for Effective Removal of Oil. *ACS Nano* **6,** 4445-4451 (2012).

38. Chang, S. T., Paunov, V. N., Petsev, D. N., Velev, O. D. Remotely powered self-propelling particles and micropumps based on miniature diodes. *Nat. Mater.* **6,** 235-240 (2007).

39. Chang, S. T., Beaumont, E., Petsev, D. N., Velev, O. D. Remotely powered distributed microfluidic pumps and mixers based on miniature diodes. *Lab Chip* **8,** 117-124 (2008).

40. Calvo-Marzal, P. *et al*. Propulsion of nanowire diodes. *Chem. Commun.* **46,** 1623-1624 (2010).

41. Jones, T. B., in *Electromechanics of Particles*, Cambridge University Press, New York, USA 1995, Ch. 5.

42. Israelachvili, J. N., in *Intermolecular and Surface Forces*, Academic Press, Massachusetts, USA 2011, Ch. 4.

43. Israelachvili, J. N., in *Intermolecular and Surface Forces*, Academic Press, Massachusetts, USA 2011, Ch. 14.

44. Bird, R. B., Stewart, W. E., Lightfoot, E. N. in *Transport Phenomena*, Wiley, Singapore 1960, Ch. 3.

CHAPTER 6

Summary and Future Outlook

6.1 Summary

The main theme of my dissertation is to develop and understand the fundamentals of novel principles for powering the self-propulsion of millimeter-sized particles in liquids. In the first project, we developed gel-based self-propelling particles, comprising of an ethanol infused hydrogel, that exhibit a unique pulsating propulsion mechanism in water over long duration (instead of continuous motion). The "dancing" gel-based particles are simple, inexpensive, easy to construct, and can be prepared using multiple combinations of surface active material and hydrogel matrix. The duration of motion of such particles can be tuned by adjusting the concentration of surface active material in the hydrogel. We analyzed the reason behind their pulsation and found that it is caused due to the generation of a self-sustained periodic cycle of surface tension gradient driven flows, which in turn occurs because the ethanol release from the hydrogel end takes place slightly beneath the water surface. On the basis of our proposed propulsion mechanism and the mass transfer of ethanol from the hydrogel, we developed scaling relations for the pulse interval and the distance propelled by these particles, and found them to be in agreement with the experimental data. Based on the quantification of this mass-transfer driven motion, we constructed floaters of various designs programmed to move in stunningly regular sequences of translational and rotational steps, performing various "dances" and following complex trajectories.

As a next step, we incorporated a "payload" element into the gel-based particles, which already contain an "engine" component for self-propulsion. Since the gel-based particles self-propel at the air-water interface, our choice for a "payload" was an oil absorbent material. The thus formed "engine-payload" particles propelled vigorously over the oil-covered water surface while the oil gets collected into the absorbent end, and simultaneously the release of the surface active material from the hydrogel end causes oil film dispersion. The efficiency of oil collection by mobile absorbents was found to be significantly higher, due to the presence of convective oil flux, compared to stationary absorbents that rely on diffusion or natural drifting for gathering oil. We correlated the weight of oil absorbed by the particle (predominantly due to convective transport) to the distance propelled in oil, based on an exponential relationship. Armed with this information,

we simplified the particle design by directly mobilizing the absorbent sheets by infusing them with a few drops of surfactant on one side, and analyzed the extent of oil dispersion and rate of oil collection by sheets propelled using three different surfactants of the homologous series of sodium n-alkyl sulfates. The dimensions of these oil-gathering particles can be easily scaled up or down and their shape can be optimized.

In the second project, we eliminated the need of incorporating a propulsion "fuel" on-board the particle by loading it with a catalyst and adding the "fuel" to the surrounding liquid. We developed biogenic or biocatalytic self-propelling particles that use yeast cells (immobilized in hydrogel or polyelectrolyte matrix) as catalyst to power their propulsion by fermenting glucose or decomposing hydrogen peroxide (H_2O_2) present in the surrounding solution. We found that the motion of the yeast boat in H_2O_2 solution was very vigorous relative to its sluggish motion in glucose solution. We correlated the particle velocity in H_2O_2 solution to the phenomenon of bubble bursting and obtained reasonable agreement between the two.

In the third project, we devised a novel technique for controlling the direction of motion of the diode-based self-propelling particles on water. The diodes are remotely powered by an external uniform AC electric field, as reported earlier by Velev group. We found that by introducing a short-duration DC component into the AC signal, the self-propelling diodes could be rotated and made to shuttle back and forth on water. Diode rotation occurs due to its orientation-dependent polarizability. We show that the diodes prefer to orient in a direction such that the DC field across them is anti-parallel with respect to the external field, analogous to the tendency of a dipole to orient anti-parallel with respect to another dipole. Application of a short-duration DC component, implemented by modifying the wave symmetry of the applied AC signal and transmitting it through a capacitor, induces counterionic redistribution that can be used to rotate the diode on-demand while eliminating the undesirable fluid flows present during the application of constant DC fields.

6.2 Future Outlook

The research on principles, engineering and applications of self-propelling particles is a relatively new but rapidly developing research field. Novel propulsion techniques are being actively explored and the proof-of-principle of performing practical functions using particles, which take advantages of a wide diversity of propulsion mechanisms, is being extensively tested. This is an interdisciplinary research topic, requiring simultaneous efforts from several areas of science and engineering. The results obtained so far in the preliminary tests have been promising and suggest that exciting possibilities exist in the future for such novel particle systems. Certain challenges continue to persist, as elaborated in Sections 1.2 & 1.3 of this dissertation. In this section, I have pointed out the potential directions for future work in reference to the self-propelling particles that we have developed, and have highlighted some of the challenges facing these particle systems.

In the gel-based self-propelling particles project, we observed that there is a strong correlation between the particle design parameters and the nature of particle motion. A particle releasing surface active material on the water interface moves in a continuous manner. In the particles that we constructed, ethanol release from the hydrogel takes place slightly beneath the water surface, due to the submerged hydrogel end, which causes the particle to propel in a periodic fashion rather than continuously. This suggests that by simply modulating the depth of immersion of such particles in water, by controlling their weight or buoyancy force, it may be possible to switch between the continuous and periodic modes of propulsion on demand. The ease of designing particles with novel shapes and motion trajectories, as well as the ability to predict the pulsation parameters of such particles using the mass-transfer based scaling relations suggests that with additional efforts it may be possible to precisely tune and control the propulsion of such Marangoni effect driven particles in predefined trajectories. Additionally, we noticed that these floaters have a tendency to assemble due to capillary attraction between their casings. In future, it may be interesting to study the “on the fly” self-assembly of such autonomously propelling gel boats (into dimers, trimers, and larger assemblies) and the emergent complex motion pattern of the ensembles.

Our approach of mobilizing an oil absorbent material for increasing the efficiency of oil collection is applicable to any type of absorbent and can potentially be implemented for environmental remediation operations following oil spills. However, their design can be improved further. Currently, we are employing magnetic steering to control the direction of motion of the self-propelling absorbents on top of oil-covered water by incorporating magnetic particles into the absorbent material. Magnetization of the absorbent also allows us to pick up the absorbent at the end of oil collection using a magnet. Potentially, the absorbed oil can be recovered from the magnetized absorbents by using a strong magnetic field for "squeezing out" the oil from them. An alternative, more efficient, steering approach can be to functionalize these particles such that they can independently sense the gradient of oil in their environment and respond to it (similar to the chemotactic behavior of bacteria, which has been observed in the case of some synthetic self-propelling motors as well, as discussed in Section 1.4). Such chemotactic absorbent particles would eliminate the need of applying external magnetic fields for steering purposes. Due to the small size of our particles, viscous drag has a significant impact on their propulsion. We have used light mineral oil in all our experiments, which may not be an accurate representation of an actual oil spill in terms of viscosity. Future research should involve testing the propulsion of such particles in high viscosity oil samples and developing means of overcoming the viscous resistance. The application of chemical dispersants for remediating oil spills is topic of an ongoing debate. Hence, in place of Marangoni effect, other techniques of self-propulsion may be applied to move the absorbent materials. One such technique may be aluminum catalyst-driven bipolar electrochemical propulsion based on water-splitting reaction (discussed in Section 1.3.4).

The general principle of enhancing the rate of mass-transfer by imparting self-propulsion ability to originally stationary particles, applied by us to an absorption process, may be relevant to other widely used chemical processes such as catalysis. We believe that self-propelling catalytic particles would be more effective in enhancing the rate of a reaction compared to passive catalysts that rely on diffusive transport of reactants towards the catalysts. Catalytic particles can be engineered to actively self-propel towards reactants,

thereby enhancing the convective mass-transport, using a variety of techniques such as self-electrophoresis, bubble recoil and osmophoresis.

Catalytic motors are believed to hold potential for a range of potential applications and extensive efforts are invested into optimizing their propulsion by rational engineering of their design and careful selection of the catalyst-fuel combination. Catalytically driven propulsion in H_2O_2 has been reported earlier by several groups using synthetic catalysts or immobilized enzymes of biological origin. Our biocatalytic yeast boats are the first demonstration of applying live cells directly as catalysts of a kind for this process. We correlated the velocity of the yeast boats in H_2O_2 solution to the rate of bubble formation and bursting. Future research efforts should examine the physics behind the particle motion in terms of the various forces acting on it when the generated bubbles burst. A clear insight into the physics behind the particle motion would enable us to model and control its motion pattern. Benign propulsion media, such as glucose, are particularly attractive for the future development of self-propelling particles with applications in the biomedical field. However, the propulsion of the yeast boats in glucose solution was very slow compared to that in H_2O_2, which we believe is due to the slow rate of metabolitic glucose fermentation by yeast. Further work needs to be done to increase the propulsion speed of the yeast boats in glucose solution by accelerating the rate of the fermentation process. We believe our work opens up interesting possibilities in this research area as well as encourages others to explore novel biocatalyst-fuel combinations.

The new principle of precisely controlling the direction of motion of the self-propelling microdevices that we developed is a first step towards the development of "intelligent" and "microbot" particles that can perform practical functions in the fields of MEMs and micro-robotics. We observed that when the applied short-duration DC component does not completely rotate the diode, the partially rotated diode starts moving sideways. We believe that the sideways movement is an outcome of reactive propulsive force and rotational torque acting simultaneously on the diode. Interestingly, we have observed diode's ability to perform sideways motion in multiple directions for a given duty cycle change. Future research should focus on determining the source of directional variability in these

experiments by understanding how each of the various electrohydrodynamic effects taking place in the Petri dish influences the direction of sideways motion when the diode partially rotates. This would enable additional level of control on the precise direction of diode motion without using a four-electrode setup. In addition to controlling the back and forth movement of the diode, this would allow us to tilt and propel the diode at a desired angle on demand. Overall, this thesis makes a step towards the future development of microbots and intelligent functional microdevices.